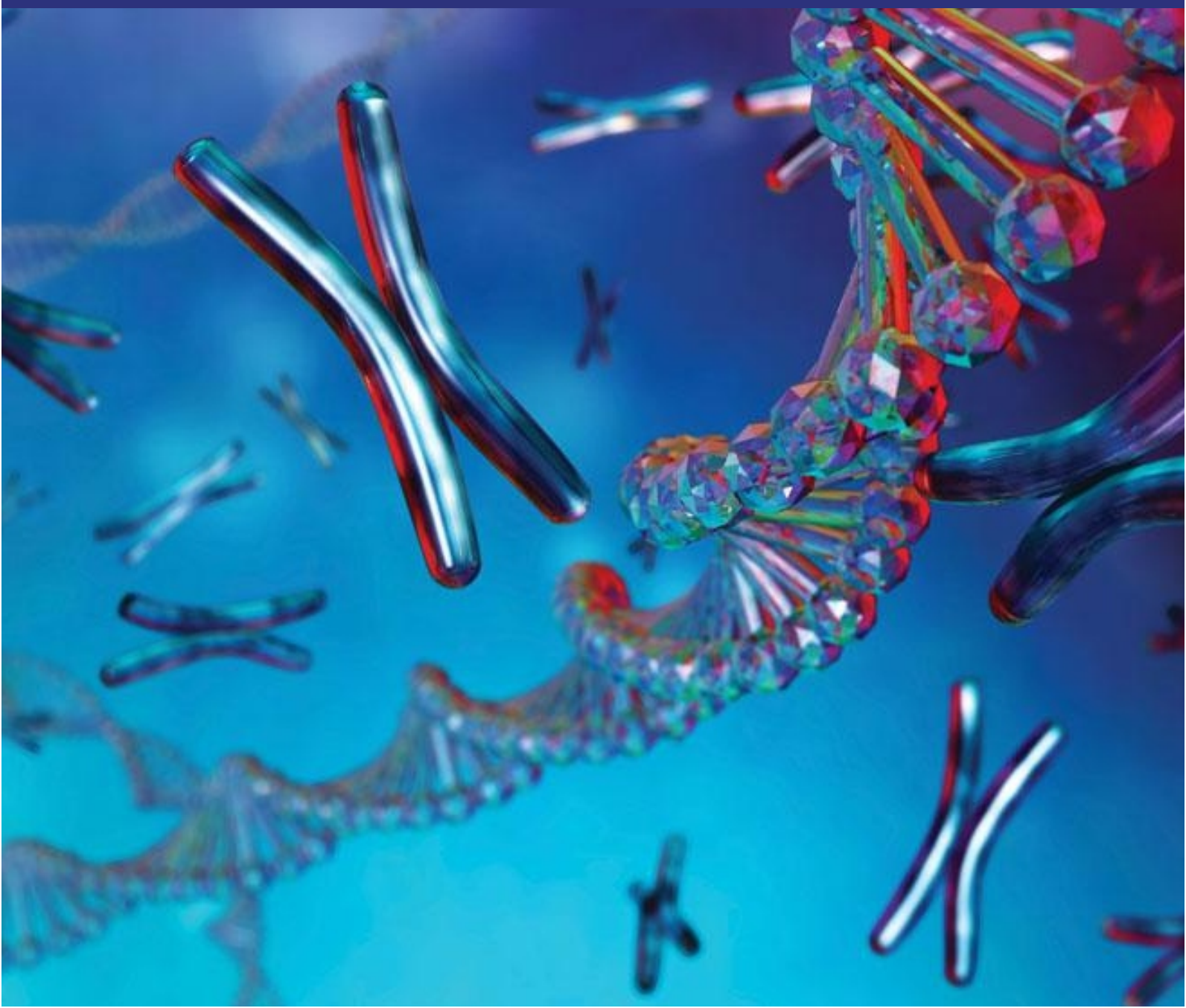


University Handbook of DNA Expression and Analysis

**Padmalakshmi Dey
Shashikant Patil**





***University Handbook of
DNA Expression and Analysis***

.....

Padmalakshmi Dey

Shashikant Patil



*University Handbook of
DNA Expression and Analysis*

.....
Padmalakshmi Dey
Shashikant Patil

Dominant
Publishers & Distributors Pvt Ltd
New Delhi, INDIA



Knowledge is Our Business

UNIVERSITY HANDBOOK OF DNA EXPRESSION AND ANALYSIS

By Padmalakshmi Dey, Shashikant Patil

This edition published by Dominant Publishers And Distributors (P) Ltd
4378/4-B, Murarilal Street, Ansari Road, Daryaganj,
New Delhi-110002.

ISBN: 978-81-78886-53-4

Edition: 2023 (Revised)

©Reserved.

This publication may not be reproduced, stored in a retrieval system or transmitted, in any form or by any means, electronic, mechanical, photocopying, recording or otherwise, without the prior permission of the publishers.

Dominant

Publishers & Distributors Pvt Ltd

Registered Office: 4378/4-B, Murari Lal Street, Ansari Road,
Daryaganj, New Delhi - 110002.

Ph. +91-11-23281685, 41043100, Fax: +91-11-23270680

Production Office: "Dominant House", G - 316, Sector - 63, Noida,
National Capital Region - 201301.

Ph. 0120-4270027, 4273334

e-mail: dominantbooks@gmail.com
info@dominantbooks.com

w w w . d o m i n a n t b o o k s . c o m

CONTENTS

Chapter 1. DNA Fragment Length and Methylation Status Are Associated with Self-DNA Mediated TLR9-Related Gene	1
— <i>Shashikant Patil</i>	
Chapter 2. Chemical Exposure Causes Changes in Gene Expression and DNA Copy Number.....	6
— <i>Mohamed Jaffar A</i>	
Chapter 3. Functional Expression of Cryptosporidium Parvum DNA-Topoisomerase IB	14
— <i>Somayya Madakam</i>	
Chapter 4. DNA Methylation Controls Genome-Wide Microrad Expression in Hepatocarcinogenesis.....	19
— <i>Suresh Kawitkar</i>	
Chapter 5. Age-Related Dynamic Alterations in DNA Methylation and Transcriptome Expression in Porcine Ovaries	26
— <i>Somayya Madakam</i>	
Chapter 6. Patient Survival Is Affected by Aberrant Expression of N-Methylpurine-DNA Glycosylase in Malignant Gliomas	34
— <i>Rajesh Kumar Samala</i>	
Chapter 7. A Mixed DNA/LNA Microarray: Expression Profiling of a Heterogeneous Population of Mornas.....	40
— <i>Thiruchitrambalam</i>	
Chapter 8. DNA Repair Capacity Levels-Stratified Microrad Expression Alterations in Women with Breast Cancer	46
— <i>Thiruchitrambalam</i>	
Chapter 9. An Effective Gene Expression Tool for Yeasts: DNA Microspheres Coated with Bioavailable Polymer.....	52
— <i>Ashwini Malviya</i>	
Chapter 10. Breast Cancer Homologous Recombination Deficiency Correlated with DNA Helicase Gene Expression	57
— <i>Raj Kumar</i>	
Chapter 10. DNA Double-Strand Breaks Related Genes, ATM And Gammah2ax, Have Abnormal Expression in Thyroid Carcinoma.....	66
— <i>Swarna Kolaventi</i>	
Chapter 11. Neutrophil Receptor Expression Affected by Bacterial Infections: DNA Virus Infections and RNA Virus Infections.....	74
— <i>Shweta Loonkar</i>	

CHAPTER 1

DNA FRAGMENT LENGTH AND METHYLATION STATUS ARE ASSOCIATED WITH SELF-DNA MEDIATED TLR9-RELATED GENE

Shashikant Patil, Professor

Department of uGDX, ATLAS SkillTech University, Mumbai, Maharashtra, India

Email Id-shashikant.patil@atlasuniversity.edu.in

ABSTRACT:

We examined the impact of self-DNA bound to Toll-like Receptor gene and methyltransferase expressions as well as cell differentiation in cells in order to comprehend the biologic relevance of this molecule. or type-4 self-DNAs were each incubated individually with HT29 cells. qtr.-PCR was used to measure the expression levels of TLR9-signaling and proinflammatory cytokine-related genes. DNA methyltransferase and cytokeratin antibodies were used to assess methyltransferase activity and cell differentiation. TLR9 expression increased significantly after treatment with type-1 DNA. Overexpression of the IL8 gene and signaling molecules associated with TLR9 was brought on by type-2 therapy. Significant overexpression of Nfk, IRAK2, and IL8 as well as downregulation of were found in the case of type-3 therapy. gene expression was increased using type and gene expression was decreased. Only after type-1 DNA treatment was CK expression noticeably increased. Type-1 DNA therapy may also increase DNMT3A expression. The activation of the TLR9-dependent and even independent proinflammatory pathways may be significantly influenced by DNA shape. There could be a biological connection between DNMT3A and TLR9 signaling. The method used to address self-DNA may affect how differently HT29 cells differentiate.

KEYWORDS:

Deoxyribonucleic, Lymphoid Follicles, Proinflammatory, Ribonucleic Acid.

INTRODUCTION

Toll-like receptors are innate immune receptors that recognize and eliminate microbial infections that are invading the body. The nucleic acids double-stranded ribonucleic acid, single-stranded RNA, and CpG deoxyribonucleic acid generated from microbial components are particularly recognized by intracellular TLRs. This recognition acts as a crucial connection between innate and adaptive immune responses. Monocytes, macrophages, dendritic cells, and some kinds of B cells that express TLR9 in the colonic mucosa tend to assemble around lymphoid aggregates and isolated lymphoid follicles. and -9 are examples of TLRs that may also be expressed by altered epithelial cells. TLR9, which may be triggered by DNA sequences originating from pathogens, is also expressed by HT29 colon cancer cells. Colonic homeostasis has been found to be maintained by bacterial DNA fragments activating apical epithelial TLR9. Self-DNA and artificial oligodeoxynucleotides that include unmethylated CpG sequences may both activate TLR9.

Pro- and anti-inflammatory cytokine synthesis as well as increased B-cell proliferation are ultimately produced as a consequence of TLR9-signaling activation. It is unknown what range of TLR9-dependent gene expression exists, despite the fact that TLR9 ligation is anticipated to trigger a broad range of protective innate immune responses[1], [2].It is well known that CpG DNA binding to TLR9 improves innate immunity. Despite substantial research on TLR9-mediated signaling networks, the size, length, and extent of changes in gene expression caused by CpG-DNA are still unclear. A single-dose CpG DNA injection has been shown to cause an initial fast surge in gene activation, similar to an increase in mRNA

levels, which returns to a baseline level in 2–3 days. However, the immune response is still influenced for many weeks. Additionally, it has previously been shown that following the insertion of CpG DNA, the first gene activation exhibits two induced peaks, occurring respectively after 3 hours and 5 days. Sequence changes to the CpG oligonucleotides that targeted the secondary structures were shown to have an impact on the invasion-inducing effect in the instance of the MDA-MB-231 human breast cancer cell line.

As opposed to the parent CpG oligonucleotide's unmethylated counterpart, methylation of the cytosine residues had no impact on the TLR9-mediated invasion. Certain human tumors and aberrant development are linked to altered methylation patterns. Three primary DNA methyltransferases have been hypothesized to have a role in an etiology of colorectal neoplasia's: DNMT1, -3A, and -3B. After DNA replication, DNMT1 is in charge of maintaining the DNA methylation pattern. During gametogenesis and development, the DNMT3 family predominantly affects de novo methylation. Additionally, it may work with DNMT1 to control the upkeep of DNA methylation. In contrast to healthy colon tissues, human colon cancer cell lines have distal DNMT3B promoters that are hypermethylated. This is consistent with the low expression level that leads to hypomethylation of many of its target gene promoters, which is significant for the a etiology of sporadic Carcaterra is currently no solid evidence regarding how the properties of self-DNA fragments that activate TLR9 affect downstream signaling pathways, cytokine response, cell differentiation, and expression of DNMTs, which may have significant immunobiological implications in the case of inflammatory and tumorous colonic disorders[3], [4].

In this work, we examined how pure, variously fragmented, and methylated self-DNA sequences affected the early, short-term gene expression of TLR9 in HT29 colon carcinoma cells. We also investigated the relationship between the expression of DNA methyltransferases and cytokeratin after self-DNA treatment and the stimulation of TLR9 signaling 1st Department of Pathology and Experimental Oncology at Semmelweis University in Budapest, Hungary, sold HT29 colon cancer cells. A particular pathogen-free cell culture facility was used to cultivate the cells 160 g/mL gentamycin, and 125 g/mL amphotericin B were added to RPMI 1640 to sustain HT29 cells. The media were changed every other day.2.3. DNA Treatment and Total RNA Isolation six-well treatment plate containing 0.5 10⁶ HT29 cells was filled with RPMI 1640, gentamycin, amphotericin B, and FBS as previously mentioned. The initial medium was changed to RPMI 1640 with gentamycin and no FBS after 24 hours. Then, 200 L of sterile phosphate buffered saline was used to dissolve 15 g of each kind of pretreatment DNA individually. Following that, the cells were treated with dissolved DNA samples that had not been tainted by protein, RNA, or lipopolysaccharide. There was just 200 L of sterile PBS added to the untreated controls. Cells were incubated at 37°C with 95% humidity, 5% CO₂, and air. Cells were twice washed in 5 mL of sterile PBS after 24 hours. Cells were finally resuspended in 5 mL of PBS after the second washing. The remaining cell solution was utilised for immunocytochemistry, and 2.5 mL of it was used for total RNA isolation. According to the manufacturer's instructions, total RNA was extracted from the isolated HT29 cells using the RNeasy Mini Kit.

Following the selection of TLR9-associated signaling genes and interleukin-8 as a marker of epithelial TLR9-pathway stimulation, oligonucleotide primers were created. Reverse transcription was carried out using 1 g of total RNA after quantitative and qualitative analysis. SYBR green and Probes Master PCR were used in the procedure. Each sample's gene expression levels were normalized to 18S expression. The 2-C approach was used to calculate differences and the mean relative gene expression. Immunocytochemistry.2.5 mL of each cell solution was utilised for the immunocytochemical tests. To penetrate the cells and prevent nonspecific protein-protein interactions, cells were centrifuged on a glass slide, fixed in

acetone at 20°C for five minutes, and then incubated in 1% bovine serum albumin/10% normal goat serum/0.3 M glycine in 0.1% PBS-Tween for an hour. Mouse anti-human monoclonal anti-TLR9 antibody was treated with TLR9 ICC Cells for an overnight period at 4°C. Lung tissue from humans was employed as a positive control. Rabbit monoclonal anti-DNMT1 antibody was treated with cells for an overnight period at 4°C. Positive checks were made using HeLa cells. Monoclonal anti-DNMT3a antibody was treated with cells for an overnight period at 4°C. Positive checks were made using HeLa cells. Rabbit polyclonal anti-DNMT3B antibody was treated with cells for an overnight period at 4°C. As a positive control, human hepatocellular cancer tissue was used. Mouse monoclonal anti-pan cytokeratin antibody was treated with cells for one hour at 37°C. As a positive control, human healthy colonic mucosa was employed. The secondary antibody was a goat polyclonal that had been conjugated to biotin. The Liquid DAB + Substrate Chromogen System was used to convert signals. Hematoxylin staining was done after the last PBS rinse[5], [6].

DISCUSSION

Innate immunity is mediated by the toll-like receptor which can recognize DNA from microbial and endogenous sources. Recent research reveals that TLR9 expression may be found in a variety of normal and tumorous cells, including HT29 colon cancer cells, in addition to immune cells. Recent research has shown that activating TLR9 with agonistic CpG sequences promotes invasion in a variety of cancer cells via partly reliant TRAF6 and MYD88-independent mechanisms. The purpose of this work was to examine the effects of self-DNA features on TLR9 signaling, DNA-methyltransferase expression, and HT29 cell differentiation. The self-DNA's typical physiological methylation pattern was intentionally altered, becoming hypermethylated, using the Messienzyme. Our findings suggest that varied pretreatment self-DNA induces various kinds of gene expression and cellular responses in HT29 colon cancer cells. While hypermethylation of self-DNA also increased IL8 synthesis, typically methylated no fragmented self-DNA largely activated the MYD88-dependent TLR9 signaling pathway. While self-DNA hypermethylation and fragmentation largely had an inhibitory impact on both the essential components of MYD88-dependent TLR9 signaling and IL8 production, they moved MYD88-dependent signaling to the MYD88-independent route. After type 4 DNA treatment, the upregulation of MYD88A and TRAF6 may suggest the participation of other, as of yet unmeasured Toll-like receptor-signaling pathways.

TLR9 was first described as a receptor that recognizes CpG sequences that are not methylation in microbial DNA. Synthetic oligodeoxynucleotides have been shown to activate epithelial TLR9. In order to investigate structural characteristics and their relationship to TLR9 activation, changes to self-DNA were employed in this work, both in length and methylation status. Our findings imply that the activation of the TLR9-mediated signaling pathways is significantly influenced by DNA structure, including methylation status and fragment length. There has previously been written on a similar immunobiological impact of DNA shape on cell invasion tests. To describe the structural properties of oligonucleotides required to elicit a TLR9-mediated inflammatory response, more biophysical investigations are required. The DNA methyltransferase 3A protein expression varied according on the kind of self-DNA.

Our discovery suggests that there could be a molecular connection between DNMT3A and TLR9 signaling. Recent research has shown that DNMTs mRNA levels are elevated in a variety of cancers, including colorectal, hepatocellular, and gastric cancer. It has previously been shown that gastrointestinal malignancies have poor DE methyltransferase expression and high amounts of DNMTs. Together, DNMTs and DE methyltransferase cause genomic instability, which ultimately speeds up the development of cancer. Recently, it was shown that

lung cancer patients with overexpression of the DNMT3A protein had considerably poorer overall survival. The DNA methylation pattern changes in cancer cells, which causes a group of genes to experience promoter hypermethylation and become transcriptionally quiet. A successful treatment approach for treating several illnesses involves reactivating genes that have been silenced by methylation by altering the expression and activity of DNA methyltransferases. One cannot rule out the possibility that, under normal or pathological conditions, self-DNA released by necrotic or apoptotic cells may have paracrine effects on nearby cells via TLR9 signaling, and that the cell's reaction will depend on the methylation state of the attached DNA. The released self-DNA is probably a physiologically active molecule in the immediate environment. Our research also shows that the way self-DNA is treated affects how differently HT29 cells differentiate. Due to the nondifferentiated nature of the HT29 colon cancer cell line, cytokeratin expression is often quite low. It has significant therapeutic value that self-DNA therapy encourages HT29 cells to express cytokeratin. An intriguing innovative method for treating colorectal cancer that has the potential to become a significant alternative therapeutic option is the use of self-DNA to separate aggressive carcinomas into less aggressive malignancies [7], [8].

Only treatment with type-3 DNA caused significant changes in the expression of the IL8 gene, a marker of epithelial TLR9-pathway induction, and only incubations with hypermethylated DNAs caused changes in the expression of the CK and DNMT proteins, suggesting that the methylation status of self-DNA may be a more important factor than fragment length regarding its biologic effect. However, since there might be significant variations in cancer cell lines, our findings also need to be validated in other cell lines. As a result, our research suggests that the biological impact of self-DNA derived from the HT29 colon carcinoma cell line on TLR9-related signaling, methyltransferase expression, and cell differentiation depends on the DNA fragment length and methylation status, though the latter seems to have a more striking biologic impact. It is necessary to do more research to determine the precise structural and biophysical characteristics of the DNA sequences that cause inflammation and the functions that these pathways play in the pathophysiology of colonic illness [9], [10].

CONCLUSION

Only treatment with type-3 DNA caused significant changes in the expression of the IL8 gene, a marker of epithelial TLR9-pathway induction, and only incubations with hypermethylated DNAs caused changes in the expression of the CK and DNMT proteins, suggesting that the methylation status of self-DNA may be a more important factor than fragment length with regard to its biologic effect. Our findings must to be verified in different cell lines since there might be significant variations in cancer cell lines.

Our study concludes that the length of the DNA fragment and its level of methylation affect the biological effects of self-DNA derived from the HT29 colon carcinoma cell line on TLR9-related signaling, methyltransferase expression, and cell differentiation; however, the methylation pattern appears to have a more striking biologic impact. To determine the precise structural and biophysical characteristics of the DNA sequences that cause inflammation and the functions that these pathways play in the pathophysiology of colonic illness, further research is needed.

REFERENCES:

- [1] T. M. Gradziel and J. Fresnedo-Ramírez, "Epigenetic selection in almond breeding," in *Acta Horticulturae*, 2018. doi: 10.17660/ActaHortic.2018.1219.3.
- [2] Renstrom, "Authors' reply.," *Knee Surg. Sports Traumatol. Arthrosc.*, 2013.

- [3] S. Akiyama *et al.*, “Pre-trial inter-laboratory analytical validation of the FOCUS4 personalised therapy trial.,” *Br. J. Cancer*, 2014.
- [4] Y.-X. Zou *et al.*, “Homocysteine lowering therapy in hypertensive subjects at low cardiovascular risk: Role of nutraceuticals,” *Zhurnal Nevrol. i psikhiatrii Im. S.S. Korsakova*, 2018.
- [5] M. Pieretti *et al.*, “Absence of expression of the FMR-1 gene in fragile X syndrome,” *Cell*, 1991, doi: 10.1016/0092-8674(91)90125-I.
- [6] Z. Lin *et al.*, “Identification of disease-associated DNA methylation in B cells from Crohn’s disease and ulcerative colitis patients,” *Dig. Dis. Sci.*, 2012, doi: 10.1007/s10620-012-2288-z.
- [7] J. Gao, X. Qiu, X. Wang, C. Peng, and F. Zheng, “Associations of ChREBP and global DNA methylation with genetic and environmental factors in Chinese healthy adults,” *PLoS One*, 2016, doi: 10.1371/journal.pone.0157128.
- [8] V. S. Dhillon, M. Shahid, and S. A. Husain, “Associations of MTHFR DNMT3b 4977 bp deletion in mtDNA and GSTM1 deletion, and aberrant CpG island hypermethylation of GSTM1 in non-obstructive infertility in Indian men,” *Mol. Hum. Reprod.*, 2007, doi: 10.1093/molehr/gal118.
- [9] S. Xargay-Torrent *et al.*, “Methylation of the C19MC microRNA locus in the placenta: A mechanism whereby maternal body size links to that of the child,” *Horm. Res. Paediatr.*, 2018.
- [10] L. I. Fedoreyeva and B. F. Vanyushin, “Mechanisms of catalytic action and chemical modifications of endonucleases WEN1 and WEN2 from wheat seedlings,” *Biochem.*, 2013, doi: 10.1134/S0006297913010057.

CHAPTER 2

CHEMICAL EXPOSURE CAUSES CHANGES IN GENE EXPRESSION AND DNA COPY NUMBER

Mohamed Jaffar A, Professor
Department of ISME, ATLAS SkillTech University, Mumbai, Maharashtra, India
Email Id-mohamed.jaffar@atlasuniversity.edu.in

ABSTRACT:

Although DNA copy number variation has long been linked to highly penetrant genomic illnesses, it wasn't until recently that it was recognized as a significant source of genetic variation in phenotypically normal people. Additionally, it is now understood that copy number variations contribute to the beginning of complex illnesses. It has been suggested that several complicated disorders linked to CNVs may be affected by as-yet-unidentified environmental variables. Environmental chemical exposure is thought to cause CNVs and have an impact on the pathophysiology and onset of illness. In order to examine the production of CNVs utilizing array comparative genomic hybridization and the zebrafish vertebrate model system, a proof-of-concept experiment using ethyl methane sulfonate and cytosine arabinoside was accomplished. Both of the compounds caused CNVs after exposure. Multiple exposure doses using EMS allowed for the detection of CNVs in related genomic areas, and five of these CNVs were shared by the two compounds. Additionally, CNVs and altered gene expression were linked. This study contends that ambient chemical exposure results in CNVs that have an influence on gene expression and justifies more research into this issue.

KEYWORDS:

Arabinoside, Genomic, Hybridization, Sulfonate.

INTRODUCTION

Single nucleotide polymorphisms, variable tandem repeats, the presence or absence of transposable elements, and structural alterations are some of the different types of structural genetic variation found in the human genome. SNPs were formerly believed to represent the main kind of genomic variation and to be responsible for a large portion of the typical phenotypic variation. Numerous copy number variations were found in the genomes of phenotypically normal individuals as a result of recent advances and uses of genome-wide technologies. A duplication or deletion that is more than 1 kb in size is referred to as a CNV. Since the beginning of the human genome's study over 40 years ago, it has been believed that copy number variations were rare, had little effect on the overall quantity of genetic diversity in humans, and were mostly linked to highly penetrant disease phenotypes. In 2004, CNVs were widely found in the genomes of people with normal phenotypes, according to two separate investigations. Additional genome-wide analysis discovered and characterized new human CNVs after these early findings. There is currently enough evidence of widespread copy number variation in the human genome, and many of these CNVs encompass genes that are expected to have an impact on gene networks. Gene expression levels may fluctuate, gene dosage and regulatory elements can be disrupted or lost, and regulatory elements can even be lost as a consequence of CNVs[1], [2].

When an illness is caused by a single genomic variation, such as a deletion on chromosome 7 in Williams Beuren syndrome, traditional cytogenetics has found a range of genomic variants that are connected to the disorder. Initially thought to have a neutral function, CNVs are now

understood to play a role in the onset of complex diseases like schizophrenia, attention-deficit hyperactivity disorder, and autism spectrum disorder. CNVs that did not directly cause early-onset, highly penetrant genomic disorders were initially considered neutral in function. Additionally, it has been suggested that CNVs affect late-onset illnesses including Parkinson's and Alzheimer's. These disorders are thought to be impacted by environmental variables in addition to hereditary ones. Environmental variables may affect the development and course of many disorders, but the processes by which they do so are not well known. Genes important for molecular-environmental interactions are enriched, according to recent functional attribute analyses of CNV areas. Additionally, research on the postmortem brains of people with ASD suggests that exposure to polychlorinated biphenyls may be linked to a duplication event on human chromosome 15. This research suggests a connection between the environment and copy number variations and their impact on complicated illness, although it is unclear if the copy number variation was directly caused by the ambient chemical exposure.

The capacity of chemical exposure to produce CNVs has not been well studied, although it is one environmental component that may contribute to their creation. The advancement of genomic technologies, such as array comparative genomic hybridization and NextGen sequencing, has made it possible to identify copy number variations throughout the whole genome. Prior tests and methods used to look at how chemical exposure affected the genome could only find bigger chromosomal abnormalities or single nucleotide changes. Further research into the biological and functional importance of these DNA modifications is hindered by the inadequate integration of structural DNA mutations with the reference genome sequence in many of these experiments. Because of this, previous genotoxicity studies did not fully evaluate this kind of DNA change. In a cell culture system, three recent investigations started to look into the production of CNVs using aphidicolin, hydroxyurea, and ionizing radiation. Other agents have not yet been looked into. A growing concern for environmental health is the unique impact of CNVs, and it is now well acknowledged that utilizing genomics to uncover environmental chemical influences on the human genome is important[3], [4].

In order to lay the groundwork for future research into the role of environmental chemical exposure in the development of CNVs, a proof-of-concept experiment was conducted in this study using a zebrafish cell line to test the hypothesis that chemical exposure will result in CNVs detectable with the use of array CGH technology. Several fields of biology use the zebrafish model vertebrate system extensively. The ability to translate the molecular processes of toxicity shown in the zebrafish model system to humans is made possible by a complete genome sequence and genetic function that is conserved across the zebrafish and human genomes. Large-scale mutant screens show that mutations in several of these orthologs exhibit characteristics comparable to those prevalent in human disorders, and some zebrafish orthologs are reported to have a significant role in human disease. As a toxicological model and a model for DNA repair processes, the zebrafish has also long been employed in research. The zebrafish genome's CNV map demonstrates that the genome is malleable enough to allow CNV generation and that it is suitable for use in this investigation. This proof-of-concept experiment includes several exposure doses of two genotoxic compounds typically used as reference chemicals, ethyl methane sulfonate and cytosine arabinoside, to evaluate dose-response and differences between the two chemicals. A global gene expression study was also done to determine the relationship between CNVs brought on by chemical exposure and changes in gene expression.

The zebrafish fibroblast cell line utilised in this investigation is described in full in Freeman et al. and was created from roughly 100 AB zebrafish strain embryos. Because it is well-

characterized, regularly checked for cytogenetic alterations, and has been used in earlier zebrafish cytogenetic research, this zebrafish cell line was chosen for the proof-of-concept study. Additionally, using this zebrafish cell line will make it simpler to transition future investigations from in vitro to in vivo zebrafish testing. Ethyl methane sulfonate and cytosine arabinoside were examined for their capacity to produce CNVs. These reference compounds are often employed in genotoxicity experiments. For the purpose of determining the toxicity of EMS and Ara-C in this cell line, a cell confluency test was first completed. This test is an adaptation of Plewa et al. work.

A normal trypsin procedure was used to extract cells from cell culture flasks, and cell concentration was then calculated. In order to reach the correct chemical test concentrations, the assay was set up in 96-well plates with 7,000 cells per well in an adequate amount of medium and chemical stock. A first column blank and a second column negative control were included in the plate setup. Four subsample wells per chemical concentration were included on each plate. Plates were set up and then put in an incubator with 5% CO₂ at a temperature of 28°C. The cells were stained with 1% crystal violet in 50% methanol after 72 hours, and any leftover crystal violet solution was rinsed off the plate. After then, 1% SDS was applied to the cells to dissolve the crystal violet once again. The four subsample wells of each test concentration were averaged after the absorbance of each well was measured on a microplate reader at 595 nm.

For each test concentration, a percent negative control value was computed. In comparison to control cells that were not exposed to the test drug, this number shows how confluent the test compound-exposed cells were. The average % negative control results from the three duplicate plates for each test concentration were completed, computed, plotted, and fitted with a sigmoidal curve. The test concentrations for the array CGH analysis were computed for each chemical using the 50% and 75% confluency values of the negative control. These numbers were chosen so that, in the EMS experiment, it could be determined whether CNVs would be produced by exposure treatments that varied from 50% impacts on cell confluency to exposure treatments that did not affect cell confluency, and that in the Ara-C experiment, exposure treatments that did not impact cell confluency could be chosen[5], [6].

DISCUSSION

For the purpose of this investigation, a zebrafish-specific oligonucleotide platform was created and printed in collaboration with Roche Noblemen. The Roche Noblemen Maskless Array Synthesizer technology was used to create the zebrafish oligonucleotide platform utilizing photo mediated synthesis chemistry. A unique probe screening approach was used to choose DNA probes. Heuristic and AI prediction algorithms generated from their experimental database were combined with balanced probe selection. The genetic target was represented by the probe sets, which also had outstanding hybridization properties. Since certain copy number variations have been shown to be connected with these genomic segments, segmental duplications were considered for this design, but highly repetitive sequences were removed. Additionally, the array also included a variety of standards. With this platform, many self-to-self hybridizations were initially carried out in order to evaluate the array platform's performance and establish the platform's resolution. The array CGH analysis was carried out similarly to how Peterson and Freeman explained it.

Three chemical concentrations of EMS representing a concentration 50% of the negative control value, a concentration 75% of the negative control value, and a concentration where no cytotoxic effects were observed for a dose-response assessment and a corresponding negative control without chemical exposure were applied to zebrafish cells. Ara-C was exposed to two low cytotoxic exposure doses. Cell concentration was calculated after cells

were extracted from maintenance cultures. Each petri dish was given the proper amount of medium and chemical stock to obtain the necessary test concentrations. Each plate was originally seeded with 7.5×10^5 cells. Petri plates were set up and left in an incubator for 72 hours at 28°C and 5% CO₂. Cells were removed after 72 hours, and genomic DNA was recovered using the common phenol: chloroform isolation technique, as stated in Freeman et al. description. Using a Nanodrop ND-1000 and gel electrophoresis, genomic DNA quantity and quality were evaluated. A two-color hybridization technique was used to hybridize each treatment with the negative control, which served as the reference sample for each duplicate. The zebrafish array CGH platform was used to label and hybridize genomic DNA samples in accordance with the instructions provided in the Roche Nobleman User's Guide. One gramme of test DNA and one gramme of reference DNA were fluorescently labelled with dye-labeled 9 Mers for each array hybridization. Using a Nanodrop ND-1000 spectrophotometer, the quality and amount of DNA as well as dye incorporation were evaluated. According to the instructions in the Nobleman Array User's Guide, Cy3-labeled test DNA and Cy5-labeled reference DNA were mixed into one tube for each test concentration and then injected into a mixer linked to the array CGH chip. The Nobleman Hybridization System's Bay was used to house the chip while DNA hybridization took place there for 16 hours at 42°C. Following hybridization, the arrays were washed using the Roche Nobleman wash buffer kit's provided solutions, and the slides were then spun-dried using a microfuge slide drier.

On a Generics 4000B, hybridized arrays were scanned utilizing two-color scanning for Cy3 and Cy5 at a resolution of 5 microns. 1% of the features were saturated, and scans were calibrated for Cy3 and Cy5 signal intensities in the same range. The Nimble Scan software programmed was used to retrieve array picture data. Using spline normalization, a straightforward and reliable nonlinear approach of normalization for two-color investigations, the Cy3 and Cy5 signal intensities were normalized to one another. Nimble Scan produced files with normalized signal intensities. Each array CGH experiment was evaluated using internal control probes and the total fluctuation of signal strength. The Nexus Copy Number programmed was used to compute the DNA sequence areas that varied from the anticipated 1:1 molar ratio of the test to reference DNA, as was previously described. CNVs caused by chemical exposure are shown by the called areas. The genomic sites and the degree of gain or loss were compared between the chemical treatments and the experiments. The zebrafish reference sequence and the genomic sites of CNVs were combined for characterization. Comparing the genomic locations of CNVs in different samples, overlapping regions were found. Each chemical underwent two different trials[7], [8].

Analysis of global gene expression:

Using RNA obtained from a 2 mM EMS exposure and a control treatment, global gene expression analysis was carried out to examine the effects of CNVs brought on by chemical exposure on gene expression. The 2 mM EMS exposure was used since it had a little impact on cell confluency and a number of CNVs could be seen there. Three biological replicates were used, each of which had three distinct control samples and three distinct samples that had been given 2 mM EMS. Using the one-color hybridization technique, microarray analysis was carried out using the zebrafish 385 K expression platform in a manner identical to that disclosed in Peterson et al.'s study. In order to conduct this investigation, six distinct microarrays were hybridized. 385,000 60-mer probes on this platform are probing 37,157 targets with a maximum of 12 probes per target. After hybridization, arrays were cleaned and scanned using a Generics 4000B array scanner from Molecular Devices in Sunnyvale, California, at a resolution of 5 microns. The Nimble Scan software programmed was used to retrieve array picture data. According to manufacturer instructions, fluorescence signal intensities were normalized using quantile normalization and gene calls were obtained using

the Robust Multichip Average method. To identify particular genes changed as a result of EMS exposure, further statistical processing of the array data was carried out using Array Star and Ingenuity Pathway Analysis software. The Microarray Quality Consortium's guidelines were used to compile a reliable and repeatable list of differentially expressed genes. The list was then narrowed down to genes that were consistently expressed and significantly changed with a fold change of 2.0. Gene ontology analysis and molecular pathway analysis were carried out using the UCSC Genome Browser and Ingenuity Pathway Analysis software under the same conditions as in earlier experiments. The genomic location of genes with altered expression was compared to the genomic location of CNVs. All genes were transformed, and their human homologs were published. The initial step was to study the toxicity of EMS and Ara-C in the zebrafish cell line, and the findings were utilized to establish the exposure dosages for the array CGH analysis. For a dose-response evaluation in the array CGH study for EMS, test concentrations were determined at the 50% negative control value, the 75% negative control value, and a concentration where no effects on cell confluency were detected). Test doses for EMS were selected to be 5 mM, 2 mM, and 0.5 mM, respectively. Additionally, two doses of Ara-C) were introduced with little effects on cell confluency. After chemical exposure, CNVs

Around 385,000 probes, each between 50 and 75 nucleotides in length, are used to tile the zebrafish genome with a median spacing of 3.2 kb on the oligonucleotide array CGH platform. First, four self-to-self hybridization studies were carried out to evaluate the platform's functionality and establish its resolution. No calls longer than five consecutive probes in length were discovered to be present in these self-to-self hybridization studies, and the platform's resolution was approximated at 16 kb. Background noise is present in all oligonucleotide array-based systems to varying degrees, depending on the technology in question. As a consequence, single probe calls are often not taken seriously. We found that calls involving at least 6 consecutive probes had a high degree of confidence by analyzing a series of self to self-hybridizations and confirmatory studies for calls detected on this platform. The amount of false positive calls was greatly reduced by using these calling settings. Additionally, calls had an average segmentation mean of magnitude 0.075 or higher. After chemical exposure, CNVs 385,000 probes, each between 50 and 75 nucleotides in length, are used to tile the zebrafish genome with a median spacing of 3.2 kb on the oligonucleotide array CGH platform. First, four self-to-self hybridization studies were carried out to evaluate the platform's functionality and establish its resolution. No calls longer than five consecutive probes in length were discovered to be present in these self-to-self hybridization studies, and the platform's resolution was approximated at 16 kb. Background noise is present in all oligonucleotide array-based systems to varying degrees, depending on the technology in question. As a consequence, single probe calls are often not taken seriously. We found that calls involving at least 6 consecutive probes had a high degree of confidence by analyzing a series of self to self-hybridizations and confirmatory studies for calls detected on this platform. The amount of false positive calls was greatly reduced by using these calling settings. Additionally, calls had an average segmentation mean of at least 0.075 magnitude.

The contribution of chemical exposure to the development of CNVs is currently poorly understood. In order to research this phenomenon, we used a zebrafish array CGH platform in this work. Recently, CNV detection in the zebrafish genome was accomplished, which indicated that CNV creation is possible due to the flexibility of the zebrafish genome. In order to integrate these results into future in vivo investigations employing this model, a zebrafish cell line was originally employed in this proof-of-concept experiment to study CNV development linked to chemical exposure. EMS and Ara-C, two genotoxic substances, were examined for their capacity to produce CNVs. EMS is often used as a reference chemical in

genotoxicity experiments and is frequently utilised as a chemical mutagen in investigations using model organisms. It is known to directly create random point mutations in genetic material through direct alkylation. EMS has also been linked to other genetic changes, such as DNA strand breaks, even though alkylating chemicals are assumed to largely produce point mutations. In this experiment, a variety of EMS chemical treatments were used, ranging from those that reduced cell confluency by 50% to those that had no effect at all. However, CNVs were found in comparable genomic locations throughout the range of EMS test doses, suggesting a possible hotspot of genomic instability and a nonrandom genotoxic mechanism for this substance. An increase in the frequency of CNVs was not seen with increasing dosage. Additionally, 39% of the CNVs produced by EMS exposure corresponded with known CNVs in the AB strain of zebrafish's genome, suggesting that these locations may be more vulnerable to genomic rearrangements than other places. In order to reduce the detection of background CNVs and reinforce the conclusion that the CNVs seen in this investigation were caused by chemical exposure, each of these trials was begun from the same batch of cells with a comparable cytogenetic structure.

In order to determine if CNVs are chemical-specific and to further evaluate CNVs at doses with minimal effects on cell confluency, Ara-C was used as a comparison chemical. Ara-C is a chemotherapeutic drug that interferes with DNA synthesis, causes chromosomal abnormalities, and is often used as a reference chemical in genotoxicity studies. Though there were less CNVs formed at the higher exposure treatment in the Ara-C treatments and no overlapped CNVs were found across the two treatments, 44% of the Ara-C exposure-induced CNVs coincided with CNVs in the genome of the AB strain of zebrafish. 5 CNVs were created in comparable genomic areas in both the EMS and Ara-C treatments, showing these regions may be more sensitive to genomic modifications in a nonchemical-specific way even though a number of chemical-specific CNVs were called. In the particular genomic area, copy number increase and/or loss were consistent in two of the five regions.

These results match the distribution of CNVs throughout the genome with certain hotspots of development in research where CNVs were exposed to aphidicolin and hydroxyurea. Overall, the two Ara-C therapies showed a dosage response, but not the EMS treatments. This difference between the EMS and Ara-C experiments is thought to be the result of the effects on cell confluency between the two ranges of test concentrations. Global gene expression analysis for the 2 mM EMS treatment was carried out in order to further evaluate the impact of CNVs caused by chemical exposure. Gene expression changes were shown to be generally linked to cardiovascular illness, connective tissue condition, skeletal muscle abnormalities, and developmental disorders. Aside from that, changes were linked to genes involved in cellular organization and mobility, amino acid metabolism, small-molecule biochemistry, cellular assembly, and cellular function. Genes linked to tissue morphology, organismal survival, embryonic development, organismal development, and organ morphology had enriched expression changes as well. Furthermore, a direct comparison between the genomic locations of genes with changed expression in the 2 mM EMS treatment and genomic areas harboring CNVs shows that CNVs caused by chemical exposure affect gene expression. Both direct relationships and harmful associations were found by this investigation.

The adverse correlation might be of a regulatory nature. Genes involved in SNAP receptor activity, the start of transcription, the start of protein synthesis, acetyl-CoA transport, the synthesis of purine nucleotides from scratch, DNA binding, and signal transduction are among those with altered expression linked to CNVs. Additionally, a number of diseases are linked to specific genes, such as mutations in CAPN5 and autosomal dominant neovascular inflammatory vitreoretinopathy, deletions in STX16 and autosomal dominant pseudo hypothyroidism, decreases in EIF2S expression and uveal melanoma, and polymorphisms in

ARID5B and MLL rearrangements in early childhood leukemias. Additionally, CAPN5 is crucial for developmental processes, whereas ARID5B is necessary for adipogenesis and liver development. Furthermore, given that CNVs are said to have a broad impact on the transcriptome, it is possible that they are also connected to changed gene expression in other genes. It should be noted that single nucleotide alterations may occur as a consequence of exposure to genotoxic substances. The data suggests that CNVs produced by chemical treatments are likely to contribute to changes in gene expression and supports further research into the functional effects of the CNVs produced by chemical exposures. As a result, some of the detected changes in gene expression may be caused by single nucleotide mutations and/or other DNA alterations[9], [10].

CONCLUSION

According to reports, the zebrafish genome underwent two cycles of whole genome duplication during the history of evolution, with a third event taking place just before the final teleost radiation. Comparing the zebrafish genome to the rat and human genomes did prove challenging due to the duplicated genome, but a complete reference sequence is now available. These duplication events are thought to increase the number of CNVs in the zebrafish genome and may have an impact on the occurrence of segmental duplications. As a result, the genome duplication could also have an impact on the frequency of CNVs brought on by chemical exposure. To examine and better comprehend how chemical exposure affects the development of CNVs, further research using different model systems will be required. Overall, the findings of this research suggest that chemical exposure causes CNVs that change gene expression. Future research into the precise mechanism of CNV formation and expansion to evaluate environmental chemicals, additional structural genomic changes using sequencing technologies, and incorporation of in vivo systems to examine the biological and functional significance of the CNVs and their impact on disease pathways are all being set up by this study.

REFERENCES:

- [1] A. C. Mirabella, B. M. Foster, and T. Bartke, "Chromatin deregulation in disease," *Chromosoma*. 2016. doi: 10.1007/s00412-015-0530-0.
- [2] R. Mesnage *et al.*, "Integrated transcriptomics and metabolomics reveal signatures of lipid metabolism dysregulation in HepaRG liver cells exposed to PCB 126," *Arch. Toxicol.*, 2018, doi: 10.1007/s00204-018-2235-7.
- [3] V. Bollati and A. Baccarelli, "Environmental epigenetics," *Heredity*. 2010. doi: 10.1038/hdy.2010.2.
- [4] Y. Liu, Y. Zhang, S. Tao, Y. Guan, T. Zhang, and Z. Wang, "Global DNA methylation in gonads of adult zebrafish *Danio rerio* under bisphenol A exposure," *Ecotoxicol. Environ. Saf.*, 2016, doi: 10.1016/j.ecoenv.2016.04.012.
- [5] D. M. Walker, B. A. Kermath, M. J. Woller, and A. C. Gore, "Disruption of reproductive aging in female and male rats by gestational exposure to estrogenic endocrine disruptors," *Endocrinology*, 2013, doi: 10.1210/en.2012-2123.
- [6] M. Velki, H. Meyer-Alert, T. B. Seiler, and H. Hollert, "Enzymatic activity and gene expression changes in zebrafish embryos and larvae exposed to pesticides diazinon and diuron," *Aquat. Toxicol.*, 2017, doi: 10.1016/j.aquatox.2017.10.019.
- [7] J. Jacob *et al.*, "Valproic acid silencing of *ascl1b/Ascl1* results in the failure of serotonergic differentiation in a zebrafish model of fetal valproate syndrome," *DMM Dis. Model. Mech.*, 2014, doi: 10.1242/dmm.013219.

- [8] R. Mandarapu and B. M. Prakhya, "Exposure to cypermethrin and mancozeb alters the expression profile of THBS1, SPP1, FEZ1 and GPNMB in human peripheral blood mononuclear cells," *J. Immunotoxicol.*, 2016, doi: 10.3109/1547691X.2015.1130088.
- [9] M. S. Forrest *et al.*, "Discovery of novel biomarkers by microarray analysis of peripheral blood mononuclear cell gene expression in benzene-exposed workers," *Environ. Health Perspect.*, 2005, doi: 10.1289/ehp.7635.
- [10] M. J. Leaver *et al.*, "Hepatic gene expression in flounder chronically exposed to multiply polluted estuarine sediment: Absence of classical exposure 'biomarker' signals and induction of inflammatory, innate immune and apoptotic pathways," *Aquat. Toxicol.*, 2010, doi: 10.1016/j.aquatox.2009.10.025.

CHAPTER 3

FUNCTIONAL EXPRESSION OF CRYPTOSPORIDIUM PARVUM DNA-TOPOISOMERASE IB

Somayya Madakam, Associate Professor
Department of uGDX, ATLAS SkillTech University, Mumbai, Maharashtra, India
Email Id- somayya.madakam@atlasuniversity.edu.in

ABSTRACT:

One of the most significant organisms responsible for human diarrhea in children, *Cryptosporidium parvum*, has a monomeric DNA-topoisomerase IB gene on chromosome 7. The cryptosporidium enzyme is shown to be active in vivo by heterologous expression of the CpTopIB gene in a budding yeast strain missing this activity. A single polypeptide with all the structural elements characterizing a fully active TopIB has the enzymatic activity. Only when CpTopIB ORF was produced in a yeast expression system displaying time and protein dependency under steady state kinetic conditions was relaxation activity of the yeast extracts identified. The irreversible inhibitor calprotectin and its water-soluble derivatives were tested for their ability to inhibit CpTopIB-transformed yeast.

KEYWORDS:

Cryptosporidium, Chromosome, Enzyme, Human Diarrhea.

INTRODUCTION

One of the most significant causes of human diarrhea in children is *Cryptosporidium parvum*. Infections are spread by consumption of polluted, low-quality source water, specifically oocysts. In humans, immunocompetent people with the virus self-limit, whereas HIV-immunocompromised patients may have catastrophic outcomes. The illness is especially severe in newborn lambs of ruminants, who exhibit lethargy, anorexia, stomach pains, diarrhea, and a significant oocyst elimination in faces. The high incidence of this illness may be brought on by the oocysts' resilience to chemical water treatments, the ineffectiveness of the present medications, or the absence of a reliable vaccination. As a result, using disinfectants, host immune-reinforcing agents, and novel medications together is crucial in the therapy of this illness. During a hundred antibiotics and antiparasitic medications have been tried against *C. parvum* infections during the last ten years with little to no success.

Poorly absorbed aminoglycoside antibiotic paromomycin and, more recently, nitazoxanide were suggested as viable treatments for cryptosporidium infections in AIDS patients. Both drugs were effective in animal models, and newborn calves, lambs, and goats were given paromomycin as a preventative measure. Nitazoxanide, a Nita oxazole benzamide molecule, on the other hand, exhibits a broad spectrum of antibacterial action against helminthic parasites. More startling is the substantial decline in opportunistic infections caused by *Cryptosporidium* spp. in AIDS patients receiving highly active antiretroviral treatment. Novel chemicals that eliminate these diseases while having little to no negative effects on the host are thus urgently needed. The potential pharmaceutical targets of DNA-modifying enzymes in proliferative processes, such as microbial and parasite infections and tumor processes, have long been explored [1], [2]. The topological state of duplex DNA is altered throughout the processes of replication, transcription, recombination, and DNA repair by DNA topoisomerases, which are enzymes. These enzymes fall into two families and a number of subfamilies: The ATP-independent enzymes known as type I DNA topoisomerases have relaxing activity for both positively and negatively supercoiled DNA.

Multimeric proteins known as type II DNA topoisomerases hydrolyze ATP to create transient DNA double-strand breaks that are then passed through and rejoined. Topi enzymes can knot, unknot, and catenate or decatenate tightly coiled DNA in addition to relaxing positively supercoiled DNA. Numerous substances have been tested against Top enzymes, and some of them are now in use. Some fluoroquinolones are effective antibiotics of choice and have been evaluated effectively as DNA gyrase inhibitors in bacteria.

However, TopIB is being specifically targeted for the therapy of a number of tumor processes. Topotecan and the prodrug irinotecan, water-soluble derivatives of calprotectin, are now prescribed for the treatment of various malignancies, although research on topoisomerases in protozoan parasites is far less common. Though there is little known about Top in apicomplexans, the astounding discovery of a bi-subunit TopIB in Kinetoplasts has opened a new arena in the treatment of these parasites. Only PfTopIB has been functionally expressed, targeted with CPT derivatives, and been cloned. A type II DNA topoisomerase from *C. parvum* was cloned in an early paper that was published years ago, but no further information on these enzymes has since been released. We discuss the functional expression of the CpTopIB gene from the apicomplexan protozoan *C. parvum* in this study, as well as heterologous production, kinetic investigation of the recombinant enzyme, and inhibition by CPT and analogues. Roche and Amersham Biosciences provided the restriction and DNA modification enzymes. Strata gene produced the Pyro coccus furious polymerase. From Sigma, cell culture medium and reagents were bought. Sigma Genesys provided the primers for the PCR amplification. Toris provided the CPT and SN-38, while R&S Pharma hem provided the topotecan[3], [4].

DISCUSSION

CpTopIB was in accordance with. In a nutshell, overexpressing yeast extracts were placed onto a phosphoacylases column that had already been adjusted in accordance with manufacturer recommendations. The recombinant proteins were eluted at 4 using a discontinuous gradient of KCl in TEEG buffer, augmented with 0.1 mg/mL sodium basophile, 0.8 mg/mL NaF, and purified a cocktail of protease inhibitors. To load the active fractions onto a phenyl-Sepharose column preequilibrated with TEEG containing 1 M NH₂SO₄, the active fractions were combined with an equivalent volume of 2 M NH₂SO₄. A discontinuous inverse gradient of NH₂SO₄ was used to elute the column. The Microcin YM-30 was used to concentrate the eluate from the phenyl-Sepharose column to the proper concentration for the various in vitro experiments. By using SDS-PAGE, the samples' purity was evaluated. To retain the activity and keep in a freezer, 40% glycerol was added to the storage solution. Colorimetric analysis was used to assess protein concentration. Topoisomerase IB from *Cryptosporidium parvum*. Captopril's active form is produced via the expression of a single 1923 bp ORF. With 641 amino acids and a predicted molecular mass of 74.7 Kad, the expressed polypeptide that corresponds to the putative CpTopIB has a pin of 8.7 and shows 60% identity to human DNA topoisomerase IB, 75% identity to baker yeasts, and 99.8% identity with *C*. Although the protein is much shorter than those of humans and baker yeast, it nonetheless has every recognizable domain seen in a standard TopIB protein. The PCR-amplified band was cloned into the yeast expression vector Yapp-GAL controlled by GAL1 promoter and expressed in a TopIB-lacking yeast system to produce a recombinant active enzyme.

A sequence alignment of CpTopIB with its homologous from human, *P. falciparum*, and the budding yeast *Saccharomyces cerevisiae* showing that, as expected, CpTopIB contains a putative no conserved N-terminal domain, a conserved core domain, and the C-terminal domain, which shows high homology with other eukaryotic C-terminal ends. This region has

the signature, which is phylogenetically conserved. Tyr-600 is involved in DNA cleavage in this area. A coiled-coil putative linker, which is poorly conserved, connects the C-terminal domain to the core. are all amino acids that make up the so-called catalytic tetrad involved in the relaxing activity and are found in the putative cryptosporidium core domain. Significant relaxing activity was found when the CpTopIB gene was produced in the topic-defective EKY3 yeast strain using the Yapp-GAL vector. As previously mentioned, yeast extracts were combined and purified. Kinetic characterization was performed using purified CpTopIB. A distributive relaxation activity with several relaxed topological isomers was attained as early as 5 seconds after using 2 units of pure CpTopIB and 0.3 g of supercoiled DNA substrate, and the whole process took 1 minute. Starting with 0.2 g of protein in the left lane, two-fold serially diluted CpTopIB-transformed EKY3 yeast extracts were tested for relaxing activity. beyond six 2-fold dilutions, significant activity was discovered, but no obvious topoisomerase could be isolated beyond that.

By analyzing the relaxation activity of the altered proteins, site-directed mutagenesis was used to investigate the function of the amino acids in the catalytic tetrad. Based on these similarities, we made the mutations R318A, K358A, R416A, and H489A, which eliminate the electrostatic contributions to substrate catalysis and hydrogen bonding by replacing the core domain residues with the neutral amino acid alanine, which is not proton able at physiological pH. On the other hand, Phe was substituted for Tyr-600, which is located at the C-terminal end and corresponds with a homologous Tyr at position 723 in the human enzyme. Phe is sterically homologous but is unable to break DNA. The pesky vector was used to produce each of these mutations, which were then transferred to the yeast Yapp-GAL plasmid and heterologous expressed in the TopIB-deficient yeast system. The residual relaxing activity of these mutants is contrasted with that of the recombinant wild-type enzyme. According to expectations, none of the active site mutations produced under conventional test conditions utilizing undiluted extracts had any appreciable capacity to relax supercoiled DNA[5], [6].

Sensitization of Topoisomerase-Deficit Yeast to CPT:

In terms of response mechanism and drug sensitivity, CpTopIB is preserved. When cultures were driven with 2% galactose, the heterologous expression of the wild-type dimeric enzyme into a topoisomerase-deficient yeast strain and defective in double-strand breaks repair was able to give sensitivity to 30 M CPT. The pharmaceutical eradication of cryptosporidiosis is not possible. It is generally known that the immune system must be weakened for this illness to be lethal. With very little or no success, a number of antibiotics and antiprotozoal drugs have been used in clinical or experimental settings. However, certain medications might be reviewed along with some fresh ideas for developing new treatments to combat cryptosporidiosis. A growing body of research shows that UV-exposed *Cryptosporidium* oocysts are unable to restore their prior level of infectiousness. The damage to DNA produced by mutations or the lack of repair genes was not sufficiently repaired by the nucleotide excision repair process, according to an explanation provided by Rochelle and colleagues[7], [8]. Numerous Top inhibitors damage DNA, producing stable single strand breaks and double strand breaks.

Top enzymes are attractive targets for chemotherapeutic intervention against cryptosporidium infections because to this special characteristic and the fact that these substances are utilised successfully as antineoplastic drugs. Using genomic DNA from *C. parvum* as a template, we were able to clone and functionally express the expected CpTopIB gene. Similar to trypanosomiasis, efforts to produce this ORF in a common bacterial expression system failed, necessitating the use of a top-deficient yeast strain. Under galactose pressure, heterologous

expression of the CpTopIB-transformed *S. cerevisiae* strain resulted in a single, distinct band of 76 KDa, which is commensurate with the predicted molecular weight of the putative ORF. By using a traditional low-pressure liquid chromatography technique, yeast extracts were purified and obtained from a highly enriched solution of CpTopIB, which was then utilised to relax supercoiled DNA. CpTopIB is a single polypeptide that distributes the structural and functional characteristics of all TopIB enzymes to relax supercoiled DNA. The irinotecan metabolite SN38, which interestingly was unable to break DNA at the utilised doses, did not target the enzyme. Instead, it was targeted by CPT and the water-soluble derivative topotecan, both of which formed irreversible linkages with DNA. Both the point replacement of the cleaving Tyr-600 by Phe and site-directed mutagenesis of the amino acids making up the catalytic tetrad in the putative core domain produced no enzymatic activity at all. The presence of a conserved active core that matched that of the human enzyme well was corroborated by all of these findings. At the moment, just one TopIB apicomplexan has been examined. From infected erythrocytes, Riou and colleagues isolated and characterized PfTopIB. The plasmodial enzyme, like *C. parvum*, is a monomeric protein of 104 KDa that corresponds to a peptide of 839 amino acids. Its gene is found on chromosome 5 of the plasmodial genome and is developmentally controlled throughout the several phases of the Plasmodium life cycle. Additionally, CPT, which incites cleavable complexes with DNA *in vitro*, successfully targets the enzyme [9], [10].

CONCLUSION

Consequently, *C. parvum* is becoming more resistant to a wide variety of chemotherapeutic drugs, some of which are effective against other apicomplexan parasites. The intracellular phases of the life cycle, which are essentially enveloped within the host cytoplasm, may be responsible for this.

Novel targets for drug screening are therefore urgently needed. The aforementioned findings demonstrate that the TopIB enzyme, which is presumed to be involved in resolving DNA structural issues throughout the replication, transcription, and repair processes, is present and active in *C. parvum*. Unlike other protozoa, the enzyme is made up of a singular protein that is encoded by a single gene and that has all the structural characteristics of a fully functional TopIB. Understanding the unique molecular properties of CpTopIB and how the enzyme's expression is controlled during the parasite life cycle may be helpful for the creation of new, selective CpTopIB inhibitors that have the potential to be effective anticryptosporidial medicines.

REFERENCES:

- [1] R. Balaña-Fouce, C. Ordóñez, J. Alfonso, and D. Ordóñez, "Functional expression of a DNA-topoisomerase IB from cryptosporidium parvum," *J. Biomed. Biotechnol.*, 2009, doi: 10.1155/2009/837608.
- [2] X. Zhang, C. Y. Kim, T. Worthen, and W. H. Witola, "Morpholino-mediated *in vivo* silencing of *Cryptosporidium parvum* lactate dehydrogenase decreases oocyst shedding and infectivity," *Int. J. Parasitol.*, 2018, doi: 10.1016/j.ijpara.2018.01.005.
- [3] R. Zhou, G. Hu, J. Liu, A. Y. Gong, K. M. Drescher, and X. M. Chen, "NF-kappaB p65-dependent transactivation of miRNA genes following *Cryptosporidium parvum* infection stimulates epithelial cell immune responses," *PLoS Pathog.*, 2009, doi: 10.1371/journal.ppat.1000681.
- [4] R. Zhou, A. Y. Gong, A. N. Eischeid, and X. M. Chen, "MiR-27b targets KSRP to coordinate TLR4-mediated epithelial defense against *Cryptosporidium parvum* infection," *PLoS Pathog.*, 2012, doi: 10.1371/journal.ppat.1002702.

- [5] M. E. Mirhashemi, F. Noubary, S. Chapman-Bonofiglio, S. Tzipori, G. S. Huggins, and G. Widmer, "Transcriptome analysis of pig intestinal cell monolayers infected with *Cryptosporidium parvum* asexual stages," *Parasites and Vectors*, 2018, doi: 10.1186/s13071-018-2754-3.
- [6] C. Lippuner *et al.*, "RNA-Seq analysis during the life cycle of *Cryptosporidium parvum* reveals significant differential gene expression between proliferating stages in the intestine and infectious sporozoites," *Int. J. Parasitol.*, 2018, doi: 10.1016/j.ijpara.2017.10.007.
- [7] A. P. Rooney, "Mechanisms underlying the evolution and maintenance of functionally heterogeneous 18S rRNA genes in apicomplexans," *Mol. Biol. Evol.*, 2004, doi: 10.1093/molbev/msh178.
- [8] G. Zhu, Y. Li, X. Cai, J. J. Millership, M. J. Marchewka, and J. S. Keithly, "Expression and functional characterization of a giant Type I fatty acid synthase (CpFAS1) gene from *Cryptosporidium parvum*," *Mol. Biochem. Parasitol.*, 2004, doi: 10.1016/j.molbiopara.2003.11.011.
- [9] J. J. Millership and G. Zhu, "Heterogeneous expression and functional analysis of two distinct replication protein A large subunits from *Cryptosporidium parvum*," *Int. J. Parasitol.*, 2002, doi: 10.1016/S0020-7519(02)00135-2.
- [10] N. N. Umejiego, C. Li, T. Riera, L. Hedstrom, and B. Striepen, "Cryptosporidium parvum IMP dehydrogenase: Identification of functional, structural, and dynamic properties that can be exploited for drug design," *J. Biol. Chem.*, 2004, doi: 10.1074/jbc.M407121200.

CHAPTER 4

DNA METHYLATION CONTROLS GENOME-WIDE MICRORNA EXPRESSION IN HEPATOCARCINOGENESIS

Suresh Kawitkar, Professor

Department of ISME, ATLAS SkillTech University, Mumbai, Maharashtra, India

Email Id-suresh.kawitkar@atlasuniversity.edu.in

ABSTRACT:

It is unclear from previous research, including our own, whether the control of microRNAs by DNA methylation happens across the whole genome in hepatocellular carcinoma. Subjects/Methods. To investigate the possible involvement of methylation changes in the control of miRNAs, we carried out genome-wide screening for DNA methylation and miRNA expression using a two-phase experimental design. Results. We discovered that the expression of 25 miRNAs accurately distinguished the HCC tumor from non-tumor and was statistically substantially different between tumor and non-tumor tissues. In tumors, 19 miRNAs were repressed whereas six were overexpressed. Eight miRNAs of the 133 miRNAs with inverse relationships between methylation and expression showed statistically significant expression variations between tumor and nontumor tissues. A total of 56 additional paired HCC tissues were used to verify six miRNAs. MiR-125b and miR-199a showed substantial negative correlations, which is in line with the inactive chromatin pattern seen in HepG2 cells. Conclusion. These findings demonstrate that DNA hypermethylation, a critical factor in the development of hepatocarcinogenesis, substantially controls the expression of miR-125b and miR-199a.

KEYWORDS:

Genome, Hepatocarcinogenesis, Methylation, Methylation.

INTRODUCTION

MicroRNAs are a group of naturally occurring, small, single-stranded RNAs that play a role in the regulation of gene expression and are involved in a number of physiological processes, including cell division, proliferation, and death. A tumor suppressive function for miRNAs in hepatocarcinogenesis has been suggested by recent studies that reveal the expression levels of miRNAs are largely downregulated in hepatocellular carcinoma tumor tissues when compared with neighboring nontumor/cirrhotic or normal liver tissues. In animal models and cancer cell lines, aberrant miRNA expression has repeatedly been linked to altered DNA methylation in the miRNA host genes, suggesting possible epigenetic pathways for their control. Our study and others before it looked at whether changes in DNA methylation may control the abnormal production of miRNAs in human HCC. There are a few host genes for miRNAs that are consistently hypermethylated in HCC tumor tissue, including miR-1-1, miR-10a, miR-122, miR-124, miR-129-2, miR-137, miR-203, miR-335, miR-503, miR-517a, miR-517c, and miR-520e. Many tumor-suppressing miRNAs, including as miR-22, miR-122, miR-125b, miR-152, miR-194, miR-199, and miR-215, are selectively expressed in liver tissues; however, the relationships between their expression and methylation status remain unexplained. As a result, it is mainly unclear whether this epigenetic process often takes place at a genome-wide level in the development of hepatocarcinogenesis, which limits the interpretation of dysregulated miRNAs and their potential use as diagnostic or therapeutic targets[1], [2].

We used a two-phase research design to analyse DNA methylation and miRNA expression patterns in a cross-sectional analysis of HCC tumors and surrounding nontumor tissues. We aimed to discover the most frequent alterations in miRNA expression in tumor tissue that are controlled by aberrant DNA methylation, which may have clinical importance, by thoroughly investigating the relationships between DNA methylation and miRNA expression patterns at a genomic level.

Study Participants and Biospecimens:

The Columbia University Medical Center's Institutional Review Board gave their approval to this investigation. The Centre for Liver Disease and Transplantation gathered 132 frozen HCC samples from 66 individuals and kept them in the Molecular Pathology Shared Resource of the Herbert Irving Comprehensive Cancer Centre. The existence, viability, and percent of the liver tumor were evaluated histologically in 4-micron thick slices of frozen liver tumor and surrounding nontumor tissues kept at 20°C. To guarantee that the tumor samples were >80% pure, they were macro dissected. Tissue slices were cut from frozen tissues and H.E. stained to ensure that the DNA/RNA retrieved from nearby normal tissue did not include tumor cells. The study pathologist examined the stained sections to make sure no tumor tissues or cells were present. The criteria of the American Joint Committee on Cancer were used to assess the tumor stage.

The same tissues were then divided into several pieces for DNA/RNA extraction. Additionally, it was determined if adjacent tissues had cirrhosis or not. Medical records were used to gather data on clinicopathological characteristics such as α -fetoprotein levels, tumor size and number, tumor grade, presence of vascular invasion, and capsular infiltration. Medical records were used to assess the immunoassay-based HBV and HCV status. The discovery set for analyzing miRNA expression patterns consisted of ten matched HCC tumor/adjacent nontumor tissues. To evaluate potential miRNAs, the remaining 56 pairings were utilised as a validation set. RNeasy Microarray Tissue Mini Kits were used to collect total RNA, including miRNAs, from 66 frozen HCC tumor and 66 surrounding nontumor tissues in accordance with the manufacturer's instructions. Genome-wide miRNA profiles for the discovery set were created using TaqMan Low Density Arrays, which covered 733 miRNAs. The data were then deposited in NCBI's Gene Expression Omnibus database under the accession number GSE54751. Six potential miRNAs were measured for expression using TaqMan MicroRNA assays in both the validation and discovery sets. The method was utilised to normalize the relative expression of target miRNAs by comparing it to the endogenous control U6 snRNA stable by liver tumor/adjacent tissue status [3], [4].

DNA was isolated using the usual proteinase K/RNase treatment, phenol/chloroform extraction, and the tumor and nearby nontumor tissues. Using an EZ DNA Methylation Kit, 1 g of DNA was bisulfite modified in accordance with the manufacturer's instructions. The Illumina standard methodology was used to carry out the Infinium Methylation 450 K experiment, as was previously published. These data were utilised for further investigation. The 450 K array has 3,439 CpG sites encompassing 727 human miRNAs. Beta-values intensity of the methylated allele were used to determine the methylation levels of CpG sites. Methylation measurements with a detection value > 0.05 and samples with a CpG coverage 95% were eliminated for quality control. The comprehensive methylation profiles are accessible through series accession number GSE54503 in the GEO database of the NCBI. Integrative analyses using OncoPrint Data and the Encyclopedia of DNA Elements.

In order to examine the collaborative role of histone modifications and deoxyribonuclease hypersensitivity in chromatin activity, DNA methylation data from miRNA host genes were combined with ENCODE data for the human hepatoblastoma cell line and the seven other

cancer cell lines. Previous results suggest that H3K4me1 is associated with active chromatin outside of promoters H3K4me3 is primarily associated with active promoters; H3K27ac is associated with both active promoters and enhancers and DNase I hypersensitive sites are associated with active histone marks and transcription factor binding. The Stanford Microarray Database and the Oncoming database were used to analyse the expression of miRNA host or target gene mRNAs in HCC tumor and/or precursor/normal liver tissues. The standard deviation was normalized to one per array, and the gene expression data were log₂ transformed and median-centered.

DISCUSSION

In order to detect aberrant miRNA expression, we examined genome-wide miRNA profiles in HCC tissues using the univariate test and Benjamini-Hochberg false discovery rate correction using Lima. Distances between miRNA expression levels in various tissues were calculated using the uncentered Pearson correlation coefficient. Based on significant miRNAs, the average linkage hierarchical clustering was carried out using Cluster 3.0 and visualized with Java Tree view. To assess the connections between changes in DNA methylation and miRNA expression, Spearman correlation coefficients were performed. The CpG sites of miRNA host genes that are differently methylated between tumor and nearby nontumor tissues were found using paired tests with Bonferroni adjustment for multiple testing. A CpG site with a Bonferroni-corrected value 0.05, or a raw value of 1.45×10^5 , was considered to have a significant difference. The Statistical Analysis System 9.0 and the R programming language were used for all statistical studies. HCC Patient Clinical and Pathological Characteristics

In the Supplementary Material, which is published comparisons of the clinical and pathological features for HCC patients in the discovery and validation sets are shown. The proportions of each ethnic group, HBV/HCV positive individuals, cigarette smokers, and alcohol consumers were comparable, as were the mean ages. The discovery set's gender distribution was different from the validation set's, with fewer female HCC cases, since we chose five male and five female patients to assess miRNA differences by gender. In the validation set, there were more transplant recipients than there were liver resection patients. Other clinical characteristics in the discovery and validation sets, such as AFP levels, tumor size, grade, cirrhosis, and survival result, showed no statistically significant variations, demonstrating the comparability of the two sets overall. Using the FDR to account for multiple comparisons, we discovered 25 miRNAs were substantially dysregulated in HCC tumor tissues, with 6 miRNAs upregulated and 19 miRNAs downregulated. The overexpressed miRNAs had fold alterations ranging from 2.6-fold for miR-18a to 18-fold for miR-196b. For downregulated miRNAs, the fold changes varied from 2.5-fold for miR-99a to 7.5-fold for miR-144#. The abnormal expression of a few miRNAs in HCC tumor tissues was originally discovered. The cluster diagram and heatmap containing the 25 substantially aberrant miRNAs provide a complete separation of the HCC tumors from nontumor tissues, indicating their potential clinical use as HCC diagnostic biomarkers[5], [6].

Changes in DNA Methylation in HCC Tumor Tissue In the discovery set, we examined the DNA methylation patterns of 3,439 miRNA-relevant CpG sites in 10 pairings of HCC tumor and nontumor tissues. 28 miRNA CpG sites had substantially different DNA methylation between tumor and surrounding nontumor tissues after Bonferroni correction. Demethylation was often the most common DNA methylation alteration in HCC tumors. Without error, the 28 significant CpG sites separated tumor from non-tumor tissue. In 56 additional pairings of tumor and nontumor tissues, we verified DNA methylation for those CpG sites and found 100% consistent findings. We also looked at the relationships between the expression of the 222 important miRNAs detected in at least 80% of samples and the DNA methylation of

1,515 CpG sites, which was covered by TLDA and 450 K arrays. For 133 miRNAs, including 55 upregulated and 78 downregulated miRNAs, there was an inverse relationship between DNA methylation and miRNA expression. Eight miRNAs were significantly expressed differently in tumor and nontumor tissues in the discovery set, out of the 133 miRNAs that displayed inverse correlation patterns between methylation and miRNA expression.

Four miRNAs showed statistically significant Spearman rank correlations between methylation and expression. At a raw value of 0.05, only the variations in DNA methylation levels between mir-125b-1 and mir-199a-1 were significant; none remained so when multiple comparisons were taken into account. Using inverse methylation/expression correlations, we verified the expression levels of 6 miRNAs. All 6 miRNAs were consistently over- or under-expressed in tumor tissues in both the discovery and validation sets. While miR-18a-5p, miR-182, and miR-1180 were consistently overexpressed in tumor tissues, miR-10a-5p, miR-125b-5p, and miR-199a-3p were consistently suppressed. Five miRNAs that were abnormally expressed in HCC tumor tissues in the validation set showed statistically significant differences. From 2.58-fold for miR-199a-3p to 2.45-fold for miR-182, the fold changes ranged. When the validation and discovery sets were combined, the expression of miR-18a-5p across tumor and nontumor tissues became significantly different.

For mir-18a, mir-125b-1, mir-182, mir-199a-1, and mir-1180, inverse Spearman rank correlations between methylation and expression were found; mir-125b-1 and mir-199a-1 reached statistical significance. From 0.23 to 0.63, the correlation coefficients were found. For miR-125b or miR-199a, 84% of individuals showed inverse methylation and expression patterns. These findings confirmed the discovery set's findings that DNA hypermethylation may have regulatory effects on the expression of miR-125b and miR-199a. For HBV negative or positive tissues, miR-125b expression levels were respectively 1.15 and 1.45 and 1.19 and 1.09 for HCV negative or positive tissues. According to data not provided, the expression levels of miR-199a were 1.98 and 2.51 for HBV negative or positive tissues and 2.41 and 1.58 for HCV negative or positive tissues, respectively.

In order to evaluate the collaborative function of histone alterations and DNase I hypersensitivity in chromatin activity, we combined ENCODE data with DNA hypermethylation findings for the markers mir-125b-1 and mir-199a-1 in HepG2 and seven additional cancer cell lines. In HepG2 cells, no active histone marks or DNase I hypersensitive sites were seen near to the hypermethylated CpG sites of mir-125b-1. In the same area, higher concentrations of H3K4me1, H3K4me3, and H3K27ac were discovered in the seven additional cancer cell lines. In HepG2 cells, the hypermethylated region of mir-199a-1 was not accompanied by any active histone marks, active regulatory areas, or both). The seven additional cancer cell lines included high to moderate amounts of H3K4me1, H3K4me3, and H3K27ac, indicating active chromatin. These findings point to a possible synergistic function for DNA hypermethylation and histone alterations, particularly in the HepG2 cell line, in the suppression of mir-125b-1 and mir-199a-1.

On chromosome 19p13.2, intron 16 of the host gene DNM2 is where mir-199a-1 is found. Integrating our findings with the Oncoming data, we discovered that miR-199a was suppressed or expressed with DNM2 mRNA; consequently, a significant under expression of DNM2 was found in HCC tumor tissue, compared to precursor, and normal liver tissues. This finding is consistent with the under expression of miR-199a in HCC tumor tissue. As opposed to precursor and normal liver tissues, HCC tumor tissues had considerably higher amounts of mRNA for the target genes of miRNAs, and these levels were negatively correlated with the expression of tumor suppressive miRNAs. For miR-125b, overexpression of the target genes in HCC tumor tissues has been found for avian erythroblastic leukemias

viral oncogene homolog avian erythroblastosis virus E26 oncogene homolog myeloid cell leukemias sequence 1 , interleukin 6 receptor , and Lin-28 Homolog B . Due to a paucity of Oncoming data, it is uncertain how one target gene, Erman, is expressed. Mammalian target of rapamycin, met protooncogene, HIF-1, clathrinid heavy chain, discoidin domain receptor, and CD44 were some of the target genes for miR-199a that were examined. As compared to precursor and healthy liver tissues, HCC tumor tissues have overexpressed mTOR, Met, CHC, and DDR1. For the target genes CD44 and HIF-1, no discernible disruption was seen. Two typical target genes for miR-125b and miR-199a, which were overexpressed in HCC tumor tissues[7], [8].

Recent research, like this one, shows that miRNA dysregulation aids in the development of HCC. After accounting for false discovery rates, we discovered 25 miRNAs that were highly dysregulated in HCC tumor tissues and could accurately distinguish between tumor and nontumor tissues. For the first time, the aberrantly expressed miRNAs miR-139, miR-381, miR-486, and miR-1180 in HCC tumor tissue were discovered. 133 miRNAs demonstrated negative correlation patterns between methylation and expression by genome-wide screening for DNA methylation and miRNA expression and integrative analysis using ENCODE data. In the discovery collection, only 8 miRNAs had expression levels that substantially differed between tumor and nontumor tissues. The number of miRNAs with significant inverse methylation and expression associations was even lower: mir-125b-1, mir-144, mir-199a-1, and mir-1180. Five miRNAs that were aberrantly expressed in HCC tumor tissues showed statistically significant differences after being validated in 56 additional matched HCC tissues. Only the inverse associations between mir-125b-1 and mir-199a-1 were confirmed to be significant. According to Supplementary, the correlation coefficients varied from 0.23 to 0.63.

The decreased amounts of active histone marks and DNase I hypersensitive sites that result in closed chromatin, especially in HepG2 cells, corroborated this regulatory pattern. No cooperative histone marks were seen in seven more cancer cell lines. These findings imply that DNA hypermethylation and histone changes work together to regulate the suppression of miR-125b and miR-199a as tumor suppressors in the development of hepatocarcinogenesis. With the exception of BLID, which is 16 kb distant, there are no other coding genes close to mir-125b-1 on chromosome 11q24.1, where it is being therapeutically studied with demethylating drugs and HDAC inhibitors in HCC. According to earlier research, miR-125b expression levels were frequently downregulated in HCC tissues as well as in those of other malignancies as prostate, breast, ovarian, and thyroid anaplastic carcinomas. Importantly, miR-125b's tumor suppressive effect was suggested by the fact that ectopic expression of the gene prevented cancer cells from growing, proliferating, migrating, invading, and tumorigenesis.

The lowering of miR-125b expression in breast cancer was reported to be partly accounted for by promoter hypermethylation of mir-125b-1 in just one research toofar. In HCC, we discovered for the first time a substantial negative association between relevant miR-125b under expression and mir-125b-1 hypermethylation, which is associated with closed chromatin. By repressing target protooncogenic or oncogenes such BCL2, ERBB2/3, Erman, SIRT7, ETS1, Mcl-1, IL6R, and LIN28B, miR-125b primarily achieves its biological tasks. In accordance with the under expression of miR-125b, we discovered that the majority of target genes were highly activated in HCC tumor tissues after analyzing Oncoming data. The significant regulatory function of DNA hypermethylation in miR-125b under expression was further confirmed by this reverse correlation. Numerous cancer types exhibit various deregulations of miR-199a expression. It is markedly elevated in cervical, colorectal, gastric cancer,hepatoblastoma, but dramatically downregulated in breast,bladder,ovarian, and

testicular germ cell tumor. Additionally, in colorectal and gastric cancer, overexpression of miR-199a was thought to be a marker for a poor prognosis for the disease and to be a factor in more advanced lymphatic invasion, lymph node metastases, and late TNM stage. However, both in human HCC cell lines and tumor tissues, there has continuously been a noticeable downregulation of miR-199a. DNA hypermethylation has been observed to lower the expression of miR-199a in TGCT, and treatment with 5-azaC or silencing of DNMT1 with siRNA may increase miR-199a expression.

The genomic region of DNMT3 that encodes mir-199a-2, a different precursor of miR-199a, was the site of this methylation shift, nevertheless. Only the host gene of DNMT2 in mir-199a-1 was discovered to have DNA hypermethylation; DNMT3 was not affected. Our findings revealed that miR-199a typically expresses in concert with its host gene. DNMT3 expression was not shown to be abnormal in HCC tumor tissue. The expression of miR-199a's target genes, including as mTOR, the Met protooncogene, HIF-1, CHC, DDR1, and CD44, should, however, be negatively correlated with each other in HCC. Our comprehensive investigations confirmed the upregulation of four target genes in HCC tumor tissue, however CD44 and HIF-1 targets did not show any discernible alterations. These findings imply that the control of miR-199a and the consequent activation of downstream target genes in hepatocarcinogenesis depend on DNA hypermethylation, particularly of the precursor of mir-199a-1 but not of mir-199a-2.

For the treatment of HCC, miR-199a's target genes Met and mTOR are being inhibited. In terms of time to progression and overall survival, a subset of HCC patients with high Met expression showed the most clinically meaningful benefits of Tivantinib, an inhibitor of Met, which shows a greater response to the treatment by inhibiting the relevant pathway. These findings contribute to the mounting evidence for miR-199a's critical regulatory function in HCC. Our data in HCC may be partly explained by methylation caused by reactive oxygen species. By attracting DNA methyltransferase1 to oxidative stress-induced damaged chromatin before the DNA is repaired, ROS can increase the promoter methylation of miR-125b-1 and miR-199a-1, which causes overexpression of target genes for both miR-125b and miR-199a in vitro and in vivo.

The use of genome-wide arrays for both DNA methylation and miRNA expression profiles, which give thorough data for identification of miRNAs epigenetically controlled by DNA methylation, is one of the study's highlights. We have enough statistical power to confirm the association patterns between DNA methylation and miRNA expression thanks to the two-phase research design and high sample size. We may better understand the relationship between DNA methylation and histone modification, as well as the relationship between miRNA and mRNA expression of host and/or target genes, by doing integrated studies utilizing ENCODE and OncoPrint data. One drawback is that the two arrays cover different quantities of miRNAs. For instance, the Infinium Methylation 450 K arrays did not cover two important dysregulated miRNAs on the TLDA array. As a result, we were unable to determine how methylation affected the regulation of these two miRNAs. Second, a number of miRNAs showed positive correlations between DNA methylation and miRNA expression patterns, suggesting there may be other biological regulatory mechanisms at play that need further investigation.

Because HCC cell lines were not included in the ENCODE data, we carried out the integrative analysis using HepG2 cells generated from a human hepatoblastoma. As a consequence, we recognize that the important DNA methylation and miRNA expression patterns for the two kinds of cell lines might vary, and the findings should be evaluated with care [9], [10].

CONCLUSION

In conclusion, our findings that two miRNAs, miR-125b and miR-199a, are primarily controlled by DNA hypermethylation corroborate their tumor suppressor function in the inhibition of their downstream target oncogenes. This finding shed further light on the etiological significance of epigenetic modification in the development of hepatocarcinogenesis. In order to manage this aggressive tumor that is now rising in the US population, more research is being conducted that aim to directly restore miRNA expression and/or indirectly alter DNA methylation. The study's concept was created by Jing Shen, who also took part in data gathering, carried out data analysis and interpretation, and authored the publication. Data analysis was done by Shuang Wang, who also edited the manuscript. Data was collected by Abby B. Siegel, who also edited the manuscript. Iryna Sirosh and Qiao Wang took involved in the data collecting. Helen Remote contributed to data collecting and edited the final version of the manuscript. Regina M. Santella developed the research plan, took part in the analysis of the data, and reviewed the manuscript. The final manuscript was reviewed and approved by all authors.

REFERENCES:

- [1] M. Cowley *et al.*, “Effects of cadmium exposure on DNA methylation at imprinting control regions and genome-wide in mothers and newborn children,” *Environ. Health Perspect.*, 2018, doi: 10.1289/EHP2085.
- [2] D. M. Messerschmidt, B. B. Knowles, and D. Solter, “DNA methylation dynamics during epigenetic reprogramming in the germline and preimplantation embryos,” *Genes and Development*. 2014. doi: 10.1101/gad.234294.113.
- [3] B. Labonté *et al.*, “Genome-wide epigenetic regulation by early-life trauma,” *Arch. Gen. Psychiatry*, 2012, doi: 10.1001/archgenpsychiatry.2011.2287.
- [4] P. A. Dugué *et al.*, “Genome-wide measures of DNA methylation in peripheral blood and the risk of urothelial cell carcinoma: A prospective nested case-control study,” *Br. J. Cancer*, 2016, doi: 10.1038/bjc.2016.237.
- [5] M. D. Long, D. J. Smiraglia, and M. J. Campbell, “The genomic impact of DNA CpG methylation on gene expression; relationships in prostate cancer,” *Biomolecules*. 2017. doi: 10.3390/biom7010015.
- [6] K. J. Howell *et al.*, “DNA Methylation and Transcription Patterns in Intestinal Epithelial Cells From Pediatric Patients With Inflammatory Bowel Diseases Differentiate Disease Subtypes and Associate With Outcome,” *Gastroenterology*, 2018, doi: 10.1053/j.gastro.2017.10.007.
- [7] J. M. SanMiguel and M. S. Bartolomei, “DNA methylation dynamics of genomic imprinting in mouse development†,” *Biology of Reproduction*. 2018. doi: 10.1093/biolre/i0y036.
- [8] J. Alexander *et al.*, “Offspring sex impacts DNA methylation and gene expression in placentae from women with diabetes during pregnancy,” *PLoS One*, 2018, doi: 10.1371/journal.pone.0190698.
- [9] S. A. Waters, A. Capraro, K. L. McIntyre, J. A. M. Graves, and P. D. Waters, “The methylome of vertebrate sex chromosomes,” *Genes*. 2018. doi: 10.3390/genes9050230.
- [10] L. Booij *et al.*, “DNA methylation in individuals with anorexia nervosa and in matched normal-eater controls: A genome-wide study,” *Int. J. Eat. Disord.*, 2015, doi: 10.1002/eat.22374.

CHAPTER 5

AGE-RELATED DYNAMIC ALTERATIONS IN DNA METHYLATION AND TRANSCRIPTOME EXPRESSION IN PORCINE OVARIES

Somayya Madakam, Associate Professor

Department of uGDX, ATLAS SkillTech University, Mumbai, Maharashtra, India

Email Id- somayya.madakam@atlasuniversity.edu.in

ABSTRACT:

Ageing causes the biological function of human ovaries to diminish. Pigs were employed as model animals to determine the underlying molecular alterations during ovarian ageing. High-throughput sequencing was used to evaluate the genome-wide DNA methylation and transcriptome-wide RNA expression in the ovaries of young and elderly pigs. In addition, 2,243 mRNAs, 95 microRNAs, 248 long noncoding RNAs, and 116 circular RNAs were all differently expressed throughout both developmental phases, revealing 422 distinct methylation sites between old and young pigs. These genes associated with various methylation and expression patterns were shown to be involved in the cycle of ovarian ageing by gene ontology analysis. These specifically participate in ovarian cumulus growth, cell apoptosis, death effector domain binding, embryonic development, reproduction, and the fertilization process. In the ovarian ageing cycle, competitive endogenous RNA networks were created and multigroup cooperative control linkages were also evaluated. These findings will provide light on possible molecular alterations in DNA methylation and transcriptional patterns linked to ovarian ageing.

KEYWORDS:

Apoptosis, Biological Function, Multigroup Cooperative, Transcriptome.

INTRODUCTION

In addition, oocyte quantity and oocyte quality are directly tied to the decline in follicular reserve in the ovary, which is one of the primary concerns in women's reproductive health. Age-related acceleration of the follicular reserve decline in the ovary is nonlinear. By a mean age of 51 to 52 years, this results in near-complete exhaustion, which is referred to as menopause. Numerous variables, including genetics, have been specifically related to ovarian ageing. In conclusion, it has been emphasized that several illnesses, including premature ovarian insufficiency and polycystic ovary syndrome, have a genetic basis. Changes in DNA sequence are not a part of the idea of epigenetics, which is concerned with heritable modifications to chromatin structure and gene expression. DNA methylation, histone modification, and the production of noncoding RNA, such as microRNAs and long noncoding RNAs, are the recognized groups of epigenetic modification. Furthermore, a network is really being formed by these three epigenetic pathways. A recent area called "ovarian epigenetics" has produced several intriguing discoveries. Recent studies have shown that DNA methylation is crucial in the control of ovarian cancer and conditions like PCOS and POI.

In addition, a number of noncoding RNAs, including miRNAs and lncRNAs, are essential for controlling ovarian physiology. These findings, however, largely clarify the role of epigenetics in phenotypes related to ovarian health [1], [2]. Due to the timing of menarche and menopause, epigenetic processes in the context of ovarian ageing have been explored much less. Importantly, the epigenetic changes that occur as ovaries age naturally provide an excellent chance to comprehend the phenotypes of ovaries that are associated with health.

The rationale is that these investigations provide light on the intricate networks of interactions between various ovarian characteristics as well as the processes behind ovarian ageing. Investigating the female ovarian processes is challenging and unethical. Despite the fact that laboratory rodents like mice are good study subjects for biomedical research, their small size and brief ovarian cycles make them less helpful for studying ovarian alterations in mammals. It has been shown that large animal models including equines, cattle, and ovine are beneficial and effective for research on female ovarian function.

Due to their similar cycle length, luteinizing hormone receptor location and function, length of ovulation, and LH surge, as well as their anatomical, physiological, and biochemical similarities to humans, pigs can be a useful model to study human ovarian ageing or disease. In fact, a lot of studies have determined that the pig is the perfect model system to study the effects of metabolic syndrome and obesity on the operation and steroidogenesis of the ovaries. Between the two life stages when a woman's reproductive system opens and closes, there occurs what is known as female natural ovarian ageing. Menarche and menopause occur on average about age 14 and 50, respectively. Both times are crucial for ovarian function, and a number of recent genome-wide association studies have clarified the genetic basis of features for both the timing of menarche and menopause. In line with this, the first ovulation's adolescence stage and the reproductive fatigue stage are two crucial stages in the ovarian cycle. The first ovulation stage of sow puberty and the reproductive exhaustion stage have median ages of around 180 days and eight years, respectively [3], [4].

The pig was utilized as a model animal to investigate possible molecular alterations that may take place during normal ovarian ageing. High-throughput sequencing was used to examine the transcriptome and genome of ovaries from young and elderly sows. This made it possible to identify some genes or regulatory elements that had varying levels of methylation and expression as well as several previously unidentified multigroup cooperative control networks in the ovarian ageing cycle. These findings will aid in the explanation of ovarian aging-related alterations in DNA methylation and transcriptional patterns. In this experiment, four healthy female Yanan pigs were used. In the past, the mountainous regions of western Sichuan Province gave rise to the indigenous Chinese pig breed known as the Yanan. It is in risk of becoming extinct due to its low growth performance and carcass composition. Two eight-year-old sows at the reproductive exhaustion stage and two 180-day-old young sows in the puberty stage of first ovulation were among the four pigs.

Over the previous three generations, there was no collateral or direct blood link between these pigs. Piglets were weaned at 28 +/- 1 days of age. After weaning, an initial meal was given that comprised 3.40 McCall kg 1 of metabolizable energy and 20.0% crude protein. Pigs were fed a meal containing 14.0 MJ/kg of metabolizable energy, 18% of which was crude protein, from the 61st to the 120th day. From the 121st day, they received crude protein and dietary metabolizable energy of 13.5 MJ/kg and 16%, respectively. Pigs were maintained in comparable circumstances and had unlimited access to food and water. Pigs were transported, restrained from eating or drinking for two hours, shocked electrically for 10 seconds at 90 V and 50 Hz, and then exsanguinated to lessen suffering the night before being slaughtered. The Institutional Animal Care and Use Committee at the College of Animal Science and Technology, Sichuan Agricultural University, Sichuan, China, approved all animal experiments and procedures and they were carried out in accordance with the Regulations for the Administration of Affairs Concerning Experimental Animals. This was done under the license number SKY-S20150804. The Sichuan Weimar Modern Agricultural Science and Technology Co., Ltd., Chengdu, Sichuan 611536, People's Republic of China provided all of the study animals. Each cadaver's ovarian tissues were swiftly removed, separated, and immediately frozen in liquid nitrogen.

When it came time to extract the DNA and total RNA, all of the obtained samples were kept at 80°C. Using the Zymo EZ DNA Methylation Lightning Kit, 50–100 ng of pure genomic DNA were treated with bisulfite. In a thermal cycler, Zymo Lightning Conversion Reagent was applied to 50 to 100 ng of isolated genomic DNA for 8 minutes at 98°C and then for 60 minutes at 54°C. Using the Epigenome Kit, bisulfite-treated DNA was purified using a spin column and utilised to create a sequencing library. This method produced DNA with a specific sequence tag by randomly priming bisulfite-treated single-stranded DNA with a polymerase that can read uracil nucleotides. The freshly created DNA strands' 3' ends were marked with a second distinct sequence, resulting in damaged DNA molecules having recognized sequence tags at both their 5' and 3' ends. These tags were then utilised in a polymerase chain reaction to add Illumina adapters P7 at the 5' and P5 at the 3' ends of the original DNA strand. The only DNA that was employed as a sequencing template was the complement to the original bisulfite-treated DNA, hence the final read always had the same sequence as the original bisulfite-treated strands. The Illumina HiSeq 4000 platform was then used to sequence DNA libraries including bisulfite genomes using 150PE reads [5], [6].

After quality filtering, reads were fed into the Socrata 10.2 using Bismark tools. Bismark invoked Bowtie2 after readings were mapped to a reference. The parameters were minimal alignment score function L, 0, and 0.2 and multispeed length of 20 bp with 0 mismatches. This would imply that an alignment must have a minimum alignment score of 30 for 150 bp readings before it can be considered genuine. This is about equivalent to 4 Indwells of 1-4 bp in the read or 4 mismatches. SAM tools were used to handle the bam file that came from Bowtie2 after readings were alienated. The UCSC genome browser was used to obtain information on CpG island loci, and bed tools was used to determine the CpG island methylation level of each sample. The R package DSS was used to first name differentially methylated loci with threshold 0.001 and then distinct methylation regions with delta 0.1 with threshold 0.001 in order to find differentially methylated areas between both phases. Togo enhanced the DMR target gene's function gene ontology. Last but not least, R and Python scripts were used to do further data statistics and visualizations.

DISCUSSION

Each sample's 5 g of RNA total was utilised as the starting point for RNA sample preparations. Following the manufacturer's instructions, the NE Next® Ultram Directional RNA Library Prep Kit for Illumina® was used to create sequencing libraries from the rRNA-depleted RNA, and the Agilent Bioanalyzer 2100 system was used to evaluate the quality of the libraries. Illumina HiSeq 4000 was utilised to sequence the libraries after cluster creation, and 150 bp paired-end reads were produced. Clean readings were acquired from the raw data after the adaptor, ploy-N, and bad reads were eliminated. TopHat2 was used to align these clean reads to the ensemble using the default settings. The mapped reads per sample were put together using the String Tie programmed, which was successful in at least one of the two repetitions. The acquired transcripts were blasted to Ensemble and the mapped transcripts were immediately identified as recognized lncRNA or mRNA. Transcripts per million of both lncRNAs and mRNAs per sample were determined using Salmon. The transcript's coding potential was then examined using the coding potential calculator and Pfams Scan v1.5. The transcripts without coding potential were considered a prospective group of new lncRNAs after the transcripts projected to have coding potential were eliminated.

Each sample's 5 g total RNA was utilised as the starting material for the creation of a small RNA library. Following the manufacturer's instructions, sequencing libraries were made using NE NextMultiplex Small RNA Library Prep Set. Codes were appended to attribute sequences in each sample index. The quality of the libraries was examined using the Agilent

Bioanalyzer 2100 instrument. Following the manufacturer's instructions, the clustering of index-coded samples was done using a cot Cluster Generation system using Trusses SR Cluster Kit v3-cBot-HS from Illumina. Following the creation of clusters, single-end reads at a length of 50 bp were produced as part of the library sequencing preparations on the Illumina MiSeq platform. In order to identify prospective miRNA and forecast new miRNA, miRbase 21 was utilised as a reference, and mirdeep2 was employed. The miRNA target was predicted using the Miranda and cutoffs. Then, using the normalization formula: normalized expression = mapped read count/total readings 10,000, miRNA expression was evaluated by Ptashne edgeR programmed was used to identify differentially expressed mRNAs, lncRNAs, miRNAs, and carcass. In many comparisons, differential expression was defined as a differential expression value 0.05 and a fold change >2. Togo carried out the GO enrichment. R scripts that were self-written were used to do additional data statistics and visualizations.

Bioinformatics target prediction of miRNA-mRNA, miRNA-lncRNA, and miRNA-circa was used to create the network of RNAs with MRE, which was then visualized using the graph R package. Based on Pearson's correlation of expression, the expression network of mRNA, miRNA, lncRNA, and circa was developed. For the purpose of building networks, the Pearson correlation coefficient between two RNAs of 0.85 was deemed significant. Statistical significance was defined as a value less than 0.05. Primer software V5.0 was used to create the primers for BSP. The Epithea Fast DNA Bisulfite Kit was used to treat the examined DNA in accordance with the manufacturer's instructions. The p.m.-T Fast Cloning Kit with Competent Cell was used to clone the PCR product after it had been purified using the UNIQ-10 Spin Column DNA Gel Extraction Kit for PAGE. Per gene, ten successful clones were chosen, and sequencing was done on an ABI 3730 DNA sequences. All sequences were examined using DNAMAN 7.0. Using the Prime Script RT Master Mix kit and the oligo and random 6-mer primers supplied, total RNAs were extracted from ovaries using the HI Pure Universal RNA Mini Kit. Following the manufacturer's instructions, the q-PCR was carried out on a Bio-RadCFX96 Real-Time PCR Detection system using a standard SYBR Premix Ex Taq kit. Glyceraldehyde-3-phosphate dehydrogenase, -actin, and small nuclear RNA were employed as three endogenous control genes in this test. Objective mRNA, miRNA, lncRNA, and circa expression levels were assessed using the 2Ct technique.

These primers are shown. DNA methylation profiles were established using WGBS comparing old pig ovarian tissues at reproductive exhaustion stage and young pig ovarian tissues at the puberty stage of first ovulation in order to analyse the changes in DNA epigenetic marks caused by ageing that happened throughout ovarian development. The four ovarian samples yielded around 951,440,304 clean reads, providing a 30x sequencing depth. Approximately 61-68% of reads per sample were uniquely aligned to Ensemble Muscoda 10.2 after ambiguous reads were removed from clean reads. For YP and OP, the global methylation levels were 70.8% and 72.9%, respectively[7], [8]. Most chromosomal areas in each group had methylation in both the CpG and non-CpG contexts, according to analysis of the sequence context of cytosines. CpG context areas exhibited the greatest differences in methylation across the two ovarian developmental phases. The metagene profiles of CG methylation in the whole pig genome of the ovarian tissue were examined in order to understand the preferred position of the CG methylation on and around the gene body region. Both the GBR and the surrounding intergenic regions were highly methylated; however, gene bodies had slightly higher levels of methylation than the intergenic regions next to them and their distribution was comparable to that of the human primordial germ and prenatal germline cells, as well as pig skeletal muscle cells. Correlation study between genetic traits and methylation levels was carried out to explore the dynamics of methylation on a global scale. Chromosome length was negatively correlated with methylation levels, while GC content,

gene and repeat recurrence were positively correlated which may be attributable to the increased GC content found in gene areas, also raises the possibility that methylation dynamics play a role in the control of gene transcription

Various DNA Methylation Linked to Ovarian Ageing:

variable methylation regions between OP and YP were found in order to learn more about the variable CG methylation during ovarian ageing. The outcome was the identification of 422 DMRs between the two developmental phases, of which 303 were up methylated and 119 were down methylated in OP as compared to YP. The dynamical DMR level at both ovarian developmental phases provided evidence that DNA methylation may be a significant factor in the ageing of the ovary. Furthermore, only 12 of these 422 DMRs were found at the gene promoter regions, whereas 146 of them overlapped at gene body areas. This was consistent with the CG methylation's preferred placement on the gene body regions). Additionally, earlier studies revealed that in the gene bodies of pig skeletal muscle, DMRs are more abundant than in the promoters. GO enrichment was done to define the function of the genes connected to these DMRs. According to the findings and Supplementary Database S1), hypermethylated genes connected to DMRs were engaged in a variety of biological processes, including protein binding, death effector domain binding, and cysteine-type endopeptidase activity connected to the apoptotic signaling pathway. Apoptosis signaling pathway, embryonic skeletal/brain system development, digit morphogenesis, negative regulation of immunological response, and hypomethylated genes linked with DMRs all showed substantial enrichment for these processes. For instance, the CASP8- and FADD-like apoptosis regulator gene was considerably up methylated in aged pigs. CFLAR is a crucial component of the innate immune regulatory network and a critical suppressor of steatohepatitis. But the Meckel syndrome Type 1 gene in Meckel-Gruber syndrome produces cilia abnormalities and embryonic deformities and was markedly down methylated in aged pigs.

Additionally, the WGBS data between OP and YP and the BSP findings for the two genes' methylation levels agreed. According to reports, one significant method for controlling the transcription of genes is the influence of methylation on promoter regions. The particular functions of DNA methylation in the gene body have not yet been identified. The correlation of DMR-mRNA pairings using the RNA sequence data allowed researchers to investigate how gene expression affects intergenic methylation. It was discovered that changes in the methylation levels in the gene bodies and changes in gene expression levels had a strong negative association. Previous methylation research in gene bodies reported a strongly negative connection with the levels of mRNA expression, which is consistent with present results. However, earlier researchers found either no discernible association patterns or a favorable link with gene expression levels.

RNA and small RNA libraries were created for the OP and YP samples, respectively, to examine transcriptional expression changes throughout ovarian ageing. High-throughput sequencing was then used to identify the transcriptome-wide profile. Each of the four samples produced an average of over 75 million clean reads for the RNA sequencing libraries, and more than 69% of these reads could be specifically aligned to Ensemble Muscoda 10.2. Additionally, for short RNA sequencing libraries, each of the four samples yielded around 10.89–13.50 million clean reads, and 80.77–90.5% of these reads were specifically aligned to Ensemble Muscoda 10.2. These four samples included a total of 20,357 mRNAs, or around 59.82% of all the transcripts found in pigs. Additionally, 1,196 miRNAs were found in these four samples, and 869 of these may be unique miRNAs since their sequences did not match any previously published ones. These four samples included a total of 4,879 lncRNAs and

7,600 carcass, 2,243 differentially expressed genes, including 1,660 upregulated genes and 583 downregulated genes, were discovered in both phases of ovarian development based on the selected screening criteria and Supplementary Database S3). According to GO analysis, these DEGs were primarily enriched in the extracellular space and were involved in a number of cellular processes, including the establishment of embryonic patterns, controlling cell death, responding to viruses, and reproduction and Supplementary Database S4).

For example, ISG15 inhibited interferon- γ overamplification and autoinflammation, and the greater level of ISG15 expression in elderly pigs showed that old females were more vulnerable to viral infection. Additionally, SRY-Box 9 and Forehead Box L2 engage in a war of the sexes and play a critical role in the maintenance of the ovary and the somatic sex reprogramming of mature ovaries to testing. The increased SOX9 expression level in OP suggested that older females' reproductive capacities were declining.

In all phases of ovarian development, 95 differentially expressed miRNAs were found, and 37 of these DEMs showed upregulation while 58 showed downregulation and Supplementary Database S3). Supplementary Database S4 demonstrate that GO analysis revealed that the target genes of DEMs are abundant in the G-protein coupled receptor signaling pathway, apoptotic signaling pathway, female pregnancy, fertilization process, embryonic development, and ovulation cycle. For instance, the increased miR-9 is important for determining the neural fates of ES cells during differentiation and may be useful as a diagnostic for recurrent ovarian cancer. 248 DELs, including 202 upregulated DELs and 46 downregulated DELs, were found for differentially expressed lncRNAs associated with ovarian ageing in both ages and Supplementary Database S3. According to GO analysis, these DEL target genes were considerably more enriched for regulation by the host I-kappa kinase/NF-kappa cascade, meiotic cell cycle phase involved in oocyte maturation, female pregnancy, and uterine development and Supplementary Database S4. Additionally, 116 differentially expressed carcass were found in both ages; 103 of these DECAs had upregulated carcass, while 13 of them had downregulated carcass and Supplementary Database S3. The transmembrane receptor protein serine/threonine kinase activity, in utero embryonic development, reproductive process, ovarian cumulus expansion, and ovulation cycle were all enriched in these DEC source genes and Supplementary Database S4.

The number of genes and their percentages were initially determined in each possible combination of regulation, with the goal of identifying the coordinated regulatory link between DNA methylation and various RNA species during ovarian ageing. 9,633 and 8,845 genes were methylated or concurrently expressed among DNA methylation, mRNA, and miRNA. The number of genes that were methylated or expressed concurrently reduced overall, and almost 600 genes were not methylated or expressed simultaneously in OP or YP, with the exception of each of these three combination groups. Similar to this, 1,465 and 1,354 genes were methylated or expressed concurrently among DNA methylation, lncRNA, and miRNA. The smallest number of genes were not concurrently methylated or expressed. Each chromosome also displayed the links between gene transcriptional regulation and gene posttranscriptional regulation. The findings show that several genes tended to be regulated in conjunction by DNA methylation and transcriptome expression. In OP, the pattern of used combination regulation may be more obvious. To find the overlap between DMRs and DEGs, the differentially expressed transcriptome and DMRs were also evaluated. The findings revealed that just one gene was differentially methylated in the gene promoter region during ovarian ageing, and seven DEGs were determined to be so. However, in these methylated genes in gene body areas, no discernible pattern of change in the relationship between methylation and expression levels was discovered. It's interesting to note that as the ovary aged, the gene with methylation in the promoter region was both up expressed and

hypomethylated. These findings suggest that methylation alterations happened in the gene promoter area rather than the gene body region, which may be relevant to how the expression level of a gene is regulated as we age. GO keywords of genes associated to DMRs and four distinct RNA species with differently expressed levels were overlapping to further emphasize the possible coordinated regulation functions of DNA methylation and various RNA species implicated in ovarian ageing. Numerous molecular processes and signaling pathways connected to the ovarian ageing cycle, including embryonic development, the apoptotic process, reproduction and fertilization, ovarian cumulus expansion, and female pregnancy, were discovered among DMRs and these differentially expressed RNAs [9][10].

CONCLUSION

The differentially methylated and expressed genes in the ovarian tissues of OP and YP were found using microarray analysis. The functions of differentially methylated and expressed genes, associated pathways, and reciprocal regulatory interactions between coding and noncoding genes were examined by GO enrichment studies and the development of carnal networks. The acquired data provide the groundwork for future investigations into the molecular processes behind ovarian ageing and further our knowledge of the ageing process in ovaries.

Future research will be needed to examine how diverse gene expression and DNA methylation patterns vary with ageing in various cell types. Additionally, this research had a small sample size and only chose two age groups. To better comprehend the variations in epigenetic alterations associated to age, in addition to complex processes underpinning the ageing process, further research on pigs of extra sequential ages and the use of more samples are required. Additionally, genomic/epigenomic research on pigs may be useful in identifying the underlying genetic underpinnings of the economic features of pigs in addition to offering unique data for medicinal investigations. Such information may be utilised to increase the effectiveness of artificial selection so that more piglets are produced.

REFERENCES:

- [1] K. R. Müller-Vahl, G. Loeber, A. Kotsiari, L. Müller-Engling, and H. Frieling, "Gilles de la Tourette syndrome is associated with hypermethylation of the dopamine D2 receptor gene," *J. Psychiatr. Res.*, 2017, doi: 10.1016/j.jpsychires.2016.11.004.
- [2] P. Salpea *et al.*, "Postnatal development- and age-related changes in DNA-methylation patterns in the human genome," *Nucleic Acids Res.*, 2012, doi: 10.1093/nar/gks312.
- [3] K. Day *et al.*, "Differential DNA methylation with age displays both common and dynamic features across human tissues that are influenced by CpG landscape," *Genome Biol.*, 2013, doi: 10.1186/gb-2013-14-9-r102.
- [4] C. Murgatroyd *et al.*, "Dynamic DNA methylation programs persistent adverse effects of early-life stress," *Nat. Neurosci.*, 2009, doi: 10.1038/nn.2436.
- [5] A. G. Fisher *et al.*, "Transcriptomic and epigenetic regulation of disuse atrophy and the return to activity in skeletal muscle," *FASEB J.*, 2017, doi: 10.1096/fj.201700089RR.
- [6] A. Lomniczi and S. R. Ojeda, "Neuroendocrine control of female puberty: Genetic and epigenetic regulation," in *Molecular Neuroendocrinology: From Genome to Physiology*, 2016. doi: 10.1002/9781118760369.ch18.
- [7] M. R. Damani, L. Zhao, A. M. Fontainhas, J. Amaral, R. N. Fariss, and W. T. Wong, "Age-related alterations in the dynamic behavior of microglia," *Ageing Cell*, 2011, doi: 10.1111/j.1474-9726.2010.00660.x.

- [8] J. C. Singer, W. E. McIlroy, and S. D. Prentice, “Kinetic measures of restabilisation during volitional stepping reveal age-related alterations in the control of mediolateral dynamic stability,” *J. Biomech.*, 2014, doi: 10.1016/j.jbiomech.2014.08.022.
- [9] T. Zhao *et al.*, “Age-related changes in the topological organization of the white matter structural connectome across the human lifespan,” *Hum. Brain Mapp.*, 2015, doi: 10.1002/hbm.22877.
- [10] K. L. Stauch, P. R. Purnell, and H. S. Fox, “Aging synaptic mitochondria exhibit dynamic proteomic changes while maintaining bioenergetic function,” *Aging (Albany. NY)*, 2014, doi: 10.18632/aging.100657.

CHAPTER 6

PATIENT SURVIVAL IS AFFECTED BY ABERRANT EXPRESSION OF N-METHYLPURINE-DNA GLYCOSYLASE IN MALIGNANT GLIOMAS

Rajesh Kumar Samala, Assistant Professor
Department of ISME, ATLAS SkillTech University, Mumbai, Maharashtra, India
Email Id-rajesh.samala@atlasuniversity.edu.in

ABSTRACT:

Examine the expression of N-methylpurine-DNA glycosylase gene and protein and its relationship to patient survival in glioma samples with various WHO grading. Methods. The expression of the MPG gene and protein was examined using an immunohisto chemistry test, quantitative real-time PCR, and Western blot analysis in 128 glioma and 10 non-neoplastic brain tissues. Results. In comparison to non-neoplastic brain tissues, the expression level of the MPG gene was considerably greater in glioma tissues. Additionally, immunohisto chemistry demonstrated that the MPG protein was overexpressed in glioma tissues, supporting the findings of the Western blot study. Additionally, the outcomes of real-time PCR, immunohisto chemistry, and western blot analysis show that the expression levels of the MPG gene and protein both rise from grade I to grade IV glioma. Additionally, MPG-positive patients had considerably poorer survival rates than MPG-negative patients. By using multivariate analysis, we were able to further establish that the over-expression of MPG was a significant and independent prognostic predictor in glioblastoma. Conclusions. Our findings demonstrated that the MPG gene and protein are overexpressed in human gliomas and, for the first time, revealed that MPG may be a poor independent prognostic factor for glioma patients.

KEYWORDS:

Glioblastoma, N-Methylpurine, Predictor, Prognostic Factor.

INTRODUCTION

Around 50% to 60% of all intracranial tumors in humans are gliomas. Gliomas are histologically divided into four categories, according to World Health Organization recommendations: pilocytic astrocytoma, low-grade diffuse astrocytoma, anaplastic astrocytoma, and glioblastoma multiforme. Despite significant advancements in diagnostic and treatment techniques, glioma continues to be one of the deadliest malignancies in humans. Patients with low-grade and high-grade gliomas in China had 5-year survival rates of 75.4% and 18.2%, respectively. Particularly, individuals with GBM still have a 12-month median survival time. Indeed, glioma patients continue to provide a significant challenge for neurooncologist specialists in terms of early detection and extending survival. Age, preoperative symptom duration, Karnowski performance status score, histopathological grade, tumor necrosis, surgical resection extent, postoperative radiation treatment usage, and likely adjuvant chemotherapy are some of the predictive markers for glioma patients. The heterogeneity of glioma patients prevents these clinical characteristics from fully explaining the observed difference in survival.

As a result, it is necessary to carry out more research on the molecular causes of gliomas and to find reliable prognostic markers for estimating survival. If exogenous and endogenous alkylating and oxidative DNA damage is not repaired, it may result in carcinogenesis, cell death, and ageing[1], [2]. This damage is addressed through the DNA-base excision repair

pathway. This process starts with a DNA glycosylase identifying and removing damaged bases, then an AP endonuclease cutting the resultant a basic site, DNA polymerase synthesis, and strand ligation. The BER pathway is a key possibility for intervention into the cellular reactions to DNA alteration as a result. A key element of the BER process is the DNA repair enzyme N-methylpurine-DNA glycosylase. In a previous work, Kaina et al. discovered that Chinese hamster ovary cells overexpressed the human MPG in an effort to comprehend the relevance of beginning lesions cleared by the BER pathway. MPG is in charge of the glycolytic elimination of the modified base, which results in the production of apurinic sites, during the N-alkylpurine repair procedure. Although it has not been shown that N-alkylpurines are directly mutagenic, the apurinic sites left behind by this repair procedure may obstruct replication and cause mutation.

Additionally, 8-hydroxyguanine and hypoxanthine are repaired by MPG. Numerous research has been conducted to look at the relationship between MPG and different human malignancies since DNA base lesions may play a role in mutagenesis and carcinogenesis. By using northern analysis, southern blots, immunofluorescence, immunohistochemistry, and western blot analysis, Cerda et al. identified the elevated MPG gene and protein expression in breast cancer cells compared to normal breast epithelial cells. A role for MPG in the development of cancer was suggested by Sohn et al.'s 2001 study indicating high-risk HPV-infected cervical neoplasia's had higher MPG expression levels and changed MPG protein intracellular distribution. Many studies have been interested in the effects of MPG on tumour sensitivity to the clinical chemotherapeutic drugs in an attempt to increase the effectiveness of cancer chemotherapy by interfering in the cellular responses to chemotherapeutic alteration. According to their findings, ovarian cancer, osteosarcoma, and breast cancer cells that overexpress MPG are markedly more sensitive to the effects of clinical chemotherapeutic agents, indicating that overexpressing MPG may be a potential gene therapy strategy to make tumour cells more susceptible to the cell-killing effects of chemotherapeutic alkylating agents. The balance between glycosylase activity, which generates apurinic sites and strand breaks, and subsequent excision repair processes may be a key factor in determining cellular cytotoxicity and resistance to alkylating agents, which may be the biological mechanism underlying the increase in sensitivity to chemotherapeutic agents in MPG overexpressing cell lines [3], [4].

We concentrate on MPG's role in human gliomas as one of our main areas of study. According to a recent study, MPG mRNA expression was found to be higher in astrocytic tumour tissues than in brain tissues next to the tumour, and MPG protein localization in an immunohistochemical study was only found in the nucleus of all tumour tissues, suggesting an MPG's role in human astrocytic tumour's and raising the possibility that the altered MPG expression and intracellular localization could be linked to astrocytic tumorigenesis. Furthermore, Tang et al. showed that MPG overexpression and the suppression of BER might make glioma cells more susceptible to the alkylating agent. However, little is known regarding the predictive importance of MPG expression in human gliomas of various clinical stages. The expression pattern of the MPG gene and protein in glioma specimens and healthy control brain tissues was examined using quantitative real-time PCR, immunohistochemistry test, and western blot analysis in order to solve this issue. The association between MPG expression and the stage of the glioma as well as patient survival was then examined.

Patient data and tissue samples:

The Institute for Functional Neurosurgery P.L.A., Tandan Hospital, Fourth Military Medical University, Xi'an, P.R. China's Research Ethics Committee authorized this research. All of the patients provided written, fully informed consent. All samples were treated with care and

kept anonymous in accordance with the law and ethical norms. The pathology department archives at Wangdu Hospital, Fourth Military Medical University, P.R. China, were searched for a total of 128 formalin-fixed, paraffin-embedded specimens of gliomas removed between 2000 and 2010. Two pathologists reevaluated each slide in accordance with the WHO criteria, and any discrepancies were carefully discussed. The study's participant population consisted of 76 men and 52 women, or a ratio of 1.46 to 1, with a median age of 42 years. One hundred and eighty-six of the 128 gliomas were categorized as high-grade gliomas, which included 58 primary glioblastomas and 38 anaplastic astrocytoma's and thirty-two low-grade gliomas. Prior to surgery, none of the patients had undergone radiation or chemotherapy.

All of the patients' clinicopathological traits and treatment plans were included. As controls, nonneoplastic brain tissues from 10 individuals with uncontrollable epilepsy were likewise cut into paraffin and snap-frozen slices. A five-year follow-up was conducted, and all patients received full care up to their deaths. From the date of the first surgical procedure to death, the overall survival time was computed. Patients who passed away from illnesses unrelated to their gliomas or as a result of unplanned circumstances were not included in this research. In addition, 20 glioma specimens, including 9 primary glioblastomas, 3 anaplastic astrocytoma's, 3 diffuse astrocytoma's, and 5 pilocytic astrocytoma's, were snap-frozen in liquid nitrogen after surgery[5], [6].

DISCUSSION

The preparation and reverse transcription of total RNA isolated from all 20 glioma samples and 10 control brain tissues. The ABI 7900HT was used to monitor polymerase chain reactions in real-time. Random primers, Oligo 18dT, and Superscript II Reverse Transcriptase were used to create cDNA. The SYBR green I dye, which binds to double-stranded DNA preferentially, and 10 ng of template were used to measure gene expression. At the conclusion of each cycle, fluorescence signals are detected and promptly presented on a computer screen. These signals, which are proportional to the concentration of the PCR product, allow for real-time monitoring of the PCR. The quantity of PCR product collected after a certain number of cycles is not what defines the reaction; rather, it is the time during cycling when the first sign of amplification of PCR products is seen. An rise in fluorescence is seen sooner the larger the initial amount of the template is. The fractional cycle number at which fluorescence crosses a certain threshold over the baseline is known as the threshold cycle. The SDS system software was used to translate fluorescence data into cycle threshold measurements, which were then exported to Microsoft Excel. The amounts of MPG mRNA and -actin were compared. Biphasic melting curves, which show if primer dimers or other unspecific products could be contributing to the amplification signal, were looked for in thermal dissociation plots.

Twenty glioma tissues and ten control brain tissues were homogenized in lysis buffer, 0.5% sodium deoxycholate, 0.1sodium dodecyl sulphate100 ug/mL aprotinin, 100 g/mL phenylmethylsulphonyl fluoride, sodium orthovanadateat 4°C throughout all procedures. Bradford's technique was used to assess the protein concentration, and bovine serum albumin was utilised as a reference. Protein samples were heated in 2 sample buffers containing 5% -mercaptothion for 5 min. After size separation on 15% polyacrylamide gel while SDS was denaturing, the proteins were then transferred to a nitrocellulose membrane at 90 V for 2 h. To determine the effectiveness of the transfer, the nitrocellulose membranes were dyed with ponceau S. The membranes were hybridized with a mouse monoclonal antibody to MPG and then incubated with a horseradish peroxidase-labeled goat anti-mouse IgG. Nonspecific binding was blocked by incubation in block buffer overnight at 4°C. Amersham Life Science,

Little Chalfont, UK, used enhanced chemiluminescence to find the bound secondary antibody. The loading control was the common protein β -actin. Using the Leica Q500IW image analysis system, positive immunoreactive bands were measured densitometrically and represented as the ratio of MPG to β -actin in optical density units. According to the protocol of the Department of Neurosurgery, Institute for Functional Neurosurgery P.L.A, Tandan Hospital, Fourth Military Medical University, Xi'an, P.R. China, an immunohistochemical assay was carried out using the traditional immunoperoxidase method. In a nutshell, specimens were blocked with phosphate-buffered saline containing 5% normal horse serum after peroxidase blocking with 0.3% H₂O₂/methanol for 30 min.

A mouse monoclonal antibody to MPG was used in all incubations, which were conducted overnight at 4°C. Following a quick PBS wash, the specimens were incubated with the anti-mouse antibody and avidin-biotin peroxidase at room temperature. After being cleaned in PBS, the specimens were coloured using a diaminobenzidine solution. The samples were counterstained with Meyer's hematoxylin after being washed with water. Nonimmune IgG was utilised as a negative control antibody for immunohistochemical staining, while non-malignant brain tissues served as control tissues. A microscope was used to view stained slices. Two independent, skilled pathologists who were blinded to the clinicopathologic criteria and clinical outcomes of the patients graded the immunostaining. The use of an immunoreactivity scoring system was done as previously mentioned. The extensional standard was composed of two components: the number of positively stained cells and the stain's intensity. Add together. According to the quantity and intensity of positively stained cancer cells, the staining score was divided as follows: -, +, point discrepancy in the results of two pathologists, samples were rescored [7], [8].

The programmed SPSS version 13.0 for Windows was used for all calculations. The ranked data were examined using the rank sum test. One-way ANOVA was used to analyse the measurement data. ANOVA using a randomized block design was used to examine the statistical variance between various tissue types. We evaluated the marginal effects of each component in the study of glioma morbidity for all patients using the Kaplan-Meier estimator and univariate Cox regression analysis. By using log-rank analysis, the differences between the groups were examined. With the use of multivariate Cox regression, the combined impact of several components was evaluated. To investigate the relationship between MPG mRNA and protein expression levels, a Spearman's analysis was used. When $P < 0.05$, differences were regarded as statistically significant. Quantitative Evaluation of MPG Gene Expression in Gliomas Based on WHO Grades

Real-time PCR was used to identify the gene expression of MPG normalized to β -actin in 20 glioma and 10 control brain tissues. The expression levels of the MPG gene were noticeably greater in human glioma tissues than they were in control brain tissues. We also examined the MPG gene's expression dependent on WHO grade. It's interesting to see that MPG gene expression increased when WHO grades rose from I to IV. Immunohistochemistry test was used to identify the expression and subcellular location of MPG protein in 10 nonneoplastic brain tissues and 128 glioma samples. Which is similar with the earlier investigation the positive staining for MPG was mostly seen in the tumour cells' nuclei in glioma tissues. MPG immunoreactivities in nonneoplastic brain slices varied from undetectable to low, whereas 102 of the glioma specimens were positively stained for MPG). Additionally, real-time PCR and Western blot cannot detect MPG immunostaining in nonneoplastic brain samples. In line with the findings of the Western blot analysis, the statistical analysis revealed that the expression level of MPG protein in glioma tissues was substantially greater than that in nonneoplastic brain tissues. In order to apply individualized therapies that particularly target the pathophysiologic and molecular characteristics of glioma patients, innovative

specific and effective prognostic indicators must be discovered immediately due to the poor prognosis for patients with glioma, especially those with GBM. In the present work, we examined MPG expression in 128 human glioma cases and linked it to tumor grade and patient survival rates. Our findings showed that glioma brain tissue had higher levels of the MPG gene and protein than non-cancerous brain tissue. Between WHO grade I and WHO grade IV glioma, we observed an increasing tendency in both the MPG protein level and gene level. These findings imply that human MPG transcriptional and translational activation may contribute to glioma carcinogenesis and progression. DNA is continually exposed to exogenous and endogenous alkylating and oxidative chemicals in all somatic and germ cells of the body, which causes DNA damage. Genetic mutation, chromosomal aberration, ageing, and cancer may result from unrepaired DNA damage.

Therefore, DNA repair is necessary for life to exist. Defective embryogenesis, tissue-specific malfunction, hypersensitivity to DNA-damaging substances, early senescence, genetic instability, and increased cancer rates may result from a lack of precise DNA repair processes. One of the most common routes for DNA repair is the BER pathway. MPG, an alkyl adenine DNA glycosylase, starts the repair of DNA bases damaged by alkylation in mammalian cells. The bulk of repair that is started by MPG happens via a process called short-patch BER, in which just one nucleotide is changed. MPG has a wide range of selectivity for various broken DNA bases. MPG eliminates the bulk of base damage brought on by methylation, including the main adducts 3-meA and 7-meG. According to reports, a number of DNA-damaging agents, including viruses, have the ability to cause MPG expression. For instance, in SV 40 T-antigen-expressing transgenic mice, the elevated expression of the MPG gene was investigated in breast cancer, cervical neoplasia, and thymic carcinoma. Mammalian cells actively control DNA repair genes and enzymes during cell growth, according to earlier research. DNA repair enzymes have a specific temporal pattern of expression throughout the cell cycle in relation to the stimulation of DNA replication. DNA repair preserves the nucleotide sequences of genomic DNA across time in brain cells that are not engaged in DNA replication. According to Kim et al. , MPG expression was relatively high in the brain one week after birth and remained low 400 days later in mature individuals, indicating that brain tissue is terminally differentiated and nonproliferating tissues[9], [10].

CONCLUSION

The overexpression of the MPG gene and protein in human gliomas was shown by our results, which also for the first time revealed that MPG may be a poor independent prognostic factor for glioma patients. DNA repair enzymes have been shown to be crucial in the development of a number of malignancies. One finding that caught our attention was the up to 24-fold overexpression of MPG in breast cancer as compared to normal primary breast epithelium. Kim et al. reported that MPG mRNA levels in astrocytomas were substantially greater than those in brain regions around the tumour in 2003. In this investigation, we also discovered the overexpression of MPG protein and gene in glioma tissues with comparable outcomes. In addition, we provide proof that MPG protein is located in nuclear localization in glioma tissues, which was in line with Kim et al.'s findings. The nuclear localization of MPG in glioma tumour cells may indicate a function for MPG in the control of cell cycle and division. Furthermore, the association between MPG expression and patient survival rates was the study's most significant discovery. According to our results, about 80% of glioma patients had positive MPG staining. Patients who had positive MPG staining had a poorer survival rate than those who did not. High MPG protein levels are a signal of a bad prognosis for patients with gliomas, according to Kaplan-Meier and multivariate analyses, which both demonstrated a substantially lower overall survival for patients whose tumor's had high MPG

levels. This study is the first to show the prognostic use of MPG in human malignancies. It is necessary to do further validations using greater sample sizes and other approaches.

REFERENCES:

- [1] A. Davidson, "What is damaging the kidney in lupus nephritis?," *Nature Reviews Rheumatology*. 2016. doi: 10.1038/nrrheum.2015.159.
- [2] A. Perfetti *et al.*, "Genome wide identification of aberrant alternative splicing events in myotonic dystrophy type 2," *PLoS One*, 2014, doi: 10.1371/journal.pone.0093983.
- [3] P. M. Yang *et al.*, "Zebularine inhibits tumorigenesis and stemness of colorectal cancer via p53-dependent endoplasmic reticulum stress," *Sci. Rep.*, 2013, doi: 10.1038/srep03219.
- [4] P. A. Tsuji *et al.*, "Knockout of the 15 kDa Selenoprotein Protects against Chemically-Induced Aberrant Crypt Formation in Mice," *PLoS One*, 2012, doi: 10.1371/journal.pone.0050574.
- [5] M. Zhou *et al.*, "Morphology and Outcomes of Total Endovascular Treatment of Type B Aortic Dissection with Aberrant Right Subclavian Artery," *Eur. J. Vasc. Endovasc. Surg.*, 2017, doi: 10.1016/j.ejvs.2017.09.014.
- [6] J. Varshney, M. C. Scott, D. A. Largaespada, and S. Subramanian, "Understanding the osteosarcoma pathobiology: A comparative oncology approach," *Veterinary Sciences*. 2016. doi: 10.3390/vetsci3010003.
- [7] T. A. Costa Casagrande *et al.*, "The value of molecular expression of KIT and KIT ligand analysed using real-time polymerase chain reaction and immunohistochemistry as a prognostic indicator for canine cutaneous mast cell tumours," *Vet. Comp. Oncol.*, 2015, doi: 10.1111/vco.12010.
- [8] A. Sepsa *et al.*, "Emerging role of linker histone variant H1x as a biomarker with prognostic value in astrocytic gliomas. A multivariate analysis including trimethylation of H3K9 and H4K20," *PLoS One*, 2015, doi: 10.1371/journal.pone.0115101.
- [9] X. Cui, Y. Shirai, T. Wakai, N. Yokoyama, S. Hirano, and K. Hatakeyama, "Aberrant expression of pRb and p16INK4a, alone or in combination, indicates poor outcome after resection in patients with colorectal carcinoma," *Hum. Pathol.*, 2004, doi: 10.1016/j.humpath.2004.06.010.
- [10] L. Lu, D. Katsaros, H. A. Risch, E. M. Canuto, N. Biglia, and H. Yu, "MicroRNA let-7a modifies the effect of self-renewal gene HIWI on patient survival of epithelial ovarian cancer," *Mol. Carcinog.*, 2016, doi: 10.1002/mc.22285.

CHAPTER 7

A MIXED DNA/LNA MICROARRAY: EXPRESSION PROFILING OF A HETEROGENEOUS POPULATION OF MORNAS

Thiruchitrambalam, Professor

Department of ISME, ATLAS SkillTech University, Mumbai, Maharashtra, India

Email Id-thiru.chitrambalam@atlasuniversity.edu.in

ABSTRACT:

Non protein coding RNAs make up the majority of mammalian transcriptomes. These ncRNAs participate in several regulatory pathways and serve a variety of activities in all cells. NcRNAs have also lately been referred to be useful diagnostic tools. Although microarray-based technologies are gradually being replaced by RNA-seq methods for high-throughput expression profiling, diagnostic application of these methods is still uncommon. While using locked nucleic acid arrays, microarrays are increasingly often employed for diagnostic profiling, particularly for extremely tiny ncRNAs. While DNA arrays may not provide satisfactory findings for the investigation of short RNAs, LNA microarrays are relatively costly for high-throughput research targeting larger ncRNAs. Here, we offer a mixed DNA/LNA microarray technology that enables sensitive and precise investigation of a complex RNA population on a single array in a single experiment by hybridizing directly labelled short and longer ncRNAs on LNA probes or bespoke DNA probes, respectively. The investigation of differential ncRNA expression in mouse embryonic stem cells and adult brain cells was accomplished with the help of the DNA/LNA system, which effectively conforms with diagnostic criteria while using only small quantities of total RNA.

KEYWORDS:

Diagnostic, Microarrays, Protein, Transcriptomes.

INTRODUCTION

Up to 90% of the human genome is being transcribed, but only around 1.5% of these transcripts correspond to protein-coding exons, according to the ENCODE project's high-resolution investigation of 1% of the human genome. With the expected presence of up to 0.5 million transcripts of regulatory non-coding RNAs in the human genome, it was hypothesized that the majority of transcripts may act as a source for these RNAs. However, the majority of these transcripts still have unidentified functions, and their functional significance is even under question. Therefore, new techniques for high-throughput profiling of ncRNA expression are needed to address these unique and intriguing features of the cellular transcriptome content. High-throughput sequencing, often known as RNA-seq, has recently become the most popular expression profiling approach, and there are several benefits to this. RNA-seq offers complete genome coverage and enables the identification of RNA editing events as well as single nucleotide polymorphisms, irrespective of hybridization artefacts. However, there are still certain RNA-seq flaws and artefacts that are often related to reverse transcription or library building techniques [1], [2].

Additionally, since sequencing dataset analysis is still time-consuming and needs substantial bioinformatics knowledge, it is not now appropriate for quick diagnostic or clinical profiling. Based on microarrays, an alternative high-throughput method is used. Locked nucleic acid arrays have recently been developed in innovative microarray technologies to effectively monitor miRNA expression or identify single nucleotide polymorphisms. LNAs are synthetic RNA analogues that have superior nucleic acid duplex thermostability, enabling for higher hybridization temperatures and better mismatch discrimination.

Because of the growing interest in ncRNAs as biomarkers, ncRNA microarrays may be a useful tool for profiling ncRNA expression in medical settings. However, most of these apps would not be able to finance an LNA platform. In this article, we provide a mixed DNA/LNA microarray technology that enables the hybridization of directly and concurrently labelled short and longer ncRNAs onto microarrays made up of both LNA-modified and specifically created DNA capture probes, respectively. This approach satisfies the majority of current biomedical diagnostic criteria in terms of cost and sample needs by enabling a sensitive and specific examination of a complex and diverse RNA population on a single array in one experiment. Exaton sold the mercury LNA miRNA array ready-to-spot probe set as an LNA capture probe set for short ncRNAs identification. This collection includes 2,056 capture probes that are all covered by miRbase and have a consistent T_m of 72°C. We bought the DNA probes from Microsite in Switzerland. They were 5'-C6 amino-modified, created to adhere to a 72°C T_m , desalted, and diluted to a final concentration of 20 M in 3xSSC, 1.5 M Betaine buffer.

Using the Microgrid II Microarray Spotter, the self-designed DNA-based capture probe set for long ncRNAs and the LNA-based capture probe set for short ncRNAs were spotted on Hsien's epoxy-coated glass slides. To assure quality control and dependability, each probe was detected twice on the slide in four duplicates. According to the Exaton protocol for hybridization with the miRNA LNA platform, hybridizations have been carried out using the Tecan HS400 hybridization station. At 56°C or 64°C, hybridizations were carried out. Following the manufacturer's instructions, total mouse brain RNA and total mouse embryonic stem cell RNA were extracted from C57/B16 mice and E14 stem cells, respectively, using Tri Reagent. Using a nanodrop spectrophotometer from Fischer Scientific, RNA was measured. Following the manufacturer's procedure with the following changes, total mouse brain RNA and total mouse embryonic stem cell RNA were directly labelled using the Node Rapid miRNA Labelling System. Prior to poly-A tailing, RNA was centrifuged, denatured at 90°C for 3 min, and chilled on ice for 2 min; and the kit's reaction buffer was swapped out for a custom reaction buffer comprising 50 mM Tris-HCl, 250 mM NaCl, and 10 mM MgCl₂. Two biological replicates of whole mouse brain RNA and total mouse embryonic stem cell RNA were utilized to determine differential expression[3], [4].

In order to create the probes, Olikodi was used. Steps for post-processing, such as confirming the specificity of the probes or the coverage of the processing events, were included. See for a detailed description. Creation of a Mixed DNA/LNA Microarray, Section 3.1 We looked at the possibility of using a combined DNA and LNA platform dedicated, respectively, to the expression analysis of long ncRNAs and tiny ncRNAs for the expression profiling of a heterogeneous population of ncRNAs. In order to do this, we created a customized microarray that was spotted using DNA capture probes for tRNAs, 7SK RNA, as well as C/D and H/ACA box snoRNAs and the commercially available mercury LNA miRNA ready-to-spot probe set from Exaton. All spotted probes required to have the same melting temperature in order to produce a mixed DNA/LNA microarray. In order to prevent the increased background caused by unspecific hybridization that was seen when employing temperature gradients, we chose to use a fixed hybridization temperature.

DNA capture probes were created to adhere to this standard regardless of their sizes since the LNA capture probe set melting temperature equates to 72°C for an ideal hybridization temperature of 64°C. For areas of 30 to 60 nt, DNA capture probes were created to hybridize to conserved ncRNA regions. To assess the sensitivity of the method, 7SK RNA and tRNAs were used to examine the ability of highly structured ncRNAs and snoRNAs to hybridize. If the target was long enough, two or more DNA capture probes per ncRNA were created. In addition to the perfectly matching antisense probes, probes with one or two nucleotide

mismatches were also created to evaluate the system's specificity. Finally, probes with one or two nucleotide deletions were created for ncRNAs that were more organized. Negative controls comprised sense probes for each ncRNA and random DNA probes.

Direct RNA Labelling:

It was necessary to decide on the RNA labelling strategy. In fact, larger RNAs are often reverse transcribed into cDNA and labelled by inclusion of amino allyl-modified nucleotides, while short RNAs are typically directly labelled for microarray tests. We used a dual fluorescent dye RNA labelling kit that is available commercially and is based on ligating fluorophore-containing dendrimers with poly-A tails. For our first proof of concept tests, we employed 5 g of total mouse brain RNA. AlexaFluor3 and AlexaFluor5 labelled whole mouse brain RNA copies were self-self-hybridized on the bespoke DNA/LNA device to eliminate dye bias effects. Analysis of the data revealed that, in contrast to snoRNAs, which were essentially undetectable neuronal miRNAs, such as miR-9 and were well identified. While tRNAs were hardly detectable at all, 7SK RNA was hardly detectable. We included a denaturation step before poly-A tailing because inadequate polyadenylation and labelling of these longer ncRNAs may be related to secondary structure. Additionally, we investigated a Mg²⁺ tailored poly-A tailing solution since Mn²⁺ cations were known to boost poly-A polymerase activity *in vitro*, which improved labelling effectiveness most likely by promoting polyadenylation. Without affecting the identification of miRNAs and the new labelling methodology allowed for better snoRNAs, tRNAs, and 7SK RNA detection and 1, Supplementary. Finally, posttranscriptional RNA changes such pseudo uridylation or 2'-O-methylation may prevent ncRNAs from being labelled; we did not examine the magnitude of this parameter, however[5], [6].

DISCUSSION

It was required to optimize the amount of RNA utilized for labelling together with RNA labelling. For hybridization on LNA microarrays, as little as 30 ng total RNA are often adequate, but DNA microarrays need at least 10–25 g of total RNA as starting material for cDNA labelling by reverse transcription. Each labelling procedure employed 0.25 to 1 g of total RNA, with the initial hybridization temperature set at 56 °C. The hybridization temperature was then increased to 64°C in order to better accommodate the LNA platform. The amount of labelled total RNA was increased from 1 g to 2 g in order to maintain the sensitivity at this temperature. Similar findings for miRNA LNA probes were seen under these circumstances, however 7SK RNA and snoRNAs were more easily detected. While LNA probes were unaffected, we typically saw better detection for DNA probes at 64°C relative to the 56°C condition. However, as significant amounts of whole RNA may not be accessible for tissue profiling, we chose to use 2 ng of total RNA per labelling process and conduct self-self-hybridizations at 64 °C, which seemed to be the best compromise. There may be a need for additional procedure optimization for diagnostic applications with smaller volumes of material.

On the DNA/LNA combination platform, we then examined the impact of ncRNA structure on the sensitivity and specificity of hybridization. For instance, raphe was identified with a mean intensity of 7555 when the capture probe was 60 nt long, but only 1564 when the probe was 30 nt long. Comparing the 36 nt long capture probe 7SK_126-162 to the 46 and 36 nucleotide long probes 7SK_17-63 and 7SK_55-91, respectively, led to a nearly 2-fold increase in the detection of 7SK RNA). Thus, identification of highly structured ncRNAs seems to be less reliant on the length of the capture probe, and using numerous complimentary probes to one specific RNA boosts detection sensitivity. The findings revealed that antisense snoRNA capture probes identified snoRNAs effectively at 64 °C with

comparable intensities to the condition using greater quantities of labelled total RNA and lower hybridization temperatures. The detection levels of miR-9 and miR-9* remained constant whereas practically all antisense snoRNA capture probes identified their particular snoRNA, although at varying intensities[7], [8].

LNA capture probes allow for nucleotide-scale discrimination. As a result, we were interested in testing how precise the DNA/LNA platform could identify DNA capture probes. Therefore, the specificity was tested using probes that had mismatches in one or two places. The signal with the two-nucleotide mismatch probe SNOZ39_6-60MM2 was falling below threshold at 64°C, indicating that discrimination was already possible with two nucleotide mismatches. However, the snoRNA SNOZ39 was only detected by the antisense and one nucleotide mismatch capture probes. However, the MM1 probe for SNOZ39 detection exhibited a drop of 40% when the mean intensity levels between the perfect matching and one nucleotide mismatch probes were compared. However, a signal was sometimes still discernible with MM2 probes), although at weaker levels than with the perfectly matched capture probes. For instance, compared to the MM1 capture probes, the intensity levels of the 7SK_17-63MM2 and 7SK_55-91MM2 probes were further reduced by 20%. LNA capture probes allow for nucleotide-scale discrimination.

As a result, we were interested in testing how precise the DNA/LNA platform could identify DNA capture probes. Therefore, the specificity was tested using probes that had mismatches in one or two places. The signal with the two-nucleotide mismatch probe SNOZ39_6-60MM2 was falling below threshold at 64°C, indicating that discrimination was already possible with two nucleotide mismatches. However, the snoRNA SNOZ39 was only detected by the antisense and one nucleotide mismatch capture probes. However, the MM1 probe for SNOZ39 detection exhibited a drop of 40% when the mean intensity levels between the perfect matching and one nucleotide mismatch probes were compared). However, a signal was sometimes still discernible with MM2 probes), although at weaker levels than with the perfectly matched capture probes. For instance, compared to the MM1 capture probes, the intensity levels of the 7SK_17-63MM2 and 7SK_55-91MM2 probes were further reduced by 20%).3.5.

Accuracy of the DNA/LNA Platform for Expression Profiling

We next used dye swap experiments using 2 g of total mouse brain RNA and 2 g of total mouse embryonic stem cells RNA to apply our DNA/LNA platform to expression profiling. At 64°C, hybridizations were carried out. For instance, mouse embryonic stem cells were found to have approximately a 25-fold overexpression of the stem cell-specific miRNAs of the miR-290 family, whereas the mouse brain had about a 14-fold overexpression of the brain-specific miR-124 and miR-9 . The miR-125b-5p was likewise around 13.5-fold overexpressed in the brain. Additionally, let-7 was overexpressed in brain cells relative to ES cells, as was predicted given that mature let-7 is expressed following neural cell development from stem cells. Regarding DNA probes, it was possible to see that mouse embryonic stem cells overexpressed SNORD55 by approximately 2-fold and SNORA71 by about 5-fold. Northern blots, which show that SNORD55 and SNORA71 are overexpressed in embryonic stem cells compared to mouse brain, corroborated this differential expression. To confirm the observed differential expression and validate the DNA/LNA platform, we used real-time PCR. For confirmation, we examined the ncRNAs and microRNAs detected by DNA probes. We confirmed that miR-125b-5p and miR-293 were considerably overexpressed in mouse brain and mouse ES cells, by 20.7-fold and 6.5-fold, respectively, as predicted by the microarray data. The snoRNAs SNORA71 and SNORD55 were found to be 3.3- and 2.5-fold, respectively, overexpressed in mouse ES cells in contrast to mouse brain . We found no

evidence of SNORD113 or 7SK RNA differential expression between mouse ES cells and mouse brain, according to the DNA/LNA microarray platform data. Finally, real-time PCR findings suggested that SNORA18 and SNOZ39 were overexpressed in mouse ES cells or the mouse brain, respectively, even though the microarray data did not seem to indicate that they were differently expressed. This differential expression was not significant for SNORA18 but was 3.6-fold for SNOZ39, emphasizing the need for additional methods like northern blotting or real-time PCR to confirm microarray and deep-sequencing findings. However, the discovery of canonical snoRNAs with variable expression is an interesting development, particularly in light of their newly reported noncanonical roles as miRNA precursors or regulators of alternative splicing [9], [10].

CONCLUSION

NcRNAs are currently regarded by many as superior disease biomarkers. For instance, it is possible to identify the source of different tumors using miRNAs, snoRNAs, or long interspersed non-coding RNAs. Noncoding RNAs have also been shown to have a role in the control of chromatin or the development of neurological disorders. Microarrays still seem to be a less costly tool for diagnostic reasons than high-throughput sequencing, and microarray analysis also takes a lot less time. For ncRNA-based diagnostic or expression profiling, a microarray technology that allows simultaneous study of both short and long molecules was needed. Here, we created a microarray technology that enables profiling of both short and long ncRNAs on the same chip. We used the previously existing LNA technology for miRNAs, combined it with bespoke DNA capture probes for longer ncRNAs, and allowed detection of all ncRNAs using a universal direct labelling technique due to the size restriction of short RNAs. As a result, the DNA/LNA platform was able to identify long, structured ncRNAs and miRNAs, and this detection was not reliant on the length of the capture probe but rather on secondary structure. We found that capture probes that were intended to hybridize to less organized areas were more effective. Capture probes covering practically the complete molecule seemed to be the most effective in the case of highly structured tRNAs. The mixed microarray takes just a little quantity of directly labelled total RNA and is sensitive and selective. If probes are made to span low-structured sections and a denaturation phase is included before RNA direct labelling, problems caused by ncRNA structure may be resolved. As a result, this platform may end up becoming a highly desirable tool for biomedical diagnostics as well as integrated expression profiling of small and long ncRNAs.

REFERENCES:

- [1] K. Skreka, M. Zywicki, M. Karbiener, A. Hüttenhofer, M. Scheideler, and M. Rederstorff, "Expression profiling of a heterogeneous population of ncRNAs employing a mixed DNA/LNA microarray," *J. Nucleic Acids*, 2012, doi: 10.1155/2012/283560.
- [2] M. Castoldi, V. Benes, M. W. Hentze, and M. U. Muckenthaler, "miChip: A microarray platform for expression profiling of microRNAs based on locked nucleic acid (LNA) oligonucleotide capture probes," *Methods*, 2007, doi: 10.1016/j.ymeth.2007.04.009.
- [3] I. Naguibneva *et al.*, "An LNA-based loss-of-function assay for micro-RNAs," *Biomed. Pharmacother.*, 2006, doi: 10.1016/j.biopha.2006.07.078.
- [4] A. A. Koshkin *et al.*, "LNA (Locked Nucleic Acids): Synthesis of the adenine, cytosine, guanine, 5-methylcytosine, thymine and uracil bicyclonucleoside monomers, oligomerisation, and unprecedented nucleic acid recognition," *Tetrahedron*, 1998, doi: 10.1016/S0040-4020(98)00094-5.

- [5] D. Kestemont *et al.*, “XNA ligation using T4 DNA ligase in crowding conditions,” *Chem. Commun.*, 2018, doi: 10.1039/c8cc02414f.
- [6] Y. Wu, C. J. Yang, L. L. Moroz, and W. Tan, “Nucleic acid beacons for long-term real-time intracellular monitoring,” *Anal. Chem.*, 2008, doi: 10.1021/ac702637w.
- [7] M. C. Fuentes, S. Calsamiglia, V. Fievez, M. Blanch, and D. Mercadal, “Effect of pH on ruminal fermentation and biohydrogenation of diets rich in omega-3 or omega-6 fatty acids in continuous culture of ruminal fluid,” *Anim. Feed Sci. Technol.*, 2011, doi: 10.1016/j.anifeedsci.2011.05.013.
- [8] S. P. Sau, T. S. Kumar, and P. J. Hrdlicka, “Invader LNA: Efficient targeting of short double stranded DNA,” *Org. Biomol. Chem.*, 2010, doi: 10.1039/b923465a.
- [9] K. E. Lundin *et al.*, “Increased stability and specificity through combined hybridization of peptide nucleic acid (PNA) and locked nucleic acid (LNA) to supercoiled plasmids for PNA-anchored ‘Bioplex’ formation,” *Biomol. Eng.*, 2005, doi: 10.1016/j.bioeng.2005.07.003.
- [10] A. M. James, M. B. Baker, G. Bao, and C. D. Searles, “MicroRNA detection using a double molecular beacon approach: Distinguishing between miRNA and Pre-miRNA,” *Theranostics*, 2017, doi: 10.7150/thno.16840.

CHAPTER 8

DNA REPAIR CAPACITY LEVELS-STRATIFIED MICRORAD EXPRESSION ALTERATIONS IN WOMEN WITH BREAST CANCER

Thiruchitrabalam, Professor

Department of ISME, ATLAS SkillTech University, Mumbai, Maharashtra, India

Email Id-thiru.chitrabalam@atlasuniversity.edu.in

ABSTRACT:

Breast cancer is the cancer in which women are most often diagnosed globally and is the main reason why they die, particularly among Hispanic women. According to earlier research, women with poor DNA repair capacity, as determined by the NER pathway, are more likely to develop breast cancer. The expression of the microRNA let-7b was also linked to DRC levels in a prior study done on BC patients. By regulating the cell's reaction to DNA damage and the pathobiology of cancer, miRNAs have the power to cause genomic instability. Finding plasma miRNAs connected to differences in DRC levels in BC patients is the main goal of this pilot investigation. Hypothesis. Our goal is to determine if there is a relationship between DRC levels and miRNA expression levels. Methods. From 56 women enrolled as part of our BC cohort, plasma samples were chosen. The host-cell reactivation test was used to determine DRC values in lymphocytes. Low and high DRC levels were assigned to the samples. To analyse the expression profile, miRNAs were extracted. Results.

KEYWORDS:

Hispanic, Pathobiology, Prevention, Reactivation.

INTRODUCTION

According to the American Cancer Society, there will be 41,760 cancer-related fatalities and 268,600 new instances of breast cancer in the US in 2017. According to the Centers for Disease Control and Prevention, BC is the second highest cause of mortality among Hispanic women and women in the US. BC currently makes up around 30% of all new cases of cancer in women in the US and Puerto Rico. The Puerto Rico Cancer Registry reported 2,205 new BC cases and 444 BC deaths in PR in 2015. Cancer is a complicated condition involving environmental, genetic, and epigenetic risk factors. Cancer is recognized to have genomic instability, according to Hanahan and Weinberg. Due to the cell's inability to repair certain forms of DNA damage, dysregulation of several DNA repair pathways leads to this genomic instability. A risk factor for several cancers, including BC, has been shown to be inadequate DNA repair as evaluated in blood cells. About 200 DNA repair genes are found in at least 5 different DNA repair pathways. Around 30 proteins participate in the very flexible repair mechanism known as nucleotide excision repair, which functions to restore harmed nucleotides. The primary method for repairing large DNA adducts is NER. These may be produced by a variety of DNA-damaging agents, including as cisplatin, exogenous compounds, UV radiation, and other chemotherapeutics.

Through the NER route and the use of lymphocytes as surrogate indicators, prior research from our lab has shown the vital significance of total DRC levels for BC risk [1], [2]. Our team recently shown that there is significant variation in total DRC levels across the four main molecular BC subtypes, with triple-negative BC in women having the lowest levels. These results emphasize the need for more study to fully comprehend how variations in DRC levels are related to various endpoints in the intricate process of BC carcinogenesis and

reinforce the significance of the NER pathway in sporadic BC. It has been suggested that the epigenome functions as a link between genotype and phenotype. Determining the processes through which genetic and environmental variables influence illness risk therefore offers great potential when using epigenetic analysis. Once a BC tumour has established, epigenetic alterations have been linked to DRC levels. For instance, elevated DRC levels in women with BC have been linked to plasma levels of the let-7b microRNA. MiRNAs are naturally occurring, short, non-protein-coding RNAs that bind to the 3'-untranslated regions of protein-coding transcripts to control gene expression at the posttranscriptional stage. Different forms of cancer have been linked to their abnormal expression in peripheral blood. As pleiotropic molecules, miRNAs have been shown to control the expression of a wide variety of cancer-related genes. However, relatively little is understood about their function in controlling DRC levels in BC. As a result, the major goals of this pilot research were to find miRNAs associated with BC, find miRNAs associated with DRC levels in women with BC, and determine if the clinicopathological traits of the women included in the study had an impact on DRC levels [3], [4].

Resources and Techniques:

Human subjects are used. This research was authorized by the institutional review board of Ponce Health Sciences University. Each participant approved the collection of a blood sample and the reading of their pathology findings by signing an informed consent form. The research nurse provided a 7-page epidemiology questionnaire to each participant, which asked about demographic information and BC risk factors. Recruitment of patients. The 1,187 women with and without BC who were recruited for our BC cohort from 2006 to 2013 and who were reported in Matta et al. 2012 were chosen as participants in this research. Blood samples and epidemiological information were obtained from each participant through a questionnaire. The blood samples were used to isolate plasma and lymphocytes. The BC cases included in this research were individuals with primary breast tumors who had just recently gotten their diagnosis and were treatment-naïve. Six months before to study enrollment, controls were needed to have a normal mammogram and a normal breast examination done by a primary care physician. They also had to have no prior history of any sort of cancer. For the purpose of confirming the diagnosis and gathering clinicopathological details such as tumor size and grade, type of cancer, hormone receptor status, and other clinically significant data, pathology reports from BC patients were acquired. The tumors of the BC cases were divided into four main molecular subtypes based on the hormone receptor status data for estrogen and progesterone receptors, as well as HER2: luminal A, luminal B, HER2+, and triple negative. From our BC cohort, which included cases and controls with high and low DRC, 56 participants (27 BC cases and 29 controls) were chosen for this pilot investigation.

Measuring DNA repair capacity. According to earlier reports, peripheral blood lymphocytes were isolated, purified, and cultured from each patient sample. Using the host-cell reactivation test, the isolated lymphocytes were employed as proxy indicators of the patients' overall DRC. The determination of *in vivo* DRC is now possible thanks to this assay, as it was previously reported. HCR was used to test the lymphocytes' ability to repair the foreign DNA within a time period that closely matched the actual cellular process. Results were consistent with the cells' intrinsic DRC, which was mostly determined by the activity of their NER pathway. Briefly, a plasmid carrying the luciferase reporter gene that had been previously damaged by UVC radiation was transfected into the cells. The luciferase activity after UVC-damaged plasmid DNA repair was compared to the undamaged plasmid DNA to determine DRC. After the designated repair period, the quantity of residual luciferase that was still active was a percentage that showed how much DRC each person had. As previously

mentioned, DRC values were determined using a cut-off of 3.8% for high DRC and 3.8% for low DRC. Expression profile of microRNA. Applied Biosystems' TaqMan Array Human MicroRNA a Cards v2.0 were used for microRNA expression profiling. Using the Ambion Mirvana miRNA Isolation Kit, miRNAs were isolated from the 56 plasma samples. Utilizing a Nanodrop 1000 to measure RNA quantity and quality, 0.5–1 mg of total RNA underwent reverse transcription utilizing pools of miRNA-specific RT primers. To improve sensitivity, a preamplification step was carried out utilizing Megaplex Preamp Primers, Human Pool A v2.1. Using 8 Multiplex RT primer pool reactions and stem-looped RT primers that were specific to mature miRNA, single-stranded cDNA was created from 200 ng of total RNA. Following diluting and mixing with TaqMan Universal PCR Master Mix, the obtained cDNA samples were put onto the TaqMan Array. The following thermocycler settings were used for quantitative PCR: 30 min at 16°C, 30 min at 42°C, 5 min at 85°C, and then maintained at 4°C. Testing for experimental outliers was used to evaluate the experimental Ct fluorescence, and only cycles between 20 and 40 Ct were taken into account. U6 was used for sample normalization since it is an endogenous miRNA. The H. Lee Moffitt Cancer Center's Molecular Genomics Core in Tampa, Florida, handled all of the miRNA expression tests[5], [6].

A Mann-Whitney test was used to see if there were any changes in mean expression between BC patients and controls. Using the Kruskal-Wallis's test, miRNA expression levels were compared across groups. Using the Morpheus heatmap generator and the Pearson's correlation test, hierarchical microRNA clustering was carried out. Cross-tables were used to do proportion analyses, and a chi-square test was used to find differences. The Spearman's correlation was used to assess any significant relationships between DRC levels and miRNA expression. A two-tailed test with a p-value of 0.05 or less was used to determine statistical significance. Prism 8 and Minitab® 18 were used for the analyses. Analyzing several variables. To localize the samples in relation to one another, the principal component technique generates a set of fictitious coordinates from the original matrix data. The easiest way to comprehend this information is via a score plot graph. This graph consolidates the sample cluster formation, showing that sample variability decreases with increasing sample proximity. The miRNA relative expression values were used to build the PC matrix for this investigation, and the miRNAs with missing values were not included in the analysis. These miRNAs, as well as certain epidemiological and clinicopathological data for each participant, such as case-control categorization, DRC levels, tumor grade, and molecular subtype classification, were used to create the PC matrix. Minitab 18 was used to construct multivariate analyses and PC graphics.

DISCUSSION

According to the PC analysis, BC patients with high DRC were somewhat different from BC cases with low DRC on the PC1 axis and comparable to controls regardless of their DRC levels. The clinicopathological variables tumor location, type of cancer, tumor grade, and molecular subtype were considered as potential candidates to explain the data variance shown in the mean comparison analysis and on the hierarchical heatmap. Only three samples were identified as having lobular malignancies, and one sample included both ductal and lobular components. Only one tumor sample, or 3.7% of the BC cases in this pilot investigation, was determined to be in situ BC. When these samples were localised in the PC plot, however, no clustering was seen in the PC analysis for the cancer type or tumor location. When the tumor grade was analyzed on a PC, no grouping was seen. The grade I samples were dispersed along the PC1 axis. Furthermore, after stratifying samples by molecular BC subtype, no clusters were seen. The luminal B and HER2 subtypes, however, were not well represented in the sample population. This pilot study is the first to, to our knowledge, show a relationship

between miRNA expression and general DRC levels in BC patients, despite the fact that the function of miRNAs in BC has been widely researched and published. This research is one of the few that examines alterations in miRNA expression in BC in Hispanic women. Even though a large body of research has been done on the abnormal expression of miRNAs after BC malignancy develops, new data shows that ethnicity may play some role in determining variances in miRNA expression patterns. New information on the miRNA expression profile of Hispanic women with BC is provided by this pilot research, which also serves as a benchmark for comparing the miRNA profiles of women with BC from other groups. therapy may also be ruled out as a possible confounder since the 27 BC patients evaluated had just recently received their diagnoses and were uninitiated in receiving therapy.

Around 56 Hispanic women from Puerto Rico made up the research group, with 51.8% being controls and 48.2% being BC cases. To evaluate group differences, epidemiological indicators were categorized by DRC levels. Although there were no differences for a number of epidemiological factors, as we have previously reported, a low DRC level was commonly seen in BC patients. Overall, controls and BC patients in our cohort were younger, as has been shown in other BC investigations in the past. Body mass index has been shown to fluctuate with age and ethnicity, however in this investigation, no link between BMI and BC was discovered. The majority of individuals said they had at least one pregnancy while they were between the ages of 20 and 29. 5.4% of both BC patients and controls reported being nulliparous, which is a similar percentage. Another recognized BC risk factor is early menarche. We discovered a link between BC and the first menstrual cycle occurring before the age of 12 that is consistent with other investigations. Hysterectomy and oophorectomy are two surgical procedures that have been connected to lower BC risk, however none of these factors were associated in our research group. Smoking and alcohol usage, two lifestyle choices known to increase the risk of BC, were equally prevalent in our population. On the basis of the family history of BC and cancer in general, no relationship with no sporadic BC was discovered[7], [8].

Invasive ductal carcinoma was seen in the majority of BC cases, including women with high and low DRC levels. Our cohort reflects the fact that invasive ductal carcinoma is the most frequently diagnosed form of BC globally. The TNM staging approach was used to categories the tumors into grades 0, I, II, III, and IV based on the tumor grade data. Regardless of DRC levels, stage II and stage III tumors were present in the majority of BC patients. For prognosis and to assess the aggressiveness of BC, Ki-67 expression is combined with the genetic BC subtype categorization. Unfortunately, there weren't enough data on Ki-67 expression, therefore no more comparisons could be made. When patients were divided up based on DRC levels and receptor status, no changes were seen. Because of the short sample size, there was likely no correlation between DRC levels and molecular subtypes. In a recent investigation with 267 BC patients, we found significant variation in four genetic BC subtypes when DRC levels were included. Most of the women in the triple-negative BC group had low DRC levels, which is consistent with that research. The clinicopathological traits were often distributed similarly across the groups.

Between cases and controls, there were noticeably differing levels of microRNA expression. Several studies have observed a similar tendency. Based on relative miRNA expression, the hierarchical matrix also identified a distinguishing pattern for each woman with and without BC. The variability shown in mean comparison studies is also caused by these particular patterns, which may potentially represent biological variation among BC patients. Some of the 40 candidates identified as being associated to BC, such as let-7b , miR-155-5p , miR-194-5p, miR-373-3p , and miR-375-3p , have reported variations in plasma miRNA expression. These miRNAs were overexpressed in the plasma of BC patients as compared to

controls, which is consistent with our findings. Only three of these 40 candidates—miR-18a-5p, miR-372-3p, and miR-652-3p—were under expressed in BC patients. Regarding miR-18a-5p, Jankovic et al. research evaluated the expression of a number of miRNAs, including this miRNA, in invasive and noninvasive BC patients and controls. They found that women with noninvasive BC had the greatest expression of miR-18a-5p, while women with invasive BC and controls had comparable expression, even though there were no significant differences between the groups. Regarding miR-372-3p, no research has clarified the expression levels of this gene in the plasma of BC-affected women. In breast tumor tissues, where its expression is lower in tumors than in nearby normal tissue, the function of this miRNA in BC has been examined. Regarding miR-652-3p, recent research by Cuk et al. found that this miRNA was more expressed in the plasma from BC-affected women than in the plasma from BC-free women[9], [10].

Numerous genes involved in various methods of DNA repair are regulated by microRNAs. Through the NER pathway evaluated in lymphocytes, our pilot research establishes a connection between certain miRNAs and DRC levels. There haven't been many research done to clarify the connection between plasma miRNA expression and DRC in BC. Most investigations into this association have been conducted in tumour tissues or with the use of in vitro models. Let-7b, miR-18a-5p, miR222-3p, and miR-520-3p were the first four miRNAs that we discovered to have a negative correlation with DRC within the range of low DRC levels. This is the first time a negative association is shown in patients with low DRC, whereas high let-7b expression has been linked to BC patients with high DRC. MiR-18a has been shown to be elevated in BC and other cancer types, which runs counter to our findings. Additionally, mechanistic investigations demonstrate that miR-18a plays a significant part in suppressing the DNA repair protein ATM in breast tumour tissues. The inverse relationship between the levels of miR-18a-5p and DRC may be partly explained by this. Numerous studies on miR-222-3p in BC and tamoxifen resistance have been conducted. Furthermore, via suppressing the expression of RAD51 in ovarian cancer cells, this miRNA has been associated with DNA damage response. There were no reports on miR-520-3p's expression alterations in BC or any connections to DRC. Only miR-299-5p and miR-373 have been mechanistically connected to DNA repair among the 18 candidates identified as DRC-related. According to Yan and colleagues' research, miR-299-5p expression and RAD21 expression are negatively associated. A protein called RAD21 is involved in the repair of double-strand breaks. In the breast cancer cell line MCF-7, forced expression of miR-373 results in a decrease in the NER proteins RAD23B and RAD52, according to a mechanistic investigation by Crosby and associates.

Multivariate Analyses:

This was done because of the variance shown in the heatmap matrix. According to the Results, the DRC levels and case-control stratifications were the best factors to represent the data variability. The PC method has been used in several investigations to minimize and explain biological variability. This approach was utilized by Wei et al. to examine 1046 miRNAs in tumors from esophageal cancer patients. Their findings used 6 components to demonstrate all data variance. This approach was also employed by Sedna et al. to research miRNAs isolated from women's whole blood who were stratified by age. This group provided an example of a PC analysis that addressed 40.8% of the variance in the data. However, with only two components, our PC model explains 69.0% of the data variability. The best estimate based on the eigenvalue graph is two components, even though they do not accurately reflect the data since they do not account for all of its variability. It is also crucial to draw attention to the fact that the miRNAs included in the PC matrix substantially differed

in expression between cases and controls, indicating that they are relevant to BC in our cohort. The DRC levels might be connected to data variability, according to the PC analysis.

CONCLUSION

In conclusion, we discovered 40 miRNAs associated with BC that may be crucial to the epigenetics of Hispanic BC patients. Four miRNAs are shown to be adversely regulated in BC patients with low DRC levels, according to this pilot study's findings. The PC study also revealed that particular miRNA expression may not be directly influenced by clinicopathological traits. To establish a comprehensive framework addressing the overall DRC levels, miRNA expression patterns, and the tumor features, further research is required. This information will play a crucial role in the investigation of prognosis, recurrence, and treatment outcomes depending on the overall DRC levels once our findings have been confirmed with a larger sample size. A multivariate analysis was carried out to analyses data variability using the following stratifications: case or control classification, DRC levels, tumor grade, and molecular subtype classification.

REFERENCES:

- [1] N. Habermann *et al.*, "No effect of caloric restriction or exercise on radiation repair capacity," *Med. Sci. Sports Exerc.*, 2015, doi: 10.1249/MSS.0000000000000480.
- [2] J. Matta *et al.*, "Estrogen receptor expression is associated with DNA repair capacity in breast cancer," *PLoS One*, 2016, doi: 10.1371/journal.pone.0152422.
- [3] D. Nikitina *et al.*, "Relationship between caffeine and levels of DNA repair and oxidative stress in women with and without a BRCA1 mutation," *J. Nutrigenet. Nutrigenomics*, 2016, doi: 10.1159/000439110.
- [4] F. Caple *et al.*, "Inter-individual variation in DNA damage and base excision repair in young, healthy non-smokers: Effects of dietary supplementation and genotype," *Br. J. Nutr.*, 2010, doi: 10.1017/S0007114509993540.
- [5] C. Ortiz, J. Encarnación, R. Vergne, W. Vargas, and J. Matta, "Abstract 3286: Correlation between vitamin D levels and DNA repair capacity in breast cancer patients stratified by molecular subtypes," *Cancer Res.*, 2017, doi: 10.1158/1538-7445.am2017-3286.
- [6] S. Wongvijitsuk, P. Navasumrit, U. Vattanasit, V. Parnlob, and M. Ruchirawat, "Low level occupational exposure to styrene: Its effects on DNA damage and DNA repair," *Int. J. Hyg. Environ. Health*, 2011, doi: 10.1016/j.ijheh.2010.09.007.
- [7] J. L. Matta, L. Morales, J. Dutil, M. Bayona, C. Alvarez, and E. Suarez, "Differential expression of DNA repair genes in Hispanic women with breast cancer," *Mol. Cancer Biol.*, 2009.
- [8] W. Zhou *et al.*, "Gene-smoking interaction associations for the ERCC1 polymorphisms in the risk of lung cancer," *Cancer Epidemiol. Biomarkers Prev.*, 2005, doi: 10.1158/1055-9965.EPI-04-0612.
- [9] P. T. Campbell, "Abstract CN06-02: Insight into colorectal cancer etiology through MPE: Unmasking the links with obesity and smoking," *Cancer Prev. Res.*, 2013, doi: 10.1158/1940-6215.prev-13-cn06-02.
- [10] C. Rödel, "SP-0459: Biomarker-driven personalised radiation therapy," *Radiother. Oncol.*, 2014, doi: 10.1016/s0167-8140(15)30564-8.

CHAPTER 9

AN EFFECTIVE GENE EXPRESSION TOOL FOR YEASTS: DNA MICROSPHERES COATED WITH BIOAVAILABLE POLYMER

Ashwini Malviya, Associate Professor

Department of uGDX, ATLAS SkillTech University, Mumbai, Maharashtra, India

Email Id-ashwini.malviya@atlasuniversity.edu.in

ABSTRACT:

One of the processes required for gene therapy and genetic alteration is gene delivery. DNA's negative charge, which causes rejection by the negative cell membrane, makes it difficult to transfer DNA into cells. In the present study, bioavailable polymers polyethylene imine and polycaprolactone were applied to DNA spheres that had DNA encoding for a specific gene during a quick, one-step nonchemical process. The polymers were used to balance the DNA's negative charge. Our research demonstrates that the DNA nanospheres were able to enter the cell without harming it and that they also expressed the appropriate gene once inside.

KEYWORDS:

Appropriate Gene, Genetic, Gene Delivery, Polycaprolactone.

INTRODUCTION

Gene delivery is still difficult. The proper operation of nucleic acid inside a cell requires the resolution of a number of challenges. The target cell must first get the nucleic acid. Despite how simple it may seem; this is really the first and most difficult step. The negative charge of the cell membrane repels the substantial negative charge of nucleic acid. Finding methods to improve yeast transformation the absorption and assimilation of external genetic material has received a lot of attention lately. The efficacy of *S. cerevisiae*'s transformation was shown to be increased by monovalent cations like Na⁺, K⁺, Rb⁺, Cs⁺, and, notably, Li⁺, but not by divalent cations like. These monovalent cations' moderate chaotropic impact during the transition may be the cause of their efficiency. For accelerating transformation, mechanical techniques like electroporation and biolistic techniques were also developed. In the biolistic approach, DNA-coated metal microprojectiles may be fired into cells to change them. The glass beads used in the glass bead approach physically harm the cell, allowing DNA to enter more easily.

Viral vectors or polymers that make it easier for nucleic acids to enter the cell are further methods for transformation. In this study, we employed positively charged bioavailable polymers to transport genes. The DNA was coated with two polymers, polyethyleneimine and polycaprolactone, to neutralize the negative charge and allow it to enter the cell [1], [2]. An amine group and two carbon aliphatic CH₂CH₂ spacers make up the repeating units of polyethyleneimine, also known as polyuridine. Primary, secondary, and tertiary amino groups are present in the branching PEIs. Industrial-scale production of PEI is used for a variety of purposes, most of which are related to its polycationic nature. The branching PEIs at all molecular weights are liquids. After poly-l-lysine, PEI was the second polymeric transfection agent to be identified. DNA microspheres are compressed by PEI into positively charged particles that attach to anionic residues on cell surfaces that are engulfed by the cell via endocytosis.

PCL has attracted a tremendous lot of attention lately. Due to its ester group, which quickly undergoes hydrolysis in the live cell, it is known to be a biodegradable polymer. According to

research, aerobic and anaerobic bacteria that are found in a variety of environments may break down PCL. *Penicillium* spp. were also used to study the breakdown of high molecular weight PCL. Due to its mechanical characteristics, miscibility with a wide variety of other polymers, and biodegradability, polycaprolactone is a significant polymer. PCL is employed, for example, as a medicine delivery device, and has particular uses in the human body that have been authorized by the Food and medicine Administration. Additionally, it has been researched as a framework for tissue engineering-based tissue healing. As soon as the amines are within the cell, protonation causes them to become counter-ions, which lowers the osmotic potential. Osmotic swelling causes the vesicle to rupture, releasing the polyplex into the cytoplasm.

The DNA may freely diffuse to the nucleus if the polyplex unpacks. We created DNA microspheres in one step using a nonchemical approach, and then son chemically coated these microspheres with PEI and PCL for insertion into cells. With the advancement of nanotechnology over the last two decades, several synthetic manufacturing techniques for diverse types of nanomaterials have been created. One of the most effective methods for producing organic and inorganic NP, core-shell nanostructures, nano-/microspheres, and other nanosized substances is sonochemistry. Shulick and Grin staff were the first to demonstrate that ultrasound can be used to synthesize nonaqueous liquid-filled microcapsules and air-filled microbubbles. It has been shown that a variety of proteins, including bovine serum albumin, human serum albumin, and hemoglobin, may be used to create microscopic gas- or liquid-filled proteinaceous microspheres[3], [4].

This method was recently expanded to include the encapsulation and delivery of medicines into cells using bovine serum albumin microspheres. In order to create RNA and DNA hydrophobic-solvent-filled nucleic acid nanospheres, the micro spherization technique was further expanded. The RNA nano capsules demonstrated stability at room temperature for at least a month. The DNA Nano capsules created employing ultrasonic waves were resilient to a variety of temperatures, pHs, and DNases and enable the delivery of genetic information to *E. coli* competent cells and human U2OS cancer cells, where effective protein production was obtained. Because of its widespread distribution and outstanding capacity for developing resistance, *Candida* was selected as a transfection model. *C. albicans* is a significant pathogen that may cause invasive candidiasis as well as topical infections. In their lifetime, more than 75% of women will have *C. albicans* infection. The fourth most common cause of nosocomial infections in patients' bloodstreams is *Candida albicans*. This may cause hospital patients to develop a systemic infection that is exceedingly deadly and has a fatality rate of 30%.

In recent decades, there have been more synthetic antifungal substances and therapeutic drug classes available to treat candidiasis, including polyenes, azoles, purine analogues, and echinocandins. However, since fungal diseases are eukaryotes, they share some of their basic functions with human cells. As a result, using antifungal medications may have serious negative side effects. Additionally, the necessity for affordable therapies to address oral candidiasis and the rising pathogen resistance to synthetic drugs have sparked the hunt for innovative solutions in this area. The effective son chemical synthesis of DNA nanospheres coated in the aforementioned bioavailable polymers is described in the present work. As shown by their capacity to produce the GFP and cherry genes introduced into the *Candida* cells, the DNA nanospheres were able to penetrate *Candida albicans* cells and maintained their functionality. After the nonchemical process, a polydisperse solution containing microspheres that varied in size from 5 nm to 7 m was produced. Dynamic light scattering was used to determine the size distribution of the polymer-coated DNA spheres in aqueous solution. The results are given in.

DISCUSSION

It was made an attempt to separate the little spheres and submit them to additional investigation since it was thought that small spheres would be readily implanted into the *Candida* cells. A PVDF syringe filter with a 200 nm pore size was used for this. Despite our best attempts, we also found bigger capsules. The partial aggregation of the smaller spheres is what gives the bigger size. The tests involving live cells only used the filtered, tiny microspheres. The size of DNA polymer microspheres coated with PEI as-prepared varied from 700 nm to 6500 nm, with a mean size of 1930 nm, according to the DLS data. The solution was filtered since this size was too big for the microspheres to be used for insertion into live cells. The size of PEI-coated, filtered DNA spheres ranged from 59 nm to 712 nm, with an estimated average size of 162 nm. A bimodal distribution was found, with average diameters of 7.5 nm and 102 nm for the filtered DNA microspheres coated with PCL, which ranged in size from 5 nm to 1000 nm. By measuring the ζ -potential, the impact of the PEI and PCL polymers on the charge of the DNA microspheres was investigated. The nucleic acid phosphates are towards the outside of the capsule, as shown by the DNA sphere's surface's negative charge. It is essential to cover the sphere with a substance that will neutralize the negative charge in order to promote penetration into the cells.

For this, PEI and were the two polymers that were selected. We treated the cells with the spheres present as per the instructions in the experimental section in order to examine the capacity of DNA_PCL and DNA_PEI tiny microspheres to pass through the *Candida* membrane and enter the cell. Following incubation, the cells were fixed on cover slides and inspected with an Olympus-FV1000 confocal fluorescence microscope. The existence of the FITC-labeled microspheres in the cytoplasm and their capacity to pass through the cell membrane are confirmed by the green fluorescence that is seen within the cells. Due to their enhanced positive charge and hence greater attraction to the cell surface, DNA_PCL and DNA_PEI microspheres had similar penetration capacities when compared. But it's crucial to keep in mind that the stronger attraction of the more positively charged particles and their increased toxicity are in a very delicate balance. The PCL microspheres were the best choice because of their optimal charge, which increased their attraction to and penetration into the cell without being too high to cause significant toxicity, while the PEI caused some cell death in *Candida* culture due to its higher positive charge[5], [6].

We created cherry-encoding microspheres from DNA that were coated with PCL and included soy oil. The microspheres were delivered to *Candida* cells in their prepared state, with no further purification necessary other than filtering to remove the smallest spheres. The cells were treated with the microspheres for 16 hours at 37 degrees Celsius. They were studied using confocal microscopy after the incubation. The control group, or *Candida* cells not receiving any treatment with the microspheres. The light that was seen was the cells' natural autofluorescence, which is common in live cells. A quantitative computation of the fluorescence in both the control and experimental groups, taking the present experiment's standard deviation into account. By comparing the fluorescence intensities of cells that had been left untreated and cells that had been given the encoding microspheres' treatment, the quantitative calculations were carried out. The ImageJ software was used to analyse these fluorescence readings. A fluorescence signal of more than 160 a.u. was measured when using the mCherry encoding microspheres, compared to the control group's fluorescence of just 80 a.u. Results identical to the control group were obtained when treating *Candida* cells with microspheres made of soy oil and water together with PEI or PCL but without DNA, ruling out the hypothesis that the microspheres were the source of the fluorescence rather than the DNA encoding the gene. Conclusion: When cells are treated with son chemically created microspheres that encode for the production of cherry, the amount of fluorescence is twice as

great as it is in the control group. After determining the fluorescence of at least 300 cells, the quantitative calculations were made using the ImageJ programme. Results from a different experiment examining GFP gene expression. The results demonstrate the production of GFP in *Candida* cells after treatment with PCL-coated DNA microspheres expressing the green fluorescent protein[7], [8].

A high-intensity ultrasonic probe was used to create the DNA microspheres. The acoustic cell had a capacity of 10 mL, and the combined volume of all the contents was 1.67 mL. Acoustic power output from the ultrasonic transducer was 26.7 W/cm². The reaction cell's temperature was originally set at 22°C. The cell was subjected to 3 minutes of sonication and placed in an ice bath to eliminate any temperature gradients introduced by the acoustic waves. When making protein microspheres, the traditional ratio between the aqueous and organic phases is 3:2. When making DNA microspheres, this ratio was maintained. Making DNA_PEI Encoding Microspheres PEI, a branched chain polymer, 50% in water, Mw 750,000, was acquired from Sigma Aldrich. 1.5 g of DNA was added to 1 mL of 5% PEI aqueous solution. The aqueous solution was then given 0.67 mL of soy bean oil. A confocal microscope with Nomarski optics, the Olympus-FV1000, was used to observe and photograph materials for light microscopy. Drop by drop, 1 mL of polyline solution-coated microscope cover slip was filled with cell suspension. The droplet was removed after 30 minutes, and 1 mL PFA 4% was then applied to the cover slip for 11–18 minutes to fix the cells. PFA was removed, and the slide was then twice-washed with 1 mL of saline.

The experimental solutions were put into a disposable cuvette and measured in accordance with the recommended procedure provided by the manufacturer using a Malvern zettaliter NS equipped with an electrophoretic laser Doppler anemometry and photon correlation spectroscopy, respectively. The *C. albicans* clinical strain employed in this investigation was located in the bacteriological laboratory of the Meir Hospital in Far-Saba, Israel. To acquire fresh culture multiple colonies that were transferred into NB + 4% glucose at an initial optical density of 0.1 at 660 nm, the strains were regularly inoculated from overnight cultures of *C. albicans* maintained on NA supplemented with 2% glucose. Until mid-logarithmic phase, cultures were allowed to develop in a rotary-shaker incubator at 37°C. The cells were then taken out and put through three saline washings. The logarithmic phase cells were moved to new nutritional medium, the microsphere stock solution was added, and the cells were incubated for 16 hours at 37°C with 160 rpm of agitation. Colony forming units were counted following the proper dilution on agar plates, overnight incubation, and calculation of the number of colonies per mL to determine the survival rate. Control *Candida* cultures were grown without microspheres[9], [10]. The following equation was used to compute the viability decrease percentage.

CONCLUSION

In this paper, we show a unique, simple, one-step method for creating DNA nanospheres coated in the biodegradable polymers PEI and PCL. The DNA nanospheres have the ability to enter cells directly and express genes there. This research gives proof that DNA nanospheres might perhaps form as The *C. albicans* clinical strain employed in this investigation was located in the bacteriological laboratory of the Meir Hospital in Far-Saba, Israel. To acquire fresh culture multiple colonies that were transferred into NB + 4% glucose at an initial optical density of 0.1 at 660 nm, the strains were regularly inoculated from overnight cultures of *C. albicans* maintained on NA supplemented with 2% glucose. Until mid-logarithmic phase, cultures were allowed to develop in a rotary-shaker incubator at 37°C. The cells were then taken out and put through three saline washings. The logarithmic phase cells were moved to new nutritional medium, the microsphere stock solution was

added, and the cells were incubated for 16 hours at 37°C with 160 rpm of agitation. Colony forming units were counted following the proper dilution on agar plates, overnight incubation, and calculation of the number of colonies per mL to determine the survival rate. Control *Candida* cultures were grown without microspheres. a brand-new class of pharmaceuticals.

REFERENCES:

- [1] C. S. Tsai, S. Kwak, T. L. Turner, and Y. S. Jin, “Yeast synthetic biology toolbox and applications for biofuel production,” *FEMS Yeast Research*. 2015. doi: 10.1111/1567-1364.12206.
- [2] S. K. Gupta and P. Shukla, “Gene editing for cell engineering: trends and applications,” *Critical Reviews in Biotechnology*. 2017. doi: 10.1080/07388551.2016.1214557.
- [3] A. Weninger, A. M. Hatzl, C. Schmid, T. Vogl, and A. Glieder, “Combinatorial optimization of CRISPR/Cas9 expression enables precision genome engineering in the methylotrophic yeast *Pichia pastoris*,” *Journal of Biotechnology*. 2016. doi: 10.1016/j.jbiotec.2016.03.027.
- [4] L. Wong, J. Engel, E. Jin, B. Holdridge, and P. Xu, “YaliBricks, a versatile genetic toolkit for streamlined and rapid pathway engineering in *Yarrowia lipolytica*,” *Metab. Eng. Commun.*, 2017, doi: 10.1016/j.meteno.2017.09.001.
- [5] L. Berg, T. A. Strand, S. Valla, and T. Brautaset, “Combinatorial mutagenesis and selection to understand and improve yeast promoters,” *Biomed Res. Int.*, 2013, doi: 10.1155/2013/926985.
- [6] X. Jiao, Q. Zhang, S. Zhang, X. Yang, Q. Wang, and Z. K. Zhao, “Efficient co-expression of multiple enzymes from a single promoter mediated by virus 2A sequence in the oleaginous yeast *Rhodospiridium toruloides*,” *FEMS Yeast Res.*, 2018, doi: 10.1093/femsyr/foy086.
- [7] A. Domröse, R. Weihmann, S. Thies, K. E. Jaeger, T. Drepper, and A. Loeschcke, “Rapid generation of recombinant *Pseudomonas putida* secondary metabolite producers using yTRES,” *Synth. Syst. Biotechnol.*, 2017, doi: 10.1016/j.synbio.2017.11.001.
- [8] J. Qin, M. J. Li, P. Wang, M. Q. Zhang, and J. Wang, “ChIP-Array: Combinatory analysis of ChIP-seq/chip and microarray gene expression data to discover direct/indirect targets of a transcription factor,” *Nucleic Acids Res.*, 2011, doi: 10.1093/nar/gkr332.
- [9] E. M. Airoidi *et al.*, “Predicting cellular growth from gene expression signatures,” *PLoS Comput. Biol.*, 2009, doi: 10.1371/journal.pcbi.1000257.
- [10] K. Mysore *et al.*, “Yeast interfering RNA larvicides targeting neural genes induce high rates of *Anopheles* larval mortality,” *Malar. J.*, 2017, doi: 10.1186/s12936-017-2112-5.

CHAPTER 9

BREAST CANCER HOMOLOGOUS RECOMBINATION DEFICIENCY CORRELATED WITH DNA HELICASE GENE EXPRESSION

Raj Kumar, Assistant Professor

Department of uGDX, ATLAS SkillTech University, Mumbai, Maharashtra, India

Email Id-raj.kumar@atlasuniversity.edu.in

ABSTRACT:

The sensitivity to platinum-containing drugs and PARP inhibitors is closely related to homologous recombination deficiency, which is currently measured by the homologous recombination deficiency score, which includes the score of telomeric allelic imbalance, large-scale transition, and loss of heterozygosity. DNA helicases use ATP hydrolysis to unwind double-strand DNA, which is a crucial step in the homologous recombination repair process. In our work, the relationship between the HRD score and the expression of DNA helicase genes in breast cancer was examined. Both in BRCA-mutated and BRCA wild-type breast cancer, overexpression in half of the DNA helicase genes was shown to be strongly linked with a high HRD score. Additionally, a linear function given by five DNA helicase genes may be used to predict HRD score. Conclusion: The lack of homologous recombination repair in breast cancer is closely related to the overexpression of certain DNA helicase genes.

KEYWORDS:

Heterozygosity, Homologous, Platinum-Containing, Recombination.

INTRODUCTION

DNA helicases are proteins that use the energy from ATP hydrolysis to unwind DNA into a single-strand structure. They are also crucial elements in the homologous recombination repair process used to fix DNA double-strand breaks, where the creation of single-strand DNA was crucial. Germline mutations in certain DNA helicase genes may result in syndromes that increase the risk of developing cancer, such as the Bloom syndrome and the Werner syndrome. Additionally, it is well documented that the Branes phenotype in breast cancer and the loss of function in DNA helicase genes such as RECQL, BLM, WRN, RECQL5, and BRIP1 are closely connected with the development of breast cancer and its carcinogenesis. When there is a genomic scar present, such as telomeric allelic imbalance, large-scale transition, and loss of heterozygosity, it is known as the "Branes phenotype" in breast cancer and can be detected using single nucleotide polymorphism profiles. The HRD score is the result of adding the TAI, LST, and LOH together numerically; an HRD score of 42 or above is considered to indicate the presence of the Branes trait. In BRCA1 and BRCA2 germline wild-type triple negative breast cancer, it has been shown that the Branes phenotype is substantially linked with the responsiveness to platinum-based chemotherapy and PARP medicines. Despite the fact that the mechanism for the precise cause of HRD in those samples remained unknown, it is significant that in BRCA wild-type TNBC, the proportion of branes phenotypic was demonstrated to be above 50%. Therefore, it is crucial to identify the molecular characteristics of breast cancer with a branes phenotype in order to comprehend the precise process and create a more practical biomarker for the assessment of HRD [1], [2].

While many recent papers have demonstrated that the altered expression in DNA helicase genes including BLM, RECQL5, SLFN11, and ATM have an impact on the HRR efficiency and subsequently sensitivity to platinum-based chemotherapy and PARP inhibitors, previous studies have concentrated on the mutation of targeted genes in the HRR pathway.

Additionally, investigations revealed that DNA damage and susceptibility to PARP inhibitors might be caused by small compounds that block DNA helicases, such as BLM and WRN. Thus, it justifies our investigation into how the expression of DNA helicases, crucial elements of the HRR pathway, affects the assessed HRD status in breast cancer. In this work, we thoroughly examined the relationship between the HR status of breast cancer as determined by the HRD score and the expression of DNA helicase genes involved in HR. Both breast tumors with BRCA1/2 mutations and those with BRCA1/2 wild-type showed a significant connection between the overexpression of DNA helicase genes and HRD. Five DNA helicase genes were found to form a gene signature that is very accurate in predicting the HRD score.

Unless otherwise stated, R software was used for data collecting and analysis. RNA-seq and clinical data were retrieved using the Claviolines R/Bioconductor programmed from the TCGA dataset. In addition to the germline mutation status of the BRCA1/2 genes, the three genetic signature scores and HRD score of breast tumors from TCGA were obtained from prior research. Utilizing methods created by researchers utilizing Affymetrix SNP6 data received from TCGA, the genetic signature score is determined. The normalization of RNA transcript readings uses fragments per kilobase of transcript per million mapped reads upper quartile. According to our previous publications, the `jQuery`, `Download`, and `Deprecate` functions were used to download and prepare FPKM-UQ RNA-seq data. Using the "ComplexHeatmap" software, unsupervised hierarchical clustering and heatmap creation were carried out. The students' `t`-test was used to compare the gene expression levels and HRD scores between the groups. Values were two-sidedly computed, and statistical significance was defined as less than 0.05[3], [4].

Correlation Analysis and Model Construction:

The function from the R package was used to create the best multivariate model. Under the general convex loss scenario, the programmed employs the primal dual active set method to solve the best subset selection issue. The techniques may be used to choose variables for a linear model. The Pearson correlation coefficient was used to assess the correlation analysis between the anticipated HRD and the actual HRD score. The study comprised 871 instances of breast cancer patients, and genomic scar scores from earlier research, including TAI, LST, and HRD-LOH, were gathered. 43 of them had BRCA1 or BRCA2 germline mutations, with 23 patients having pathogenic mutations and the other patients having nonpathogenic mutations. The average HRD score in the cohort of people with BRCA pathogenic mutations, which was 58.9, served as the benchmark for identifying high and low HRD scores. As a result, a score more than 59 was deemed to indicate a high HRD, whereas a score less than 59 indicated a low HRD. This HRD cutoff score is set higher than the standard cutoff of 42. In the research, 22 DNA helicase genes involved in homologous recombination were examined. A correlation heatmap was created based on the calculation of the association between the expression of DNA helicase genes and HRD score.

As they exhibit extremely comparable correlations with each gene, the scores of TAI, LST, and LOH were substantially associated with one another. According to their link with the HRD score, the 22 DNA helicase genes may be split into 4 groups after being clustered by the K-means method. Among these, the HRD score, which was included in group 4, showed a substantially favourable connection with the expression of BLM, PIF1, POLQ, and PARPBP. Three of the 22 genes in group 1 had a modestly negative connection with HRD score, whereas six of the 22 genes were in group 3, which had a modestly positive correlation with HRD score. There was no discernible relationship between the HRD score and the other nine genes. While no correlation was found between the expression of SLFN11 and HRD

score in breast cancer in this study, SLFN11 expression has previously been shown to be correlated with homologous recombination efficiency and drug sensitivity to PARP inhibitor in non-small-cell lung cancer.

The relationship between gene expression and HRD score was next examined in individuals with and without BRCA mutations. When compared to the BRCA wild-type and nonpathogenic mutation groups, breast cancer with pathogenic germline BRCA mutations had a higher HRD score. Between the nonpathogenic mutant group and the wild-type group, there was no discernible difference. Although no single genetic alteration can be traced to explain the process, 17.5% of BRCA wild-type breast cancer cases had HRD scores that were higher than the norm for BRCA mutant cases. All of the positively correlated genes, with the exception of RECQL4, showed higher expression in HRD high patients regardless of the presence of a BRCA mutation, whereas the three negatively correlated genes showed lower expression in the HRD high group only in BRCA wild-type cases. There was no discernible change in expression between the HRD low group and the BRCA-mutated group. The aforementioned findings suggested a common mechanism that underlies HRD-high groups independent of BRCA mutant status[5], [6].

DISCUSSION

This research examined the relationship between the HRD score and the expression of DNA helicase genes. Both BRCA1/2-mutated breast cancers and BRCA1/2 wild-type breast tumors showed a significant connection between the overexpression of DNA helicase genes and HRD. Additionally, a very accurate linear model was created utilizing the mRNA expression of five DNA helicase genes to predict the HRD score. It has been shown that HRD and DNA helicase gene overexpression are related with breast cancer. BLM is involved in both BRCA1-related and unrelated homologous recombination repair, as shown by previous research that demonstrated that overexpression of BLM may accelerate the incidence of DNA damage and that knockdown or lack of BRCA1 encouraged the overexpression of BLM. The overexpression of several DNA helicase genes, however, was shown to be strongly linked with HRD in our work, revealing a common mechanism between them for the first time. The precise molecular process must be revealed via more research. As first-line and second-line treatments for breast cancer patients with hereditary BRCA1/2 mutations, PARP inhibitors such as Olaparib, rucaparib, niraparib, and talizumab have shown strong efficacy. The PARP inhibitor was similarly efficacious in BRCA1/2 wild-type cells with an HRD phenotype, as shown by molecular and early clinical studies.

In contrast to measuring gene expression, measuring HRD score is presently more costly and cumbersome. Our research shown that the expression of DNA helicase genes may accurately predict HRD score in breast cancer, providing a method for evaluating the Branes phenotype in breast cancer. Other small compounds that target the HRR pathway through DNA helicase proteins in breast cancer have been explored as possible treatments despite PARP inhibitors. The proliferation of breast cancer cells could be restricted in a RECQL5-dependent way by a small chemical that binds selectively to the DNA helicase RECQL5 and stabilizes the connection between RECQL5 and RAD51. The fact that the aforementioned work was conducted on the MCF-7 cell line, which has the wild-type BRCA1/2 gene, indicates that the HRR pathway may also be a target for BRCA1/2 wild-type breast cancer. Additionally, research revealed that utilizing a CHK1 inhibitor in cancer cells lacking in WRN might have a synergistic lethal effect. Together with the findings of our investigation, the expression of DNA helicase may serve as a diagnostic tool for determining the HRR status of breast cancer patients as well as a therapeutic target. The fact that the generated model has only been evaluated in one database places restrictions on our investigation. Future studies should

include validation using additional breast cancer databases. Additionally, as mentioned by numerous recent reports using a variety of methods, this model may be experimentally validated to demonstrate HR deficiency in cancer. For instance, a recent study evaluated the response of a PARP inhibitor using autophagy-proficient and -defective breast cancer cells and a xenograft SCID-mice model. Building breast cancer cell lines downregulating HELQ and overexpressing DNA helicases BLM, FIGL1, PIF1, or FBXO18 might be used to further validate our findings.

Measurements like the measurement of H2A γ foci should be used to assess the effectiveness of HRR in the created cell lines. It is important to assess PARP inhibitor sensitivity. 2-3% of people worldwide suffer from the chronic skin condition psoriasis, which is immune-mediated. Psoriasis's pathophysiology is still poorly understood. Currently, it is thought that genetic and environmental variables work in concert to develop an immune system dysfunction. Thus, mounting evidence supports the importance of epigenetics, notably DNA methylation, which is a covalent alteration of the cytosine in the CpG dinucleotide to generate 5-methylcytosine and is preferentially catalysed by a methyltransferase. The majority of CpG islands that are largely found in the promoter and exon sections of structural genes experience this form of methylation; as a result, these islands often take part in the control of gene transcription as a reversible and heritable epigenetic process [7], [8].

The complementary and alternative therapy known as traditional Chinese medicine has been successful in treating psoriasis. Psoriasis is separated into several syndrome kinds in order to adopt various therapy regimens in TCM, which often employs a treatment strategy based on the classification of syndromes. The two most prevalent forms of psoriasis vulgaris are blood heat syndrome and blood stasis syndrome. The TCM syndrome theory is based on the holistic idea that "man is an integral part of nature a pathological summary of the body at a particular stage of the disease's development that emphasizes the interaction between time, space, the human body, and the external environment, thus reflecting the overall state of the body at that stage. This is consistent with the emphasis of epigenetics on the significant role of acquired environmental factors in human diseases. One of the fundamental pillars of TCM theory, which guided the application of clinical treatment regimens and clinical success, is the concept of TCM syndromes. TCM syndromes are still classified as macroscopic clinical manifestations for the time being. There aren't any accurate, quantitative, systematic scientific assessment indicators since dialectics is founded on the individual clinical experience of clinicians. The principles of epigenetics and TCM are similar, and there may be some crossover in the study approaches.

Therefore, the use of epigenetics in the study of TCM diseases will open up new avenues for research. In order to participate in the research, participants had to provide written agreement. Psoriasis patients and healthy individuals were chosen from the Dermatology Clinic at the Yueyang Hospital of Integrated Traditional Chinese and Western Medicine in Shanghai, China. Basic subject data, the PASI, were recorded. At least two dermatologists made the diagnosis. To reduce clinical heterogeneity, patients with generalized psoriasis vulgaris who satisfied the diagnostic criteria of BHS and BSS for psoriasis according to TCM were included. Prior to sample collection, patients were forbidden from using any topical or systemic medications for at least a month. Peripheral blood mononuclear cells were then extracted from each patient's 2 mL of blood after it had spent 24 hours in a refrigerator set at 20°C. The following procedures, among others, were carried out using the Illumina Infinium Human Methylation 850 BeadChip according to the instruction booklet. Further methylation data analysis could be carried out since, according to the QC report test, the samples' quality control indicators complied with Illumina's standards for quality. Shanghai Biochip Company provided assistance with data analysis. The R software minfi package was used to preprocess

the chip's original data before the IMA programme was used to check for variations in methylation sites and regions across the groups. Data quality control, preprocessing, analyses of DMSs, and studies of differentially methylated areas were the four processes that made up the analysis of the complete methylation. The level of methylation of the relevant site is often gauged using the beta value. The range of values is closer values to 1 and closer values to 0 indicate greater and lower levels of methylation, respectively, at the location. Using the pool t-test technique and the screening criteria of value 0.05 and $|\text{beta difference}| > 0.14$, we evaluated the DMSs across groups.

The differentially methylated region linked genes were mapped to the terms of the GO and KEGG pathway databases using the cluster profiler programmed in R software. The number of genes in each entry was also calculated. The GO or KEGG entries that were substantially enriched in DMR-related genes as compared to the background of the total genome were then screened using the hypergeometric test. A corrected value was utilized as the threshold after the estimated value was adjusted using the Bonferroni correction. These GO or KEGG keywords were regarded as being highly enriched in the genes with differential expression. In the genome of psoriasis BHS patients, there were 674 differential CpG sites discovered to be dispersed, but in the genome of BSS patients, there were 705 divergent CpG sites. The gene body areas were primarily enriched for the DMPs of the two TCM disorders. DMPs were mostly abundant in the TSS1500 and 5'UTR regions of the promoter in BHS and BSS patients. Both BHS and BSS patients were hypomethylated in terms of methylation expression patterns across several genomic regions and S3). DMPs were most enriched in the CGIs, followed by the shore areas, and were least enriched in the shelf regions in various CpG islands, more notably in both BHS and BSS. Except for the N shelf area, which is hypermethylated in BSS patients and S3), the methylation patterns of other regions are the similar in BHS and BSS patients, indicating hypomethylation.

According to GO enrichment analysis, the biological processes of positive regulation of potassium ion transport, positive regulation of potassium ion transmembrane transport, cyclic-nucleotide-mediated signaling, and cAMP-mediated signaling were primarily enriched in the DMGs of BHS when compared to healthy controls. As shown in and 2, the DMGs of BSS were primarily enriched in nitric oxide-mediated signal transduction, hippo signaling, response to organic cyclic compound, positive regulation of potassium ion transmembrane transport, antigen processing and presentation of peptide or polysaccharide antigen via MHC class II, and antigen processing. Rheumatoid arthritis, PPAR signaling pathway, insulin resistance, inflammatory bowel disease, AMPK signaling pathway, Epstein-Barr virus infection, Herpes simplex infection, and Adherents junction were the key KEGG pathway enrichment analyses that DMGs of psoriatic BHS were enriched in. DMGs of psoriatic BSS were mostly enriched in the metabolism of propanoate, pyruvate, and tryptophan as well as the Notch signaling pathway, type I diabetes, and valine, leucine, and isoleucine degradation. The 247 difference CpG sites we discovered after comparing and analyzing the differential sites between psoriatic BHS and BSS included 53% hypomethylated and 47% hypermethylated Cogs. The BHS and BSS samples were categorized differently according to hierarchical cluster analysis and S4)[9].

Around 68 CpG sites were found, and their distribution across the genome was determined. DMPs were significantly more abundant in the gene body and 5'UTRs regions. Only one distinct CpG site was enriched in exotic regions. DMPs were mostly hypomethylated in the 3'UTR regions and hypermethylated in the TSS1500 and TSS200 regions. Additionally, the DMPs in the 3'UTRs, 5'UTRs, and exotic regions were all hypomethylated. We discovered 60 CpG sites with various levels of methylation via analysis of the distribution in CGI areas. DMPs were more abundant in the S shelf region than in the S shore area, and they were less

common in the island areas. In contrast, the N shelf and N coast region had the lowest DMP distribution. The S coast region was also hypermethylated in terms of methylation levels. The levels of methylation were comparable in other areas.

According to GO enrichment studies, the biological processes of control of synapse structure or activity, regulation of peptidase activity, regulation of endopeptidase activity, and modulation of synaptic transmission were primarily enriched in the DMGs in psoriasis BHS and BSS patients. DMGs were mostly abundant in neuronal cell bodies, receptor complexes, and cell bodies in terms of cellular components). Heparin binding, glycosaminoglycan binding, and ATPase activity were the most enriched molecular functions. The DMGs in psoriatic BHS and BSS were mainly enriched in platelet activation, complement and coagulation cascades, regulation of actin cytoskeleton, *Staphylococcus aureus* infection, glutamatergic synapse, thyroid hormone signaling pathway, bacterial invasion of epithelial cells, and ECM-receptor interaction, according to KEGG pathway enrichment analyses. Finally, we used Spearman's correlation analysis to exclude the DMGs connected to the psoriasis PASI score. There were found to be 483 DMGs where the PASI score and methylation level linked. In order to increase the precision and rigor of the data, we set the value 0.01 and the β difference and \log_2 value 2 for screening and obtained 42 DMGs, of which 21 DMGs were negatively linked with disease severity and 16 DMGs were positively correlated.

Increasingly, methylation modification has drawn interest in recent years as psoriasis research has advanced. RNA and DNA are principally involved in methylation modification. While RNA methylation mostly controls gene expression at the posttranscriptional level, DNA methylation alteration primarily affects gene expression at the transcription stage. Numerous autoimmune skin conditions linked to psoriasis, including systemic lupus erythematosus, dermatomyositis, and scleroderma, have DNA methylation as a key pathogenic factor. Currently, skin tissues have been the subject of the majority of investigations on DNA methylation in psoriasis. The skin, however, could be the final target of a succession of immune mechanism interactions since autoimmune illness is a systemic condition. As a result, systemic therapy continues to be the mainstay of treatment for moderate to severe psoriasis. Monocytes, phagocytes, dendritic cells, T and B lymphocytes, as well as a select few additional cell types, are all found in PBMCs. They are the primary parts of immune cells and are crucial to the body's immunological response. Numerous differentially expressed genes have been linked to inflammation, which is a systemic rather than organ-specific phenomena, according to several investigations on the expression of psoriatic skin samples. In contrast, PBMCs express divergent genes in a manner that is more targeted than skin tissue.

In order to evaluate the overall methylation trend in PBMCs from psoriasis patients, the MethyLamp Global DNA Methylation Quantification Kit is being employed. According to recent research, the overall methylation trend in psoriasis is substantially higher than in healthy controls. Global DNA methylation, on the other hand, can only detect changes in the overall amount of DNA methylation and is unable to identify alterations at particular loci. Skin tissue investigations of the whole genome, however, showed that psoriatic samples were hypomethylated. Therefore, more confirmation and in-depth analysis are needed to fully understand the DNA methylation level of psoriasis in PBMCs. In this investigation, we employed the Illumina 850k methylation chip, which comprises more than 90% of the original 450k chip and can determine the methylation state of around 853,307 CpG sites in the human genome. We discovered that the DMSs in PBMCs of patients with psoriasis predominantly included hypermethylation and further classified psoriasis into two TCM syndromes: the BHS and BSS. This was done by comparison of DNA methylation in PBMCs

between psoriatic patients and healthy controls. The DMSs exhibit hypomethylation in BSS and hypermethylation in BHS as compared to unharmed controls. DMPs were mostly found in the gene body and TSS1500 regions of the genome in psoriatic individuals. BHS and BSS had the same distribution pattern in psoriasis. Regions having more than 200 base pairs and more than 50% GC concentration are referred to be CGIs. They contribute in controlling gene expression and are often found close to the promoters of genes. The CGI, shelf, and coast zones of Cogs were separated. The majority of DMPs in both groups included hypomethylation and were considerably enriched in CGIs. Various psoriasis symptoms and healthy controls exhibit various biological processes connected to DMGs, according to bifunctional informatics. On DMGs from psoriasis patients, we also conducted KEGG pathway enrichment analysis and discovered that they were primarily enriched in type I diabetes mellitus, autoimmune thyroid disease, bacterial invasion of epithelial cells, ECM-receptor interaction, tryptophan metabolism, insulin resistance, hematopoietic cell lineage, inflammatory bowel disease, and cell adhesion molecules, among other conditions. Rheumatoid arthritis, the PPAR signaling pathway, insulin resistance, inflammatory bowel disease, the AMPK signaling pathway, and adherent junction were the most enriched DMGs in BHS psoriasis. Valine, leucine, and isoleucine degradation, pyruvate and tryptophan metabolism, the Notch signaling system, type I diabetes mellitus, and propanoate metabolism were primarily enriched in BSS psoriasis.

According to TCM, psoriasis BSS is the dormant stage of the illness, whereas psoriatic BHS is the advancing stage. Interestingly, we discovered that Epstein-Barr virus infection and Herpes simplex infection were concentrated in the DMGs of psoriasis BHS. Infections with respiratory viruses have a significant role in the development of psoriasis. Additionally, there is evidence that having the Herpes simplex virus may increase your chance of developing psoriasis. Psoriasis' BSS suggests that it has progressed to the chronic stage; according to TCM, the illness shifts from acute to chronic as a result of pathogenic elements damaging healthy qi during the conflict between them. The TCM concept and treatment principle of strengthening the body's resistance to chronic diseases is reminiscent of the DMGs of BSS, which are enriched in the degradation of valine, leucine, and isoleucine, pyruvate metabolism, and tryptophan metabolism. These amino acids are the building blocks of proteins required for human nutrition. Unique pathogenic concepts in TCM are BHS and BSS.

When we compared the DNA methylation patterns of the two kinds of syndromes, we discovered 247 distinct methylation sites, most of which involved hypomethylation. The location of these places throughout the genome varied across populations, however. Wound healing, blood coagulation, hemostasis, and coagulation were identified by GO function studies of DMGs. The platelet activation, complement, and coagulation cascade were highlighted by KEGG pathway analysis. According to TCM, BHS is a term used to describe heat entering the blood, which often causes the blood flow to be unrestricted. Blood stasis, blocked meridians, and uneven blood circulation are the causes of BSS. According to ultrasound studies, BHS patients' and healthy skin's venous and arterial blood vessels underneath skin lesions are expanded and dilated, and blood flow is accelerated when compared to BSS in psoriasis.

Contrarily, a substantial body of research has shown that BSS is often intimately associated to circulatory or microcirculation problems, which result in aberrant blood rheology. The TRIM14 gene was considerably and negatively connected in the correlation study between DNA methylation level and psoriasis severity, while the PRDM16 gene was significantly and favourably correlated. A RING domain, two B-box domains, and a coiled-coil region make up the proteins that make up the tripartite motif family. The TRIM family includes TRIM14, which is found on chromosome 9q22. An essential component of the immunological and

inflammatory response in psoriasis is the NF- κ B signaling pathway. Studies have shown that overexpression of TRIM14 stimulates the NF- κ B signaling pathway and enhances the phosphorylation and degradation of I- κ B caused by TNF-. The STAT3 signaling pathway is crucial for the differentiation of psoriatic TH17 cells, and TRIM14 also positively regulated the protein levels of phosphorylated STAT3, as well as the mRNA and protein expression of the STAT3 signaling pathway transcriptional targets matrix metalloproteinase 2, MMP9, and vascular endothelial growth factor. Psoriasis and metabolic syndrome are strongly associated, and a substantial body of clinical research has shown that the prevalence of diabetes and obesity in psoriasis patients is much greater than that in the general population. Clinical and fundamental research has shown a link between obesity and diabetes and the expression of PRDM16, as well as the role that PRDM16 signaling plays in their respective management. Furthermore, mice with PRDM16 overexpression had higher energy expenditure, less weight gain, greater glucose tolerance, and better responses to a high-fat diet. As a result, PRDM16 may be crucial in the etiology of psoriasis. Our study discovered that methylation levels of the genes TRIM14 and PRDM16 may be significant indicators of the severity of psoriasis, but additional investigation is needed to determine the precise mechanism of action of these related genes[10], [11].

CONCLUSION

In conclusion, the current investigation revealed a tendency of hypermethylation in the DNA methylation of psoriasis-related PBMCs. DMGs are linked to several immunological and metabolic disorders and engage a number of inflammatory signal pathways. Our research also shown that the TCM syndrome kinds of psoriasis have distinct mechanisms, as evidenced by the various DNA methylation sites between BHS and BSS of psoriasis and the biological roles of the genes implicated in associated locations.

Additionally, TRIM14 and PRDM16 DNA methylation levels may function as possible biomarkers for determining the severity of psoriasis. A non-intense but chronic pathological condition results when the immune system loses the ability to eliminate the pathogenic factors and weak pathogenic elements are unable to worsen the illness. Chinese herbs having a tonic action are often used in clinical therapy to increase blood circulation and disperse stasis.

REFERENCES:

- [1] W. D. den Brok *et al.*, "Homologous Recombination Deficiency in Breast Cancer: A Clinical Review," *JCO Precis. Oncol.*, 2017, doi: 10.1200/po.16.00031.
- [2] J. J. Pitt *et al.*, "Characterization of Nigerian breast cancer reveals prevalent homologous recombination deficiency and aggressive molecular features," *Nat. Commun.*, 2018, doi: 10.1038/s41467-018-06616-0.
- [3] E. H. Lips *et al.*, "Indicators of homologous recombination deficiency in breast cancer and association with response to neoadjuvant chemotherapy," *Ann. Oncol.*, 2011, doi: 10.1093/annonc/mdq468.
- [4] M. L. Telli *et al.*, "Homologous recombination deficiency and host anti-tumor immunity in triple-negative breast cancer," *Breast Cancer Research and Treatment*. 2018. doi: 10.1007/s10549-018-4807-x.
- [5] T. Steenbruggen *et al.*, "Abstract OT1-01-08: Intensified alkylating chemotherapy in patients with oligo-metastatic breast cancer harboring homologous recombination deficiency: The OLIGO study," *Cancer Res.*, 2017, doi: 10.1158/1538-7445.sabcs16-ot1-01-08.

- [6] Z. Sztupinski *et al.*, “Migrating the SNP array-based homologous recombination deficiency measures to next generation sequencing data of breast cancer,” *npj Breast Cancer*, 2018, doi: 10.1038/s41523-018-0066-6.
- [7] R. Buisson *et al.*, “Cooperation of breast cancer proteins PALB2 and piccolo BRCA2 in stimulating homologous recombination,” *Nat. Struct. Mol. Biol.*, 2010, doi: 10.1038/nsmb.1915.
- [8] J. Wang, Q. Ding, H. Fujimori, A. Motegi, Y. Miki, and M. Masutani, “Loss of CtIP disturbs homologous recombination repair and sensitizes breast cancer cells to PARP inhibitors,” *Oncotarget*, 2016, doi: 10.18632/oncotarget.6715.
- [9] G. R. Borst *et al.*, “Neoadjuvant olaparib targets hypoxia to improve radioresponse in a homologous recombination-proficient breast cancer model,” *Oncotarget*, 2017, doi: 10.18632/oncotarget.20936.
- [10] V. Abkevich *et al.*, “Patterns of genomic loss of heterozygosity predict homologous recombination repair defects in epithelial ovarian cancer,” *Br. J. Cancer*, 2012, doi: 10.1038/bjc.2012.451.
- [11] I. Faraoni and G. Graziani, “Role of BRCA mutations in cancer treatment with poly(ADP-ribose) polymerase (PARP) inhibitors,” *Cancers*. 2018. doi: 10.3390/cancers10120487.

CHAPTER 10

DNA DOUBLE-STRAND BREAKS RELATED GENES, ATM AND GAMMAH2AX, HAVE ABNORMAL EXPRESSION IN THYROID CARCINOMA

Swarna Kolaventi, Assistant Professor
Department of uGDX, ATLAS SkillTech University, Mumbai, Maharashtra, India
Email Id- swarna.kolaventi@atlasuniversity.edu.in

ABSTRACT:

In order to detect DNA double-strand breaks and the DNA damage response, ATM and H2AX are essential. In this research, ATM and H2AX expression in thyroid cancer will be examined, and a potential link between thyroid function tests and DNA damage will be discussed. Immunohistochemistry was used to identify the expression of ATM and H2AX in 30 instances of benign nodular goiter, 110 cases of thyroid cancer with good differentiation, 22 cases of thyroid cancer with poor differentiation, and 21 cases of anaplastic thyroid cancer. Clinical and pathological characteristics, such as differentiation phases, distant metastases, lymph node metastasis, T classification, TNM stage, and thyroid function tests, were evaluated and their relationships with H2AX and ATM were examined. Compared to benign nodular goiter and healthy surrounding tissues, thyroid cancer tissues produced more H2AX and ATM. H2AX and ATM were associated with thyroid carcinoma. FT3 was linked to both the expression of ATM and H2AX. H2AX was also related to differentiation status, FT4, TSH, TNM stage, and TNM categorization. As a result, it seems that ATM and H2AX both have a relationship with thyroid hormones, and H2AX also affects how thyroid cancer differentiates.

KEYWORDS:

Carcinoma, Immunohistochemistry, Pathological, Thyroid Cancer.

INTRODUCTION

The most prevalent cancer of the endocrine system is thyroid cancer, which is linked to radiation exposure. Thyroid cancer incidence has sharply increased in recent years, in part because of advancements in the diagnosis process. The most severe kind among them, anaplastic thyroid carcinoma, is still a medical challenge and has a short survival period after diagnosis. The hereditary risk to thyroid cancer, however, is still not fully understood. Paraffin blocks comprising representative areas from each specimen were selected from paraffin blocks containing HE stained slides using the TM-1 tissue microarray kit. These paraffin blocks were then removed. After that, the cores were positioned and inserted in empty paraffin blocks. For improved tissue fixation, the blocks were heated to 60°C for 30 minutes and then cooled to room temperature. Immunohistochemistry was performed on 3 mm thick slices that were cut from tissue microarray blocks or tissue paraffin blocks. After deparaffinization in xylene, the sections underwent a series of graded alcohol dilutions for hydration. Sections were cooked in a pressure kettle for 1.5 minutes in citrate buffer and cooled to room temperature for antigen retrieval in order to detect H2AX expression. Slices were treated with anti-H2AX antibody for 90 minutes after endogenous peroxidase activity was suppressed, and then with secondary antibody for 30 minutes [1], [2]. Sections were cooked in a microwave for 15 minutes in EDTA buffer for antigen retrieval, then chilled to room temperature to detect ATM expression. Slices were treated with anti-ATM antibody for 90 minutes after endogenous peroxidase activity was suppressed, and then with secondary antibody for 30 minutes. All slices were then counterstained with hematoxylin after being

exposed to DAB for 5 minutes. At least two qualified pathologists evaluated each portion. Positive cell percentages were classified as 0, 1, 2, 3, and 4, respectively, for 0%, 0-For no staining, light yellow, yellow-brown, and brown, the positive staining intensity was determined as 0, 1, 2, and 3, respectively. Multiplying the distribution and intensity score allowed for the evaluation of the semiquantitative expression levels of ATM and H2AX. Low expression was defined as final scores below 5, and strong expression as final scores over 5. Romy lesions brought on by radiation exposure may contribute to the development of thyroid cancer. Large DNA fragment loss, aberrant mitosis, and even the activation of the cell death process may all result from a single incorrectly repaired double-strand break. Cells use a variety of mechanisms, such as DNA recombination and repair, cell cycle arrest, and apoptosis, to reverse and lessen severe DNA damage. It has been shown that both ATM and H2AX play a role in preserving genomic integrity and DSB response

Ataxia telangiectasia is a condition caused by an ATM gene deficit that is characterized by radiosensitivity, genomic instability, progressive ataxia, and susceptibility to cancer. Autoactivated ATM phosphorylates a number of substrates, including as H2AX, NBS1, CHK2, and p53, after being attracted to the DSB sites and so effecting DSB repair. Lung, breast, and prostate cancers were among the malignancies for which certain ATM alleles were linked to an elevated risk. But it has been shown that a few certain ATM alleles may provide protection against cutaneous melanoma. Various investigations have shown that ATM plays a variety of functions in thyroid cancer. According to Wojcicki et al.'s study, the ATM variation ATM rs1801516 might change BRCA1-related risk but was not linked to PTC risk. No correlation between ATM polymorphisms and PTC risk was discovered. Other studies have shown that ATM polymorphisms may contribute to thyroid cancer development. Multiple malignancies have been shown to accumulate H2AX phosphorylation, which may be mediated by ATM.

Cellular reactions to DNA damage may include activation of ATM and buildup of H2AX. In our earlier investigation, we discovered that papillary thyroid carcinoma patients had higher levels of H2AX expression, which was inversely correlated with lymph node metastases and TNM stage. Recent studies showed that H2AX was elevated in differentiated thyroid cancer patients receiving 131I treatment as well as in human primary thyrocytes exposed to ionizing radiation. However, the function of ATM and H2AX in thyroid cancer is still not well understood. Numerous hormones, including estrogen, have been shown to cause DNA damage and hence aid in the development of cancer. Recent research indicated that thyroid cancer risk was correlated with aberrant FT3, FT4, and TSH levels in individuals with thyroid cancer, among other thyroid illnesses. The thyroid hormones have a significant impact on how energy is burned. Reactive oxygen and nitrogen species are produced as a result of the increased oxygen demand brought on by thyroid hormones. And as a result, additional antioxidants produced by cells may be eaten, and antioxidant enzymes may become inactive, which would increase oxidative stress and oxidative DNA damage. As a result, we surmise that DNA damage and thyroid diseases are related[3], [4].

The link between thyroid functioning and genes associated to DSB, however, is not well known. In this research, 30 examples of benign nodular goiter, 110 cases of thyroid cancer with good differentiation, 22 cases of thyroid cancer with poor differentiation, and 21 cases of anaplastic thyroid cancer were included to examine the expression of H2AX and ATM in thyroid cancer. Data from thyroid function tests were gathered and analyzed to explore the association between H2AX and ATM expression and thyroid function tests in thyroid cancer in this research, which sought to ascertain if thyroid hormones play a role in DNA damage. In this investigation, 153 individuals with thyroid cancer and 30 patients with benign nodular gaiter were both detected. 80 incidences of benign nodular goiter were also detected in the

thyroid cancer group. In China's Zhejiang Province Cancer Hospital, thyroid cancer patients were discovered between January 2001 and August 2014, whereas benign nodular goiter patients were discovered between January 2012 and June 2012. At least two qualified pathologists concurred on the final diagnosis of benign nodular goitre and thyroid cancer. The medical records were used to document a number of clinicopathological characteristics, including age, gender, differentiation stages, lymph node metastases, and distant metastasis. Based on the TNM staging guidelines published by the American Joint Committee on Cancer in 2002, the T classification and TNM stage of the cancer patients were assessed. Triiodothyronine, basal plasma free T₃, thyroxine, basal plasma free T₄, thyroid-stimulating hormone, and thyroglobulin levels were also investigated prior to surgery and they were evaluated in accordance with the following standards. Ages of the 30 patients with benign nodular goitre were 36 to 70, with 29 female and 1 male patients. Ages of the 153 thyroid cancer patients varied from 18 to 78 years, with 104 females and 49 men. Lymph node metastases was observed in 107 cases, whereas distant metastasis was reported in 19 instances. The postoperative histological analysis revealed that 110 of the patients had good differentiation, 22 had poor differentiation, and the remaining 21 were anaplastic. Before surgery, none of the thyroid cancer patients had ever received anticancer therapy.

DISCUSSION

The indications of DSB and DDR are ATM and H2AX. They are required in the first phase that leads to DSB and may be the first molecular activities in carcinogenesis. One of ATM's substrates, H2AX, is a potential target for phosphorylation by ATM. H2AX might boost the expression of ATM whereas autoactivated ATM could increase ATM activity. Different tumors with varying functions have been shown to express ATM and H2AX abnormally. They were linked to a higher risk of cancer, according to several studies. In this investigation, thyroid cancer tissues expressed H2AX and ATM at higher levels than benign tissues. Additionally, a correlation between H2AX and ATM was found, which is consistent with the earlier work. H2AX and ATM both contribute to thyroid carcinoma. In this research, it was discovered that H2AX was correlated with thyroid carcinoma differentiation. H2AX expression levels were greater in anaplastic thyroid cancer tissues than in well-differentiated thyroid cancer tissues and lower in poorly differentiated thyroid cancer tissues. Additionally, changes in ATM expression across several histologic kinds of thyroid carcinoma were discovered that were statistically significant. Compared to well differentiated thyroid cancer tissues, anaplastic thyroid cancer tissues expressed more ATM, while well differentiated thyroid cancer tissues expressed more ATM compared to poorly differentiated thyroid cancer cells. Previous studies have shown that high-grade breast cancer has a much higher incidence of DSB-initiated genomic loss, including ATM. Furthermore, it has been shown that ATM deficiencies cause breast cancer to poorly differentiate.

H2AX overexpression has been shown to correlate with differentiation and TNM stage in gastric cancer and may be used as a biomarker. According to this study's findings, well-differentiated thyroid cancer tissues showed greater levels of H2AX and ATM expression than poorly-differentiated thyroid cancer cells [5], [6]. However, it is still unclear why tissue from anaplastic thyroid cancer expressed more ATM than poorly differentiated thyroid cancer. It may be as a result of the study's use of inadequate specimens. It is improper to draw a direct connection between ATM expression and thyroid carcinoma differentiation. However, further studies are required to examine the possible association. In light of this, we hypothesized that whereas ATM was not specifically connected with differentiation of thyroid cancer, H2AX was. H2AX was also shown to be associated with the TNM stage and T classification. Patients with an earlier T stage had higher levels of H2AX. This finding is consistent with a prior study that found that H2AX levels were elevated in premalignant

lesions and that H2AX may be crucial in the early stages of cancer. We hypothesized that H2AX could be more significant in thyroid cancer's early stages. Thyroid hormones have an important impact on many organ systems and metabolic processes. By interacting with THRB, T3 has been shown by Zambrano et al. to stimulate ATM-dependent adenosine monophosphate-activated protein kinase signaling, which is crucial for mitochondrial respiration and results in DSB in mouse embryonic fibroblasts. T3 was unable to induce senescence in the absence of ATM, whereas ATM transfection restored the response to T3. In this research, associations between thyroid function tests and ATM and H2AX expression were examined. T3 and the expression of ATM and H2AX did not correlate, according to our research. The findings, however, indicated a correlation between FT3 and both ATM and H2AX in thyroid carcinoma. Numerous disorders might be identified by the FT3 marker for the euthyroid condition, and decreased plasma levels of FT3 could impede the conversion of T4 to T3. Recent studies revealed a correlation between the likelihood of developing thyroid cancer and lower FT3 and FT4 levels and higher TSH levels. In this research, H2AX was linked to FT4 and TSH as well. We hypothesized a connection between thyroid diseases and ATM and H2AX expression despite the data being unconvincing.

Overall, H2AX has been shown to affect the differentiation status of thyroid cancer, and both H2AX and ATM were predicted to affect thyroid hormones. Further studies are required to address the connection between thyroid functions and DNA damage as ATM activation and H2AX have been identified as markers of DNA damage. The majority of solid tumours exhibit traits not seen in healthy tissues, such as excessive angiogenesis and resulting hyper-vasculature, flawed vascular architecture, compromised lymphatic drainage/recovery systems, and significantly elevated production of a variety of permeability mediators. The increased permeability and retention effect is a characteristic of tumors that makes it possible for macromolecules like lipids to enter the interstitial space of the tumor and get trapped there as a result of decreased lymphatic filtration. SMANCS, PK-1, and DNA contained in liposomes are only a few examples of lipid- or polymer-conjugated anticancer medications that may be targeted to the tumor more precisely thanks to the EPR effect. Liu et al. demonstrated that an efficient technique for transfecting DNA into the liver, lung, kidney, and heart is the fast injection of a high volume of DNA solution into a vein. The hydrodynamic approach is a technique that increases endothelial and parenchymal cell permeability as a catalyst for *in vivo* gene transfer by applying regulated hydrodynamic pressure to capillaries. According to Gao et al., hepatocytes may achieve a transfection efficiency of up to 40% when a significant volume of DNA solution is injected into them during a short period of time. In mice and rats, this approach has been utilized to transport DNA that codes for tiny proteins such as alpha1 antitrypsin, cytokines, hepatic growth factors, and hemophilia factors. By hydrodynamically delivering the IL-2 gene, Ronaldo et al. demonstrated that up to 160 ng/mL of IL-2 protein may be produced quickly and momentarily in serum. The issue with the hydrodynamic approach for gene transfer in humans is that it is impossible to get a high transfection effectiveness in a short amount of time using a DNA solution up to 12% of body weight [7], [8].

It is typical for the protein expression of genes from plasmid DNA-delivered genes to be temporary, lasting just a few days, and then to be followed by an extended period of low-level expression. Unmethylated CpG regions in the plasmid backbone are believed to trigger innate immune responses inside of cells. It has been shown that plasmids lacking CpG sequences (minicircles) which only retain the functional portion of the plasmid and no longer carry antibiotic resistance indicators or the bacterial origin of replication, may extend the time that proteins are expressed. These tiny vectors enable the long-term transient expression of many transgenes without the immunogenic reaction hazards associated with conventional

plasmids. In mouse livers three weeks after transgene administration, Chen et al. demonstrated that minicircles produced 45 and 560-fold greater serum levels of human factor IX and human alpha1-antitrypsin than their parent unrecombined plasmids. Yew et al. demonstrated that transfection of plasmid DNA depleted of nearly 80% of CpG motifs not only resulted in significantly fewer changes in blood parameters, lower levels of inflammatory cytokines, and less liver damage than transfection of unmodified vector, but also resulted in longer transgene expression in the lung and liver of immunocompetent mice. Since Feltner et al. initially discovered that a double-chain monovalent quaternary ammonium lipid, trimethylammonium chloride, efficiently binds and transfers DNA to cultivated cells, hundreds of novel cationic lipids have been created. These cationic lipids are attractive candidates for gene transfer due to their nonimmunogenic properties and simplicity of commercial manufacture. Nonviral liposomal vectors are being used in 13% of ongoing gene therapy studies throughout the globe. The Dr. Gao and Huang-developed LPD has shown potential as a nucleic acid carrier for *in vivo* transfection. The initial purpose of LPD was to effectively transport the payload nucleic acid to the tumor cells while avoiding macrophage clearance in the reticuloendothelial system. According to reports, the LPD had extremely little immunotoxicity and hardly any cytokine production in the studied animals. LPD thus offers the ability to get beyond the hydrodynamic method's transfection restrictions. In this work, we modified the LPD formula slightly and used it for nucleic acid transfection.

By promoting HCC initiation and suppressing HCC metastasis, our team has shown that the 100-kid nuclear transcription factor androgen receptor, which is encoded by the AR gene and measures around 3.2 kb, performs two distinct functions in the development of HCC. We also shown in a prior work that, in contrast to low AR expression, Sorafenib targeted treatment combined with ectopic AR expression inhibits HCC metastasis. In this study, we investigated the effectiveness of delivering an MC-liposome vector containing a 3.2 kb androgen receptor cDNA into Hepatitis B Virus -induced HCC mouse livers and tested whether an MC-carrying AR DNA vector results in expression latency in tumors using a human-relevant HBV-HCC mouse model created by Zheng et al. For one mouse injection, 200 L of LPD were made according to earlier instructions. In a nutshell, 24 g of minicircle DNA were compressed into nanometric complexes by 18 g of protamine by electrostatic contact. The complexes were combined with 30 L of a 20 mM, 100 nm, cationic liposome made of cholesterol and 1,2-dioleoyl-3-trimethylammonium-propane. Following postinsertion of 30 L of DSPE-PEG at 50°C for 10 minutes, the LPD nanoparticles were PEGylated. Twelve-to-fifteen-day old HBV-transgenic mice were administered a single injection of the hepatic carcinogen diethyl nitrosamine, as previously mentioned. Professor Ou from the University of Southern California gave the animals. The HBV-Lowden HCC mice were administered intravenously with 20 g/100 L/mouse of LPD at the age of 54 weeks twice weekly for 4 consecutive weeks. Two months after receiving minicircle DNA injections, the mice were euthanized. The livers were removed, preserved for frozen section in Tissue-Tek OCT Compound, and then cut into slices for GFP signal detection.

In vitro delivery, long-term culture, immunoblot analysis, and the AR Transactivation Luciferase Assay are 2.4. Minicircle DNA was transfected into 293T cells using a calcium phosphate precipitation technique in order to assess the expression latency of the minicircle DNA. One out of every ten cells were subculture once they had reached confluence. At days 2, 6, 10, and 14, GFP expression was found using a fluorescent microscope. For the purpose of detecting AR by western blot, the proteins were extracted 2 days after transfection. In this work, the plasmids purl-TK and ARE-luciferase reporter were used. Briefly, 24 hours before to transfection, 1-2 10⁵ cells were planted in 24-well plates. Following transfection, DHT was added 24 hours later. Cells were collected and tested using the Dual-Luciferase Reporter

Assay System in conjunction with a luminometer around 24 hours later. The O.C.T. compound was used to embed sections of normal and tumor livers, which were then frozen at 80°C. After that, the tissue slices were cut using a microtome. The portions were then fixed for 10 minutes with 1.25% glutaraldehyde. Using a Nikon Eclipse 80i camera attached to a fluorescent microscope, all sections were examined, and pictures were taken.

In this investigation, we subcloned a human AR cDNA with a full-length of 3.2 kb onto a parental plasmid called a minicircle). We produced a 10 kbp cypher by first linearizing pMCP with the BamH1 endonuclease restriction enzyme and inserting human AR cDNA. We used plasmid-transformed ZYCY10P3S2T *E. coli* in a two-step incubation to generate minicircle DNA on a bigger scale. To clone competent bacteria on a wide scale, the first incubation was carried out. After that, we activated the phiC31 and ISce1 genes in *E. coli* and kept the temperature low so that the plasmid's backbone would be broken down. Using a CSci gradient technique, the minicircle DNA was extracted after incubation. The GFP-carrying minicircle DNA and parental plasmids were 7 kip and 3 kip in size, respectively, left panel). 10 kip and 7 kip, respectively, made up the parental plasmid and the AR-carrying minicircle DNA, right panel). According to our studies, there was very little to no contamination. We transiently transfected MC.GFP and Char into 293T cells to confirm the expression and activity of AR minicircle DNA. An immunoblot test was used to check the protein expression of AR). In 293T cells, we discovered that the AR protein was overexpressed. The correct folding and operation of AR were subsequently confirmed by looking at AR transactivation). When 10 nM DHT was administered to Char transfectants, ARE-luciferase activity was robustly increased as opposed to ARE-luciferase activity in MC.GFP transfectants.

DNA molecules, notably plasmids, may be delivered via vectors with modified viral backbones. The transgene of interest is constructed in the viral genome for therapeutic reasons, and the virus then employs its built-in infection mechanism to penetrate cells and release the expression cassette. The gene is then expressed after entering the nucleus and sometimes integrating with the host genome. High transfection efficiencies have been attained for gene expression employing viral vectors in tissues such the kidney, muscle, ovary, and liver. The use of viruses as delivery vectors raises a number of issues, however. The main issues are the viruses' toxicity and the potential for their capsids to trigger an intense immune response. Numerous animal models have shown this toxicity. For instance, the concern about potential germline tampering was increased when traces of adenovirus titers were found in the seminal fluids of a male patient who had previously undergone adenoviral-based gene therapy. It has been shown that adenoviral vectors employed in cystic fibrosis gene therapy produce a potent immunogenic response. A deadly immune reaction to the adenovirus vector used to transfer the gene was blamed for the death of a patient with respiratory and multiple organ failure who was taking part in a clinical study of gene therapy that had received FDA approval in 1999. All gene therapy experiments in the US were temporarily halted as a result of this instance. Despite the fact that clinical studies have restarted, this incident, along with a few others and, have greatly increased concerns about the safety of utilizing viruses for gene therapy. Additionally, a virus's integration of therapeutic genes into the host genome happens in a random manner. The precise spot where a gene is inserted cannot be predicted. Random gene insertion may result in insertion mutagenesis, which can have harmful effects by activating oncogenes or inhibiting the expression of normal cellular genes. Both of these two issues do not arise when employing minicircle DNA since it does not include a chromosome-insertion sequence and uses LPD technology for nonverbally mediated gene transduction.

The Minicircle-LPD Delivery System's Benefits and Potential for Cancer Therapy. Due to the surface PEGylation, lipid nanoparticles are often less immunogenic than viral delivery

methods. However, liposomal gene transfer-related harm has been noted. Animals given lipoplex injections intravenously and airway instillations have shown acute inflammatory responses. Induction of inflammatory cytokines, neutrophil infiltration in the lungs, a decline in white cell counts, and sometimes tissue damage in the liver and spleen are some of the symptoms. The unmethylated CpG sequences present in plasmids of bacterial origin are associated with a portion of the inflammatory response seen in treated lungs. Unmethylated CpG sequences, a powerful immunological stimulant, cause the production of inflammatory cytokines. The action of unmethylated CpG may be strengthened by cationic lipids found in lipoplexes. Another benefit of adopting the LPD delivery method is that, due to the EPR effect, LPD tends to accumulate in tumours, considerably boosting selectivity[9], [10].

CONCLUSION

To the best of our knowledge, this work is the first to deliver a metastasis suppressor gene to normal and spontaneous-tumor livers. In this work, we delivered a 100-kid protein to mice's normal and tumor livers using LPD incorporating minicircle DNA. Our findings indicate that the AR protein was expressed vigorously for at least two months. The following elements would see the applicability of this success: In order to have therapeutic benefits, cancer medicines often need a long-lasting concentration or expression in the target organ. This would be accomplished by our model; The systemic immune response brought on by viral particles would be one drawback of viral-mediated gene therapy. Because the LPD harboring minicircle DNA exhibits minor immunological issues, several therapies are possible. Minicircle DNA, which lacks the immunological response brought on by bacterial unmethylated CpG sequences, increases expression level and lengthens expression duration. Minicircle DNA was further compressed by protamine and enveloped as a core by lipids, reducing the likelihood that it would be exposed to immune cells and elicit an immunological response.

REFERENCES:

- [1] J. L. Hu *et al.*, "Abnormal expression of DNA double-strand breaks related genes, ATM and GammaH2AX, in thyroid carcinoma," *Int. J. Endocrinol.*, 2015, doi: 10.1155/2015/136810.
- [2] S. Deng *et al.*, "The catalytic topoisomerase II inhibitor dexrazoxane induces DNA breaks, ATF3 and the DNA damage response in cancer cells," *Br. J. Pharmacol.*, 2015, doi: 10.1111/bph.13046.
- [3] K. E. Gurley and C. J. Kemp, "Synthetic lethality between mutation in Atm and DNA-PKcs during murine embryogenesis," *Curr. Biol.*, 2001, doi: 10.1016/S0960-9822(01)00048-3.
- [4] L. G. Ball and W. Xiao, "Molecular basis of ataxia telangiectasia and related diseases," *Acta Pharmacologica Sinica*. 2005. doi: 10.1111/j.1745-7254.2005.00165.x.
- [5] K. O. Yoshiyama and S. Kimura, "Ser-Gln sites of SOG1 are rapidly hyperphosphorylated in response to DNA double-strand breaks," *Plant Signal. Behav.*, 2018, doi: 10.1080/15592324.2018.1477904.
- [6] E. J. Gapud and B. P. Sleckman, "Unique and redundant functions of ATM and DNA-PKcs during V(D)J recombination," *Cell Cycle*. 2011. doi: 10.4161/cc.10.12.16011.
- [7] M. Gandhi *et al.*, "Homologous chromosomes make contact at the sites of double-strand breaks in genes in somatic G 0/G 1-phase human cells," *Proc. Natl. Acad. Sci. U. S. A.*, 2012, doi: 10.1073/pnas.1205759109.

- [8] S. S. Pali, B. O. Van Emburgh, U. T. Sankpal, K. D. Brown, and K. D. Robertson, "DNA Methylation Inhibitor 5-Aza-2'-Deoxycytidine Induces Reversible Genome-Wide DNA Damage That Is Distinctly Influenced by DNA Methyltransferases 1 and 3B," *Mol. Cell. Biol.*, 2008, doi: 10.1128/mcb.01799-07.
- [9] T. Tanaka *et al.*, "ATM activation accompanies histone H2AX phosphorylation in A549 cells upon exposure to tobacco smoke," *BMC Cell Biol.*, 2007, doi: 10.1186/1471-2121-8-26.
- [10] S. Rooney, F. W. Alt, J. A. Sekiguchi, and J. P. Manis, "Artemis-independent functions of DNA-dependent protein kinase in Ig heavy chain class switch recombination and development," *Proc. Natl. Acad. Sci. U. S. A.*, 2005, doi: 10.1073/pnas.0409857102.

CHAPTER 11

NEUTROPHIL RECEPTOR EXPRESSION AFFECTED BY BACTERIAL INFECTIONS: DNA VIRUS INFECTIONS AND RNA VIRUS INFECTIONS

Shweta Loonkar, Assistant Professor
Department of ISME, ATLAS SkillTech University, Mumbai, Maharashtra, India
Email Id-shweta.loonkar@atlasuniversity.edu.in

ABSTRACT:

Antibiotics are inefficient for treating viral diseases or non-infectious causes of inflammation, and they also increase the risk of toxicity, allergic reactions, and antibiotic resistance, all of which raise medical expenses. Of course, inaccurate diagnosis is a key contributor to the overuse of antibiotics. Because of this, quick and precise information on whether the illness is caused by bacteria would be very helpful. We will discuss our most current research on opsonin receptor expression on phagocytes in this publication. A unique application for the diagnosis of viral and disorders is made possible by the study of the expression levels of FCRA, CR1, and CR3, as well as CRP and ESR data. The CIS point approach for a bacterial infection marker, DNAVS point for discriminating between DNA and RNA viral infections, and CRP/CD11b ratio for a sign of Gram-positive sepsis will be generated when the separate variables are merged.

KEYWORDS:

Antibiotics, Discriminating, Inflammatory, Non-Infectious, Phagocytes.

INTRODUCTION

Opsonin-dependent and opsonin-independent molecular pathways are the two main types of phagocytic cells' identification of microbes. Opsonin's, which are serum components necessary for the first mechanism, function by attaching to the surfaces of bacteria at one end and to certain receptors on the surface of phagocytes at the other. The two most well-known opsonin's are Immunoglobulin which attaches to the phagocytes' Fc receptors via its Fc domain, and the C3b and iC3b fragments of complement, which bind to the phagocytes' CR1 and CR3 complement receptors, respectively. In the absence of opsonin's, several bacterial species engage in vitro with phagocytic cells in serum-free conditions. Several integrins, including CR3, operate as receptors for microbial surface ligands in monopsonic phagocytosis. Over 75% of the immunoglobulin that circulates in the blood is IgG, making it the most prevalent Ig class in serum. It interacts with Fc receptors to provide important effector actions. There are three primary kinds of Fc receptors: FCRA, Frei, and Frei, each with unique structural and functional characteristics.

With three extracellular Ig-like domains produced constitutively by monocytes and macrophages as well as numerous myeloid progenitor cells, FCRA is a high-affinity receptor for monomeric IgG. Frei and Frei, the other two kinds of Fc receptors, have a low affinity for monomeric IgG in contrast to FCRA. They have the ability to engage with aggregated IgG via multimeric low-affinity, high-avidity interactions, which are crucial for the identification and attachment of antibody-antigen complexes during an immune response[1], [2]. IgG binding to ineffective Degranulation, phagocytosis, and the control of the generation of antibodies are just a few of the effector and immunoregulatory actions that FCRA may activate. Different cell types express the Fc RII molecule: Myeloid cells, such as polymorphonuclear leukocytes, monocytes, macrophages, platelets, and certain kinds of

endothelial cells, express the FcRI isoform; B cells, monocytes, and macrophages express the FcRII isoform; and only natural killer cells express the FcRIII isoform. There are two isoforms of the other low-affinity Fc receptor, FcRIIb. Although FcRIIa and FcRIIb demonstrate significant structural variations, they share a high degree of sequence homology. While FcRIIb undergoes posttranslational processing to become a glycosylphosphatidylinositol anchored protein without the transmembrane and intracellular domains, FcRIIa is a transmembrane protein that interacts with the FCRA chain.

While only neutrophils express FcRIIb constitutively, several leucocyte cell types, including macrophages, NK cells, and subsets of T cells and monocytes, express the FcRIIa isoform broadly. Complement receptors 1 and 3, which are present on all phagocytic cells, are the receptors for complement molecules. Resting neutrophils only weakly express these receptors on their surface, and the majority of them are stored in intracellular granules. Secretory vesicles, followed by gelatinase, particulate, and azurophilic granules, are the ones most likely to degranulate and discharge their contents. Along with exposure to proinflammatory cytokines, other factors such as various anticoagulant types, temperature fluctuations, and leukocyte separation might cause neutrophil SVs to rapidly degranulate. Increased amounts of CD35 and CD11b are seen at the cell surface as a result of SV fusion with the plasma membrane. Does the expression of phagocytes' opsonin receptors change as a result of viral and other inflammatory diseases?

By adding 10 volumes of 0.83% NH₄Cl to anticoagulated blood and allowing the mixture to sit for 15 minutes at room temperature, erythrocytes were lysed. Centrifugation was used to separate the leukocytes. Leukocytes were treated in 50 L of gabs with monoclonal antibodies in polystyrene flow cytometer vials for 30 min at +4°C prior to the assessments of receptor expression. The cells were once rinsed with cold gabs after incubation and then resuspended in the solution. To rectify leukocyte autofluorescence, leukocytes were treated with mouse non-specific immunoglobulins. By calculating the average fluorescence intensity of 5000 leukocytes, a relative estimate of receptor expression was derived. The proportion of fluorescence-positive cells in the neutrophil FCRA instance was also calculated. The %-value ranged between 5 and 70 in neutrophils, which express very little FCRA on the cell membrane. This value better captured variations in expression levels than the MFI. The %-value was 95–100 at high expression levels. When %-value was 100, only MFI was shown independent of the leukocyte's level of activation. Using fluorescently tagged receptor-specific monoclonal antibodies, leukocyte receptor expression was measured. lists the abs and the receptor panel used for the two-color immunofluorescence investigation. In a handful of our earlier research, we evaluated the receptor expression in a number of relatively small patient groups. Infections with bacteria and viruses resulted in an upregulation of all receptors in monocytes. In bacterial infections, neutrophils' CR1, CR3, FCRA, and FcRIIa were increased whereas FcRIIb was downregulated. In viral infections, CR1 and FcRIIa were downregulated, but CR3 and FCRA were increased. These findings convinced us that the receptor expression may serve as a foundation for the distinction between bacterial and viral illnesses[3], [4].

In this study, neutrophil complement receptors, CR1 and CR3, and FcRI, as well as standard clinical laboratory data (erythrocyte sedimentation rate) were collected from 292 hospitalised febrile patients. Following clinical diagnosis or microbiological confirmation, 135 individuals were determined to have either bacterial curve analysis). The most efficient differential capacity was found in neutrophil CR1, which was superior to other evaluated variables including neutrophil CR3, neutrophil count, CRP, and ESR. The fact that CR3 is expressed not only from quickly releasing secretory vesicles like CR1, but also from specialised and gelatinase granules, may help to explain why CR3 has a poorer diagnostic accuracy than CR1. Due to extracellular calcium deficiencies in blood samples, the

differential capability of CR1 and CR3 was lost when EDTA was employed as an anticoagulant in place of heparin. Since CRP and ESR levels were much greater in bacterial infections than in viral infections, their behavior was comparable to that of neutrophil CR1 expression. The neutrophil count, mean fluorescence intensity of FITC-conjugated CR1-specific monoclonal antibodies on neutrophils, and MFI of PE-conjugated CR3-specific monoclonal antibodies on neutrophils were multiplied to create a computational variable in addition to the measured variables. The total number of neutrophil complement receptors per volume of blood sample is indicated by an index created by taking the base-10 logarithm of this factorial. In order to discriminate between viral and bacterial infections, the neutrophil CR1 has a little lower specificity than the TNCR index.

DISCUSSION

Utilizing the Clinical Infection Score Point to Differentiate Between Bacterial and Viral Infections We calculated the clinical infection score point, which consists of four variables, including CRP, ESR, mean amount of CR1 on neutrophil, and TNCR index, to ascertain whether the diagnostic yield of measured individual variables increases upon combination. A result that fell below the cutoff point for each variable measured was converted to a variable score point of 0, a result that fell between the cutoff point and a second cutoff value, and a result that fell above the second cutoff value was converted to a variable score point of 2. The highest value of a variable that was discovered in patients with viral infections served as a second cutoff value. When extra second cutoff values were substituted in their place, the highest virus value, which is greater than the average value of bacterial infection, was disregarded. Combining variable scores resulted in CIS points that ranged. With 98% sensitivity and 97% specificity, the CIS points distinguished between microbiologically proven bacterial illness and viral infection at a cutoff value of >2. In a manner similar to the CIS point, we calculated the DNA virus score point, which is composed of four variables: the mean amount of CD64 on neutrophils, neutrophil CD64%, the percentage of lymphocytes, and the lymphocyte count.

For every variable measured, a result less than the cutoff point was converted to a variable score point of 0, that between the cutoff point and an additional second cutoff value was converted to a variable score point of 1, and that greater than the additional second cutoff point value was converted to a variable score point of 2. The highest value found in individuals with Serna virus infection served as a second cutoff value for a variable. After data translation, we produced SUM by summing the four variable score points, which ranged from 0 to 8. The SUM, CD64 factor, and hematopoietic factor were then multiplied to create a DNAVS point. When the variable score point for both receptor variables was 0, CF of 0.25 was used. A HF of 0.5 was applied if the variable score point for both hematopoietic variables was 0. CF and HF were 1 in each of the other situations. The DNAVS points distinguished between dsDNA and Serna viral infections with 95% sensitivity and 100% specificity at a cutoff point greater than or equal to 1.5. Using the analysis of Fc RI expression to distinguish between bacterial infections, viral infections, and inflammatory diseases When compared to healthy controls, individuals with febrile viral and bacterial infections had considerably more FcRI on the average number of neutrophil and monocyte surfaces. Additionally, we report a brand-new febrile infection diagnostic called a "CD64 score point" that uses quantitative measurement of FcRI expression on both neutrophils and monocytes[5], [6].

This marker has a 94% sensitivity and 98% specificity for identifying febrile infections from healthy controls. While levels did not significantly differ between systemic, local, and clinically diagnosed bacterial infections, analysis of FcRI expression on neutrophils and

monocytes showed poor sensitivity and specificity in differentiating between bacterial and viral infections. As a result, although an elevated Fc RI count on neutrophils and monocytes is a helpful indication of febrile illness, it cannot be used to distinguish between bacterial and viral infections or between systemic and local bacterial infections. As was already mentioned, bacterial infections are more common than viral infections in terms of neutrophil CD35 expression. The generation of the CIS point may enhance neutrophil CD35-based discrimination between bacterial and viral illnesses. The vertical and horizontal lines in the CD64/CIS point bivariate dot-plot graph (4) are set to indicate the ideal cutoff point, which is an MFI value of 1.5 for neutrophil FcRI and 2.5 for CIS point value, respectively. The upper left quadrant, upper right quadrant, lower left quadrant, and lower right quadrant may be used to categorise the bivariate dot-plot graph. Currently, 92% of bacterial infections are found in URQ, while 35% or 61% of viral infections are found in LLQ or LRQ. Distribution of inflammatory illnesses to LLQ, ULQ, and URQ. The average level of CD11b on neutrophils was substantially greater in gram-negative bacterial infection compared to gram-positive bacterial infection. Contrarily, gram-positive bacterial infections had CRP levels that were substantially greater than gram-negative bacterial infections. We developed a novel marker of Gram-positive sepsis, the CRP/CD11b ratio, by dividing the serum CRP value by the amount of CD11b on neutrophils. This marker showed 76% sensitivity and 80% specificity for the detection of Gram-positive sepsis in febrile patients with microbiologically confirmed or clinically diagnosed bacterial infection.

Hepatic carcinoma, a deadly digestive system malignancy, is the sixth most common cause of morbidity and the fourth leading cause of mortality in 2018. Hepatitis virus and alcohol intake are two crucial risk factors for HCC. With the advancement of bioinformatics and high-throughput sequencing technology, inhibitor of apoptosis protein family members, CDK1, PBK, RRM2, and ASPM, only about 5-14 percent of patients with HCC have a five-year survival rate. Han et al. discovered recently using bioinformatics that SCAMP3 could be a key marker in the development of liver cancer. Investigating the relationship between prognostic value and novel gene complexes in HCC is crucial. The micro liposome maintenance protein, which is essential for DNA replication, was initially identified in the yeast *Saccharomyces cerevisiae*. Mutants of this protein shown deficiencies in micro liposome maintenance. From yeast to humans, MCM2-7 is a collection of six structurally similar proteins that bind to create a hexamer. Nuclear proteins MCM2-7 attach to chromatin in a way unique to the cell cycle throughout the advancement of DNA synthesis, boosting cell proliferation and helicase activity.

The DNA replication mechanism may be directly disrupted by problems with these proteins, which can result in cancer growth and progression. Numerous pathologic processes, including as DNA replication, cell cycle, proliferation, invasion, migration, immunological response, and apoptosis, are regulated by the MCM complex. MCM is more strongly expressed in various malignancies than in healthy tissues, according to earlier reports in the literature. For instance, HCC, oral squamous cell carcinoma, gastric cancer, breast cancer, colon cancer, and ovarian cancer all have high levels of MCM2. The level of MCM2 might indicate a bad prognosis for osteosarcoma, gastric cancer, lung adenocarcinoma, diffuse large B cell lymphoma, and esophageal cancer. MCM2 was thought to be a possible therapeutic target for cancer therapy. MCM2 may be a possible therapeutic target for HCC, according to recent studies. Additionally, Deng et al. discovered that MCM2 suppression might boost the ovarian cancer cell's susceptibility to carboplatin. Similar to other cancer types, MCM3 showed high levels of expression in glioma, salivary gland tumours, and osteosarcoma. MCM3 has a high expression in leukaemia, lymphoma, uterine cervix cancer, colon, lung, gastric, kidney, breast, and malignant melanoma, according to Ha et al. MCM4 levels were

increased in cases of non-small-cell lung cancer, uterine cervical cancer, and esophageal cancer. MCM5, a different regulator of DNA replication, was overexpressed in many cancers, including bladder cancer, thyroid cancer, oral squamous cell carcinoma, colon cancer, and cervical cancer. In colorectal cancer, breast cancer, AO, HCC, endometrioid adenocarcinoma, lung cancer, meningiomas, cervical cancer, Hodgkin's lymphoma, and Merkel cell carcinoma, the expression of MCM6 was found to be increased, and its high level had a close relationship with an unfavorable prognosis.

Acute myeloid leukemia, prostate cancer, HCC, breast cancer, and HCC have all been linked to ectopic MCM7 expression. These investigations adequately demonstrated the varying levels of MCMs in various cancer types, but few research systematically examined the prognostic significance of the whole MCM complex in the development of cancer. We thoroughly explored the transcriptional level of MCMs in this work and discovered its predictive relevance in HCC. We also used bioinformatics to analyse the interaction network, genetic mutation, and functional enrichment of Casemore studies are now showing that ectopic production of MCMs may speed up the cell cycle, DNA replication, and metastasis. Numerous human illnesses were influenced by MCMs in their onset and development. The tetradecameric complex made up of MCM2-7 in human cancer cells has previously been thoroughly described. However, there are still a lot of issues about the expression, operation, interaction, and prognostic significance of MCMs in HCC that need to be thoroughly resolved. In order to learn more about MCM2-7's transcriptional level, functional enrichment, gene/protein interaction, and prognostic values in HCC, we carried out a thorough investigation[7], [8].

In this work, we discovered that HCC tissues had much higher levels of MCM2-7 expression than normal liver tissues. An oncogene called MCM2 was linked to the emergence and progression of HCC from cirrhosis. MCM2 protein may be helpful as a cascade screening technique for spotting precancerous alterations in cervical cancer since it is substantially expressed in high-grade squamous intraepithelial lesions. Our findings showed that in HCC patients without hepatitis virus infection, high levels of MCM2 were substantially linked with poorer OS, RFS, PFS, and DSS. MCM3 is a useful prognostic tool that is independent of ER and HER2 statuses, as Zhao et al. demonstrated when they found that it was a better marker of proliferation than Ki67. Our research found that HCC patients with high MCM3 expression had worse OS/RFS/PFS/DSS in the group of non-alcohol drinkers. MCM4 may be utilised as a more accurate proliferative marker to detect esophageal lesions, according to Choy et al. We discovered that the RFS and OS of HCC patients with higher MCM4 mRNA levels were poor.

Ectopic MCM5 expression was shown to be closely correlated with malignancy and a poor prognosis, suggesting that it might be used as a prognostic indicator for renal cell carcinoma by Gong and his colleagues. In the research, we discovered a strong link between a high level of MCM5 and a bad prognosis for HCC, particularly in OS/RFS/PFS/DSS. According to Liu et al., MCM6 might increase migration and invasion, indicate a poor prognosis, and predict preclinical early recurrence in HCC patients, indicating the need for more vigilant surveillance and vigorous treatment. We also discovered that MCM6 expression was associated with poor OS and PFS in patients with stage 1+2, stage 3+4, grade 1/2/3, or nonvascular invasion. Additionally, MCM7 is superior to conventional cell cycle indicators like Ki67 and PCNA because it is more sensitive and resistant to outside influences, such as inflammatory stimuli. The existence of MCMs at all cellular stages may be the cause of the advantage since Ki67 and PCNA expression can only be detected at certain phases of replication and may be readily tampered with. We also looked at the relationship between MCM7 level and prognosis, and the results suggested that MCM7 may possibly be a useful

prognostic marker for HCC patients. Using the corporal database, the association between MCMs and genetic change was discovered in HCC. The fact that the HCC prognosis was unaffected by the mutation, however, may mean that additional mechanisms, such as protein phosphorylation, alanylation, and ubiquitination, were responsible for the ectopic production of MCMs in HCC. It was yet unknown how the MCM complex affected epigenetic changes such DNA methylation, histone acetylation, and noncoding RNA control. As an acquired condition, HCC may be more related to aberrant molecular signal transmission and epigenetic changes than to hereditary factors and gene alterations.

Therefore, further research on protein and epigenetic modification is required in order to compare it to research on gene change. Further research was required on how these MCMs' genes are altered. Furthermore, our findings revealed that MCM proteins, which were both elevated in HCC relative to normal liver tissues, were significantly positively correlated. BLM, WRN, RMI1, and TOP3A, which forms an important network to perform a series of pathophysiological functions at the protein level. By using bioinformatics research, Wen et al. built a network related to small cell lung cancer, showing that connections between MCM2/3/6 and other hub proteins were crucial to the development of the disease. We looked at the functional enrichment of MCMs and its mechanism via Mediascape in order to better investigate the associated activities and signaling cascades of these proteins. The findings suggested that DNA replication, cell cycle, homologous recombination, pyrimidine metabolism, and viral carcinogenesis may all be implicated in MCMs. In carcinogenesis, these pathways often showed dysfunction. For instance, Lin and his colleagues discovered that the MCM complex might promote carcinogenesis by accelerating the cell cycle via DNA replication. BRCA1, a tumor suppressor protein that increases DNA double-strand break repair via homologous recombination, shields DNA replication forks from attrition. Sweeney et al. discovered that rhodexin and dimethyl aminopurine successfully blocked the vital biosynthetic route for the survival of leukemia cells by inhibiting the combination of glutamine and glutamine-derived metabolites in purine and pyrimidine production. EBV and hepatitis virus infections, respectively, have shown viral carcinogenesis in nasopharyngeal carcinoma and high-grade cervical cancer. To validate these bioinformatics hypotheses, more research and tests are required. This will allow us to better understand how MCM2-7 and associated signaling pathways contribute to the development of HCC[9], [10].

CONCLUSION

Antibiotics are inefficient in treating viral diseases or non-infectious causes of inflammation, and they also increase the risk of toxicity, allergic responses, and antibiotic resistance, all of which raise medical expenses. Of course, inaccurate diagnosis is a key contributor to the overuse of antibiotics. In order to combat antibiotic resistance, timely and precise information on whether the ailment is bacterial in origin would be very helpful. A unique application for the diagnosis of viral and inflammatory disorders is made possible by the study of the expression levels of FCRA, CR1, and CR3, as well as CRP and ESR data. When the individual variables are combined to produce the CIS point method for a reliable bacterial infection marker, DNAVS point for differentiating between DNA and RNA virus infections, CD64 score point for a marker of febrile infection, and CRP/CD11b ratio for a marker of gram-positive sepsis, the best clinical benefit from the quantitative analysis of these markers will be obtained.

REFERENCES:

- [1] E. M. Lilius and J. Nuutila, "Bacterial infections, DNA virus infections, and RNA virus infections manifest differently in neutrophil receptor expression," *The Scientific World Journal*. 2012. doi: 10.1100/2012/527347.

- [2] P. S. Martins *et al.*, “Expression of cell surface receptors and oxidative metabolism modulation in the clinical continuum of sepsis,” *Crit. Care*, 2008, doi: 10.1186/cc6801.
- [3] I. Von Scheele *et al.*, “Toll-like receptor expression in smokers with and without COPD,” *Respir. Med.*, 2011, doi: 10.1016/j.rmed.2011.02.012.
- [4] M. Herová, M. Schmid, C. Gemperle, and M. Hersberger, “ChemR23, the Receptor for Chemerin and Resolvin E1, Is Expressed and Functional on M1 but Not on M2 Macrophages,” *J. Immunol.*, 2015, doi: 10.4049/jimmunol.1402166.
- [5] K. Pauksens, G. Fjaertoft, L. Douhan-Håkansson, and P. Venge, “Neutrophil and monocyte receptor expression in uncomplicated and complicated influenza A infection with pneumonia,” *Scand. J. Infect. Dis.*, 2008, doi: 10.1080/00365540701646287.
- [6] Y. Tsuda, H. Takahashi, M. Kobayashi, T. Hanafusa, D. N. Herndon, and F. Suzuki, “Three different neutrophil subsets exhibited in mice with different susceptibilities to infection by methicillin-resistant *Staphylococcus aureus*,” *Immunity*, 2004, doi: 10.1016/j.immuni.2004.07.006.
- [7] P. G. Vallés, S. Melechuck, A. González, W. Manucha, V. Bocanegra, and R. Vallés, “Toll-like receptor 4 expression on circulating leucocytes in hemolytic uremic syndrome,” *Pediatr. Nephrol.*, 2012, doi: 10.1007/s00467-011-2014-7.
- [8] H. Fang, T. Elina, A. Heikki, and S. Seppo, “Modulation of humoral immune response through probiotic intake,” *FEMS Immunol. Med. Microbiol.*, 2000, doi: 10.1016/S0928-8244(00)00187-5.
- [9] R. Salomao *et al.*, “Toll-like receptor pathway signaling is differently regulated in neutrophils and peripheral mononuclear cells of patients with sepsis, severe sepsis, and septic shock,” *Crit. Care Med.*, 2009, doi: 10.1097/CCM.0b013e318192fbaf.
- [10] A. P. Freitas, B. C. Favoretto, P. B. Clissa, S. C. Sampaio, and E. L. Faquim-Mauro, “Crotoxin Isolated from *Crotalus durissus terrificus* Venom Modulates the Functional Activity of Dendritic Cells via Formyl Peptide Receptors,” *J. Immunol. Res.*, 2018, doi: 10.1155/2018/7873257.